



Bryan J. Dolan
VP, Nuclear Plant Development

Duke Energy
EC09D/ 526 South Church Street
Charlotte, NC 28201-1006

Mailing Address:
P.O. Box 1006 – EC09D
Charlotte, NC 28201-1006

704-382-0605

Bryan.Dolan@duke-energy.com

February 22, 2010

Document Control Desk
U.S. Nuclear Regulatory Commission
Washington, DC 20555-0001

Subject: Duke Energy Carolinas, LLC
William States Lee III Nuclear Station - Docket Nos. 52-018 and 52-019
AP1000 Combined License Application for the
William States Lee III Nuclear Station Units 1 and 2
Transmittal of Unit 1 Foundation Input Response Spectra (FIRS)
Horizontal and Vertical Component Analysis
Ltr# WLG2010.02-01

- References: (1) Letter from Brian Hughes (NRC) to Peter Hastings (Duke Energy), Request for Additional Information Letter No. 076 Related to SRP Section: 02.05.02 – Vibratory Ground Motion for the William States Lee III Units 1 and 2 Combined License Application, dated November 3, 2009
- (2) Letter from Bryan J. Dolan (Duke Energy) to Document Control Desk, U.S. Nuclear Regulatory Commission, Response to Request for Additional Information (RAI No. 3549), Ltr# WL12009.12-08, dated December 18, 2009

In preparing the response to the Nuclear Regulatory Commission's request for additional information (RAI) 02.05.02-049 included in Reference 1, Duke Energy identified the need to revise a site specific analysis for the horizontal and vertical components of the Lee Nuclear Station (Lee) Unit 1 Foundation Input Response Spectra (FIRS). This change does not affect the horizontal and vertical components of the Lee Ground Motion Response Spectra (GMRS).

The corrected Unit 1 FIRS remains below the generic AP1000 Hard Rock High Frequency spectrum, and the conclusions presented in the Lee FSAR are unchanged. The revision of this site specific analysis is addressed in Enclosure 1 to this letter, which also identifies associated changes, where appropriate, that will be made in a future revision of the Final Safety Analysis Report for the Lee Nuclear Station. In addition, revisions have been made to the supplemental technical report entitled "Development of Horizontal and Vertical Site-Specific Hazard Consistent Uniform Hazard Response Spectra at the Lee Nuclear Station Unit 1," originally provided in Reference 2. The revised technical report is included as Enclosure 2 to this letter.

DO93
NR0

Document Control Desk
February 22, 2010
Page 2 of 5

If you have any questions or need any additional information, please contact Peter S. Hastings, Nuclear Plant Development Licensing Manager, at 980-373-7820.



Bryan J. Dolan
Vice President
Nuclear Plant Development

Document Control Desk
February 22, 2010
Page 3 of 5

Enclosures:

- 1) Summary of Changes to FIRS A1 Analysis and Associated FSAR Revisions
- 2) Development of Horizontal and Vertical Site-Specific Hazard Consistent Uniform Hazard Response Spectra at Lee Nuclear Station Unit 1, Revision 3

AFFIDAVIT OF BRYAN J. DOLAN

Bryan J. Dolan, being duly sworn, states that he is Vice President, Nuclear Plant Development, Duke Energy Carolinas, LLC, that he is authorized on the part of said Company to sign and file with the U. S. Nuclear Regulatory Commission this supplement to the combined license application for the William States Lee III Nuclear Station and that all the matter and facts set forth herein are true and correct to the best of his knowledge.


Bryan J. Dolan

Subscribed and sworn to me on February 22, 2010


Notary Public

My commission expires: April 19, 2010



Document Control Desk
February 22, 2010
Page 5 of 5

xc (w/o enclosures):

Loren Plisco, Deputy Regional Administrator, Region II
Stephanie Coffin, Branch Chief, DNRL

xc (w/ enclosures):

Brian Hughes, Senior Project Manager, DNRL

Summary of Changes to FIRS A1 Analysis and Associated FSAR Revisions

In preparing the response to the Nuclear Regulatory Commission's request for additional information (RAI) 02.05.02-049 included in Reference 1, Duke Energy identified the need to revise the site specific analysis of the horizontal and vertical components of the Lee Nuclear Station (Lee) Unit 1 Foundation Input Response Spectra (FIRS). This change does not affect the horizontal and vertical components of the Lee Ground Motion Response Spectra (GMRS). A detailed description of the change, the results of the corrected analysis, and an assessment of the effects of the change are presented below.

The velocity randomization process used a correlation function to avoid unrealistic velocity variability between adjacent layers. In this case, the correlation function combined with a set of standard randomization seeds produced a large systematic bias in the randomized basement shear wave (V_s) velocity relative to the target basement V_s velocity.

The Lee Unit 1 FIRS A1 base case profile consists of 20.5 ft of fill concrete, randomized + 3 ft, with a V_s velocity of 7,500 ft/sec, randomized + 10% with a coefficient of variance (COV) of 0.1. The fill concrete overlies hard rock with a V_s equivalent to that specified in the reference rock probabilistic seismic hazard analysis (PSHA), $V_s = 2.83$ kilometers per second (km/sec) ($V_s = 9,285.2$ ft/sec). In the randomization procedure, the hard rock velocity is also randomized using a lognormal distribution with a σ_{ln} of 0.3, appropriate for basement rock conditions (EPRI, 1993) (FSAR Reference 2.5.2-273). Subsequently, the mean velocity of the concrete was found to be $V_s = 7,459.7$ ft/sec, within about 0.5% of the base case value of $V_s = 7,500$ ft/sec, and considered to be well within the judgment tolerance of about 10% used in assessing the mean values. Because amplification varies as the square root of the velocity, a 10% tolerance in mean velocity results in about a 5% tolerance in amplification, a very small and acceptable number in the context of ground motion variability.

For a typical soil site, typical ground motion analyses involve much thicker (> 20 ft) soil overlying basement material. The mean velocity of the basement has a small impact on the amplification, due primarily to the nonlinear response of the soil. As would be expected, the nonlinear response of the soil column tends to dampen fluctuations in incoming motions (EPRI, 1993) (FSAR Reference 2.5.2-273), which are affected by the basement velocity. To illustrate this case, EPRI (1993) found that the difference in soil amplification for basement velocities ranging from a base case value of $V_s = 6,000$ ft/sec to 9,000 ft/sec (a 50% increase) resulted in a maximum difference of only about 10% in amplification. For a typical soil response, this difference in basement velocity would result in a difference in amplification of about 5% or less.

For the site specific case of Lee Unit 1 FIRS, with a very thin high velocity material (concrete) that is linear in response and overlying very high velocity hard rock, the systematic variations in the randomized basement velocity relative to the base case basement velocity was found to have a more significant impact on estimated amplification. This increased sensitivity was recently discovered when it was observed that the randomizations produced a mean basement velocity of $V_s = 11,502.5$ ft/sec, a 24% increase in basement velocity relative to the target base case value of $V_s = 9,285.2$ ft/sec.

In this case, the difference in amplification varies approximately as the square root of the ratios of velocities (basement velocity divided by that of the overlying layer). The original Unit 1 FIRS V_s ratio is given by $11,502.5/7,459.7$ and the square root is 1.24. The desired target Unit 1

FIRS V_s ratio is given by $9,285.2/7,500.0$ with a square root of 1.11, or about 10% lower. Enclosure 2 of this letter provides a revision to the supplemental technical report entitled "Development of Horizontal and Vertical Site Specific Hazard Consistent Uniform Hazard Response Spectra at the Lee Nuclear Station Unit 1." This report was last revised and submitted in Reference 2. The original and updated median estimates of the amplification factors (FSAR Figure 2.5.2-141) reflect maximum amplifications of 1.22 and 1.10 near 70 Hz respectively, quite close to the theoretical values. The structural frequencies specified by the PSHA include spectral accelerations at two specific frequencies greater than 34 Hz (of 50 Hz and 100 Hz). The maximum amplification difference is about 6% and occurs at 50 Hz. The corrected Unit 1 FIRS remains below the generic AP1000 Hard Rock High Frequency spectrum, and the conclusions presented in the FSAR are unchanged.

The attached mark-ups of FSAR subsections, revised FSAR tables, and revised FSAR figures affected by the correction of the Unit 1 FIRS will be incorporated into a future revision of the Final Safety Analysis Report.

References:

1. Letter from Brian Hughes (NRC) to Peter Hastings (Duke Energy), Request for Additional Information Letter No. 076 Related to SRP Section: 02.05.02 – Vibratory Ground Motion for the William States Lee III Units 1 and 2 Combined License Application, dated November 3, 2009.
2. Letter from Bryan J. Dolan (Duke Energy) to Document Control Desk, U.S. Nuclear Regulatory Commission, Response to Request for Additional Information (RAI No. 3549), Ltr# WL12009.12-08, dated December 18, 2009.

Associated Revision to the Lee Nuclear Station Supplemental Technical Report (included in Enclosure 2 to this letter):

Report Overview

Subsection 3.4.2.3

Subsection 4.2.3

Subsection 4.3

Subsection 5.0

Subsection 6.0

Table 2

Figure 2

Figure 8

Figure 14

Figure 15

Figure 17

Figure 19

Figure 20

Associated Revision to the Lee Nuclear Station Final Safety Analysis Report:

FSAR Subsection 2.5.2.6

FSAR Subsection 2.5.2.7

FSAR Subsection 2.5.2.8

FSAR Subsection 3.7.1.1.1

FSAR Table 2.0-201

FSAR Table 2.5.2-224

FSAR Figure 2.5.2-240

FSAR Figure 2.5.2-241

FSAR Figure 2.5.2-244

FSAR Figure 2.5.2-245

FSAR Figure 2.5.2-246

FSAR Figure 2.5.2-247

FSAR Figure 3.7-201

FSAR Figure 3.7-202

Attachments:

- 1) Mark-up of FSAR Subsection 2.5.2.6
- 2) Mark-up of FSAR Subsection 2.5.2.7
- 3) Mark-up of FSAR Subsection 2.5.2.8
- 4) Mark-up of FSAR Subsection 3.7.1.1.1
- 5) Revised FSAR Table 2.0-201
- 6) Replacement FSAR Table 2.5.2-224
- 7) Revised FSAR Figures 2.5.2-240, 2.5.2-241, 2.5.2-244, 2.5.2-245, 2.5.2-246, 2.5.2-247, 3.7-201, and 3.7-202

**Lee Nuclear Station
Summary of Changes to FIRS A1 Analysis and Associated FSAR Revisions**

Attachment 1

Mark-up of FSAR Subsection 2.5.2.6

COLA Part 2, FSAR, Chapter 2, Subsection 2.5.2.6, third paragraph, is revised as follows:

For the vertical GMRS (Table 2.5.2-220), a fully probabilistic approach is used to develop the vertical hazard curves along with UHRS and GMRS to maintain exceedence probabilities consistent with the horizontal UHRS (Subsection 2.5.2.7.1.1). The method employed, Approach 3 (Subsection 2.5.2.7.1), integrates the horizontal hazard curves with distributions of V/H ratios resulting in vertical hazard curves, which are intended to maintain the same exceedence probability as the horizontal hazard. For the V/H ratios, the stochastic point source model is used to compute both horizontal (normally incident SH-waves) and vertical (incident inclined P-SV waves) motions (References 280 and 281) using the hard rock crustal model (Table 2.5.2-221). For the hard rock profile, because the shear-wave velocities are high, a linear analysis is performed for the horizontal as well as vertical motions (References 273 and 286) (Subsection 2.5.2.7.1.1). Table 2.5.2-221 lists the source distances and depths intended to cover the range in expected hard rock horizontal peak acceleration values at exceedence probabilities ranging from 10^{-2} to 10^{-7} yr⁻¹. Because V/H ratios typically vary with source distance (Reference 292), the range is also intended to cover the distance deaggregation. While the hard rock V/H ratios are largely independent of **M** (Reference 251), **M** 5.1 is selected as small magnitudes dominate the contribution at close distances and at high frequency (Figures 2.5.2-231, 232, and 233), where the V/H ratios typically reach maximum values (References 251, 286, and 292). The median estimates of the computed V/H ratios are shown in Figure 2.5.2-240. Only a subset of the computed ratios are shown in Figure 2.5.2-240, as there is little change at distances beyond about 6 to 9 mi. (10 to 15 km), with an abrupt jump in the ratios within about 6 mi. (10 km). The ratios are largely independent of frequency with a peak near 60 Hz and range in amplitude from about 0.5 to about 1 as distance decreases. These values, at low frequency, are lower than empirical hard rock central and eastern North America (CENA) V/H ratios, which average about 0.8, decreasing from about 0.9 at 1 Hz to about 0.7 at 10 Hz (References 297 and 298). While these empirical V/H ratios are for Fourier amplitude spectra and not 5% damped response spectra and are dominated by small **M** earthquakes (\leq about 4) and large distances ($D \geq$ about 125 mi.), the results illustrate the large uncertainty in vertical hard rock hazard for CENA and suggest large distant ratios may be greater than model predictions at low frequency. To accommodate the large uncertainty, a minimum V/H ratio of 0.7, the average of the empirical and simulations, is adopted. To accommodate the change in source distance with both annual exceedence probability and structural frequency shown in the deaggregation plots (Figures 2.5.2-231, 232, 233, 234, 235, and 236), V/H ratios computed at a suite of distances are given relative weights (Table 2.5.2-223). The distances selected are 17 mi. (28 km), 4 mi. (7 km), and 0 mi. (0 km) to cover ratios reflecting distant, intermediate, and near source contributions. Table 2.5.2-220 lists the resulting vertical 10^{-4} yr⁻¹ and 10^{-5} yr⁻¹ UHRS and GMRS, and Figure 2.5.2-239 shows the horizontal and vertical GMRS.

Lee Nuclear Station

Summary of Changes to FIRS A1 Analysis and Associated FSAR Revisions

Attachment 2

Mark-up of FSAR Subsection 2.5.2.7

COLA Part 2, FSAR, Chapter 2, Subsection 2.5.2.7.1.1.1.1, is revised as follows:

Horizontal amplification factors are developed using hard rock spectral shapes as control motions (Reference 251). Base Case Profile A1 is placed on top of the regional hard rock crustal model (Table 2.5.2-221, Reference 249273). A hard rock kappa value of 0.006 sec (Table 2.5.2-221) is used, consistent with that incorporated in the hard rock attenuation relations (Reference 249273). With a hysteretic damping in concrete between 0.5% and 1.0% any additional damping in the shallow concrete profile is neglected as its impacts will be beyond the fundamental shallow column resonance, well above 50 Hz.

While the site response analyses are linear and therefore strictly independent of control motion spectral shape for Fourier amplitude spectral ratios, at high frequency, 5% damped response spectral ratios may not be strictly independent of control motion shape. This can occur because the width of the simple harmonic oscillator transfer function is constant in log frequency and increases directly with frequency, averaging over a wider range in frequencies as oscillator frequency increases. At very large distances, where crustal damping has depleted high frequencies (spectral shapes shift to lower frequencies, Reference 251) and the site resonance is not highly excited, responses spectral ratios may depart from those computed using control motions relatively rich in high frequency energy (close distances). To accommodate the possibility of distance dependent transfer functions in a linear analysis, a suite of spectral shapes is used as control motions at distances of 0.6, 12, 62, 125, 250 mi (1, 20, 100, 200, and 400 km). Results are shown in Figure 2.5.2-241 and reveal the shallow site resonance, median amplification of about 25%~~10%~~ near 60 Hz to 70 Hz, with a very slight difference only at 250 mi (400 km). The width of the resonance is broadened by the profile randomization with shear-wave velocities varying $\pm 10\%$ about the Unit 1 FIRS value of 7,500 ft/sec along with depth to hard rock at 20 ft, randomly varied ± 3 ft.

COLA Part 2, FSAR, Chapter 2, Subsection 2.5.2.7.1.1.1.2, is revised as follows:

For the Lee Nuclear Station, the concrete profile is randomized between depths of 17 to 23 ft, the range in depths to hard rock conditions [shear-wave velocity exceeding, on average, 9,300 ft/sec (2.83 km/sec)] (Reference 249273). A uniform distribution is assumed for the depth randomization. For the shear-wave velocity randomization, a soft rock correlation model was used (References 277 and 280). Because concrete velocities show much less variability than firm rock, being a uniform and controlled emplacement material, variations in velocity were constrained to $\pm 10\%$ about the base case value of 7,500 ft/sec with a COV of 0.1.

COLA Part 2, FSAR, Chapter 2, Subsection 2.5.2.7.2, third and fifth paragraphs, are revised as follows:

The approximations of linear analysis for the vertical component and uncoupled vertical and horizontal components are validated in two ways. Fully nonlinear modeling using a 3-D soil model shows that the assumption of largely independent horizontal and vertical motions for loading levels up to about 0.5g (soil surface, horizontal component) for moderately stiff profiles is appropriate (Reference 280). Additionally, validation exercises with recorded motions have been conducted at over 50 sites that recorded the 1989 M 6.9 Loma Prieta, California and ~~1992 M 6.7 Northridge, California~~ earthquakes (Reference 273). These validations show the overall bias and variability is low but is higher than that for horizontal motions (References 280 and 281). An indirect validation is also performed by comparing V/H ratios from WNA empirical attenuation relations with model predictions (Reference 281) over a wide range in loading conditions (Reference 281). The results show a favorable comparison with the model

exceeding the empirical V/H ratios at high frequency, particularly at high loading levels. In the V/H comparisons with empirical relations, the model also shows a small under prediction at low frequency (≤ 1 Hz) and at large distance (≥ 12 mi.).

For Lee Nuclear Station Unit 1 FIRS the site-specific V/H ratios, Figure 2.5.2-240 shows median estimates computed with the stochastic model for M 5.1. For M 5.1, the distances range from 50 to 0 mi. (80 to 0 km) (Table 2.5.2-221) with expected horizontal hard rock peak accelerations ranging from 0.01 to 0.50g. Figure 2.5.2-240 shows that the V/H for the shallow concrete profile Unit 1 FIRS are nearly constant with frequency and increase rapidly as distance decreases, within about a 9 mi. source distance. For distances beyond 6 to 9 mi., the V/H ratio is about 0.5 and increases rapidly to about 0.9. The peak near 60 Hz is likely due to the peak in the horizontal amplification factors (Figure 2.5.2-241). In Figure 2.5.2-240, the multiple peaks beginning near 1 Hz reflect deep crustal resonances (structure below 0.5 mi., Table 2.5.2-221) that would be smoothed if the crustal model were randomized and discrete layers replaced with steep velocity gradients to reflect lateral variability and a more realistic crustal structure. The M 5.1 distance ranges more than adequately accommodate the hazard deaggregation (Subsection 2.5.2.4.5).

COLA Part 2, FSAR, Chapter 2, Subsection 2.5.2.7.4, is revised as follows:

Table 2.5.2-224 and Figures 2.5.2-244 and 245 show horizontal and vertical Unit 1 FIRS developed compared to the horizontal and vertical GMRS developed for Unit 2. Figure 2.5.2-246 shows both the horizontal and vertical FIRS. Figure 2.5.2-247 shows the horizontal and vertical UHRS at exceedence levels of 10^{-4} , 10^{-5} , and 10^{-6} yr⁻¹. Through Approach 3, both the horizontal and vertical UHRS and Unit 1 FIRS are hazard- and performance-based consistent across structural frequency from 0.5 to 100 Hz, the frequency range over which the hard rock hazard is computed (Reference 273). For frequencies below 0.5 to 0.1 Hz, the extrapolation employed is intended to reflect conservatism, likely resulting in motions of lower probability. Table 2.5.2-224 lists discrete values for FIRS and UHRS horizontal and vertical spectral acceleration values for Unit 1. Section 3.7 compares the site-specific ground motions to the AP-1000 design ground motions.

Lee Nuclear Station

Summary of Changes to FIRS A1 Analysis and Associated FSAR Revisions

Attachment 3

Mark-up of FSAR Subsection 2.5.2.8

COLA Part 2, FSAR, Chapter 2, Subsection 2.5.2.8, is revised as follows:

278. Anderson, J.G. and Hough, S.E., "A Model for the Shape of the Fourier Amplitude Spectrum of Acceleration at High Frequencies," *Bulletin of the Seismological Society of America* 74 (5): ~~1,343-1,373~~1,969-1,993, 1984.

Lee Nuclear Station

Summary of Changes to FIRS A1 Analysis and Associated FSAR Revisions

Attachment 4

Mark-up of FSAR Subsection 3.7.1.1.1

Duke Letter Dated: February 22, 2010

COLA Part 2, FSAR, Chapter 2, Subsection 3.7.1.1.1, fifth paragraph, is revised as follows:

As shown on Figure 3.7-201, the horizontal GMRS and Unit 1 FIRS exceed the horizontal CSDRS at frequencies of about 20 to 75 hertz and 20 to 85 hertz, respectively. PGA at 100 hertz of the GMRS and Unit 1 FIRS is 0.21 g and ~~0.24~~0.22 g, respectively. As shown on Figure 3.7-202, the vertical GMRS and Unit 1 FIRS exceed the vertical CSDRS at frequencies between about 25 to 70 hertz.

Lee Nuclear Station

Summary of Changes to FIRS A1 Analysis and Associated FSAR Revisions

Attachment 5

Revised FSAR Table 2.0-201

COLA Part 2, FSAR, Chapter 2, Table 2.0-201, Sheet 2 of 7, entry for SSE, is revised as follows:

TABLE 2.0-201 (Sheet 2 of 7)
COMPARISON OF AP1000 DCD SITE PARAMETERS AND LEE NUCLEAR STATION UNITS 1 & 2 SITE CHARACTERISTICS

	AP 1000 DCD Site Parameters	WLS Site Characteristic	WLS FSAR Reference	WLS Within Site Parameter
Seismic				
SSE	SSE free field peak ground acceleration of 0.30 g with modified Regulatory Guide 1.60 response spectra. Seismic input is defined at finished grade, except for sites where the nuclear island is founded on hard rock. ^(d) The hard rock high frequency (HRHF) GMRS provides an alternative set of spectra for evaluation of site specific GMRS. A site is acceptable if its site-specific GMRS fall within the AP1000 HRHF GMRS. ^(e)	GMRS PGA = 0.21g Unit 1 FIRS PGA = 0.240 .22g GMRS and Unit 1 FIRS are below the WEC hard rock high frequency spectrum at all points.	Subsection 2.5.2.6 Subsection 2.5.2.7 Subsection 3.7.1.1.1 Figure 3.7-201 Figure 3.7-202	Yes

Lee Nuclear Station

Summary of Changes to FIRS A1 Analysis and Associated FSAR Revisions

Attachment 6

Replacement FSAR Table 2.5.2-224

COLA Part 2, FSAR, Chapter 2, Table 2.5.2-224, is replaced as follows:

WLS COL 2.5-2

TABLE 2.5.2-224 (SHEET 1 OF 2)
FIRS AND UHRS FOR PROFILE A1

<u>Frequency</u>	<u>FIRS</u> <u>Horizontal</u>	<u>FIRS</u> <u>Vertical</u>	<u>UHRS(10⁻⁴)</u> <u>Horizontal</u>	<u>UHRS(10⁻⁴)</u> <u>Vertical</u>	<u>UHRS(10⁻⁵)</u> <u>Horizontal</u>	<u>UHRS(10⁻⁵)</u> <u>Vertical</u>	<u>UHRS(10⁻⁶)</u> <u>Horizontal</u>	<u>UHRS(10⁻⁶)</u> <u>Vertical</u>
<u>(Hz)</u>	<u>SA (G)</u>	<u>SA (G)</u>	<u>SA (G)</u>	<u>SA (G)</u>	<u>SA (G)</u>	<u>SA (G)</u>	<u>SA (G)</u>	<u>SA (G)</u>
100	0.224	0.168	0.110	0.086	0.497	0.374	1.439	1.192
90	0.256	0.193	0.123	0.097	0.570	0.428	1.664	1.385
80	0.298	0.224	0.141	0.111	0.663	0.497	1.956	1.637
70	0.355	0.265	0.163	0.129	0.788	0.590	2.350	1.978
60	0.433	0.323	0.193	0.154	0.962	0.718	2.905	2.462
50	0.548	0.407	0.236	0.190	1.217	0.905	3.733	3.190
45	0.569	0.424	0.240	0.193	1.264	0.942	3.859	3.274
40	0.593	0.443	0.244	0.195	1.318	0.985	4.005	3.372
35	0.622	0.466	0.248	0.198	1.383	1.036	4.176	3.486
30	0.616	0.467	0.252	0.201	1.369	1.037	4.088	3.423
25	0.598	0.460	0.257	0.205	1.329	1.023	3.912	3.298
20	0.534	0.410	0.241	0.191	1.186	0.909	3.424	2.852
15	0.461	0.353	0.222	0.175	1.024	0.781	2.883	2.365
12.5	0.420	0.321	0.211	0.165	0.933	0.710	2.586	2.100
10	0.375	0.286	0.198	0.154	0.833	0.631	2.263	1.816
9	0.352	0.267	0.190	0.147	0.778	0.588	2.097	1.671
8	0.329	0.248	0.182	0.139	0.721	0.542	1.926	1.523
7	0.304	0.228	0.173	0.131	0.662	0.495	1.748	1.371
6	0.277	0.207	0.163	0.122	0.599	0.446	1.564	1.214
5	0.249	0.184	0.153	0.113	0.533	0.394	1.370	1.052

WLS COL 2.5-2

TABLE 2.5.2-224 (SHEET 2 OF 2)
FIRS AND UHRS FOR PROFILE A1

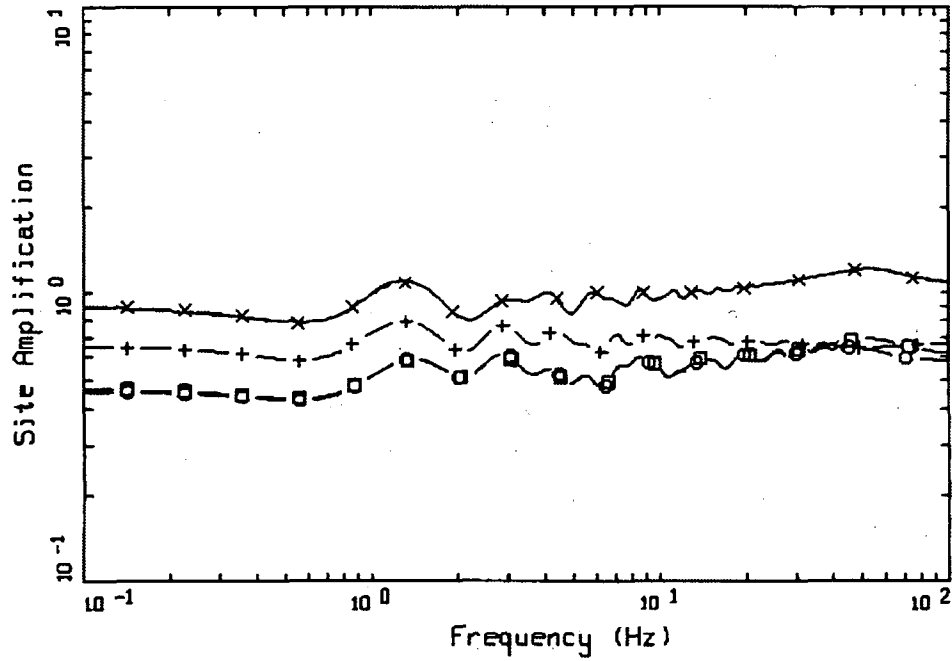
<u>Frequency</u> <u>(Hz)</u>	<u>FIRS</u> <u>Horizontal</u>	<u>FIRS</u> <u>Vertical</u>	<u>UHRS(10⁻⁴)</u> <u>Horizontal</u>	<u>UHRS(10⁻⁴)</u> <u>Vertical</u>	<u>UHRS(10⁻⁵)</u> <u>Horizontal</u>	<u>UHRS(10⁻⁵)</u> <u>Vertical</u>	<u>UHRS(10⁻⁶)</u> <u>Horizontal</u>	<u>UHRS(10⁻⁶)</u> <u>Vertical</u>
	<u>SA (G)</u>	<u>SA (G)</u>	<u>SA (G)</u>	<u>SA (G)</u>	<u>SA (G)</u>	<u>SA (G)</u>	<u>SA (G)</u>	<u>SA (G)</u>
<u>4</u>	<u>0.211</u>	<u>0.156</u>	<u>0.132</u>	<u>0.097</u>	<u>0.449</u>	<u>0.334</u>	<u>1.113</u>	<u>0.858</u>
<u>3</u>	<u>0.170</u>	<u>0.127</u>	<u>0.109</u>	<u>0.080</u>	<u>0.360</u>	<u>0.269</u>	<u>0.852</u>	<u>0.659</u>
<u>2.5</u>	<u>0.148</u>	<u>0.111</u>	<u>0.096</u>	<u>0.071</u>	<u>0.313</u>	<u>0.235</u>	<u>0.719</u>	<u>0.558</u>
<u>2</u>	<u>0.125</u>	<u>0.094</u>	<u>0.079</u>	<u>0.059</u>	<u>0.267</u>	<u>0.201</u>	<u>0.602</u>	<u>0.472</u>
<u>1.5</u>	<u>0.101</u>	<u>0.076</u>	<u>0.061</u>	<u>0.046</u>	<u>0.217</u>	<u>0.164</u>	<u>0.479</u>	<u>0.380</u>
<u>1.25</u>	<u>0.088</u>	<u>0.067</u>	<u>0.052</u>	<u>0.039</u>	<u>0.190</u>	<u>0.144</u>	<u>0.415</u>	<u>0.332</u>
<u>1</u>	<u>0.074</u>	<u>0.057</u>	<u>0.043</u>	<u>0.032</u>	<u>0.162</u>	<u>0.123</u>	<u>0.347</u>	<u>0.281</u>
<u>0.9</u>	<u>0.071</u>	<u>0.054</u>	<u>0.039</u>	<u>0.029</u>	<u>0.155</u>	<u>0.118</u>	<u>0.337</u>	<u>0.269</u>
<u>0.8</u>	<u>0.068</u>	<u>0.051</u>	<u>0.034</u>	<u>0.026</u>	<u>0.148</u>	<u>0.112</u>	<u>0.325</u>	<u>0.257</u>
<u>0.7</u>	<u>0.064</u>	<u>0.048</u>	<u>0.030</u>	<u>0.023</u>	<u>0.141</u>	<u>0.106</u>	<u>0.313</u>	<u>0.244</u>
<u>0.6</u>	<u>0.060</u>	<u>0.045</u>	<u>0.026</u>	<u>0.019</u>	<u>0.133</u>	<u>0.099</u>	<u>0.299</u>	<u>0.230</u>
<u>0.5</u>	<u>0.056</u>	<u>0.041</u>	<u>0.022</u>	<u>0.016</u>	<u>0.124</u>	<u>0.092</u>	<u>0.284</u>	<u>0.215</u>
<u>0.4</u>	<u>0.044</u>	<u>0.033</u>	<u>0.018</u>	<u>0.013</u>	<u>0.098</u>	<u>0.073</u>	<u>0.226</u>	<u>0.171</u>
<u>0.3</u>	<u>0.033</u>	<u>0.024</u>	<u>0.014</u>	<u>0.010</u>	<u>0.073</u>	<u>0.054</u>	<u>0.169</u>	<u>0.128</u>
<u>0.2</u>	<u>0.021</u>	<u>0.016</u>	<u>0.009</u>	<u>0.007</u>	<u>0.048</u>	<u>0.035</u>	<u>0.112</u>	<u>0.085</u>
<u>0.15</u>	<u>0.016</u>	<u>0.012</u>	<u>0.007</u>	<u>0.005</u>	<u>0.035</u>	<u>0.026</u>	<u>0.084</u>	<u>0.064</u>
<u>0.125</u>	<u>0.013</u>	<u>0.010</u>	<u>0.006</u>	<u>0.004</u>	<u>0.029</u>	<u>0.022</u>	<u>0.070</u>	<u>0.053</u>
<u>0.1</u>	<u>0.009</u>	<u>0.007</u>	<u>0.004</u>	<u>0.003</u>	<u>0.021</u>	<u>0.015</u>	<u>0.047</u>	<u>0.036</u>

Lee Nuclear Station

Summary of Changes to FIRS A1 Analysis and Associated FSAR Revisions

Attachment 7

**Revised FSAR Figures 2.5.2-240, 2.5.2-241, 2.5.2-244, 2.5.2-245, 2.5.2-246,
2.5.2-247, 3.7-201, and 3.7-202**



V/H RATIOS
UNIT 1 FIRS

LEGEND

- 50TH PERCENTILE, D = 80 KM, 0.01 g (D= 50 MI, 0.01g)
- 50TH PERCENTILE, D = 16 KM, 0.10 g (D= 10 MI, 0.10g)
- +— 50TH PERCENTILE, D = 7 KM, 0.20 g (D= 4 MI, 0.20g)
- x— 50TH PERCENTILE, D = 0 KM, 0.30 g (D= 0 MI, 0.30g)
- 50TH PERCENTILE, D = 0 KM, 0.50 g (D= 0 MI, 0.50g)

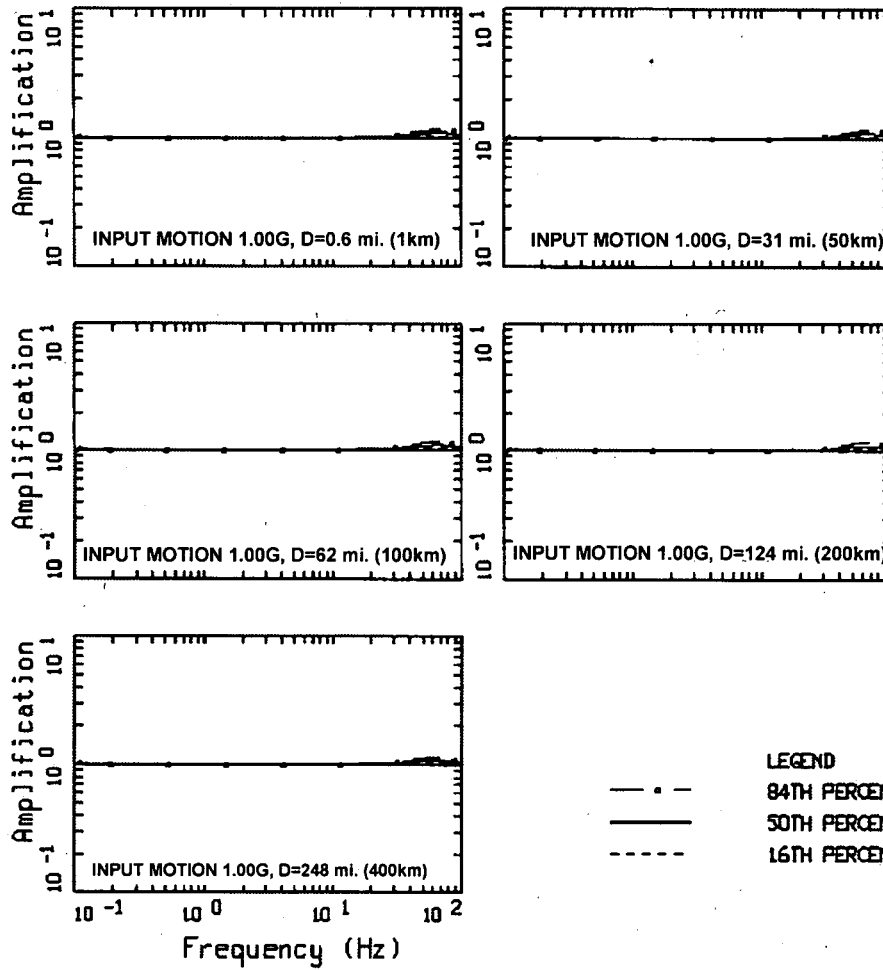
WLS COL 2.5-2

WILLIAM STATES LEE III
NUCLEAR STATION UNITS 1 & 2

Example of Median V/H Ratios Computed for
M 5.1, Single-Corner Source Model,
Unit 1 FIRS

FIGURE 2.5.2-240

Rev



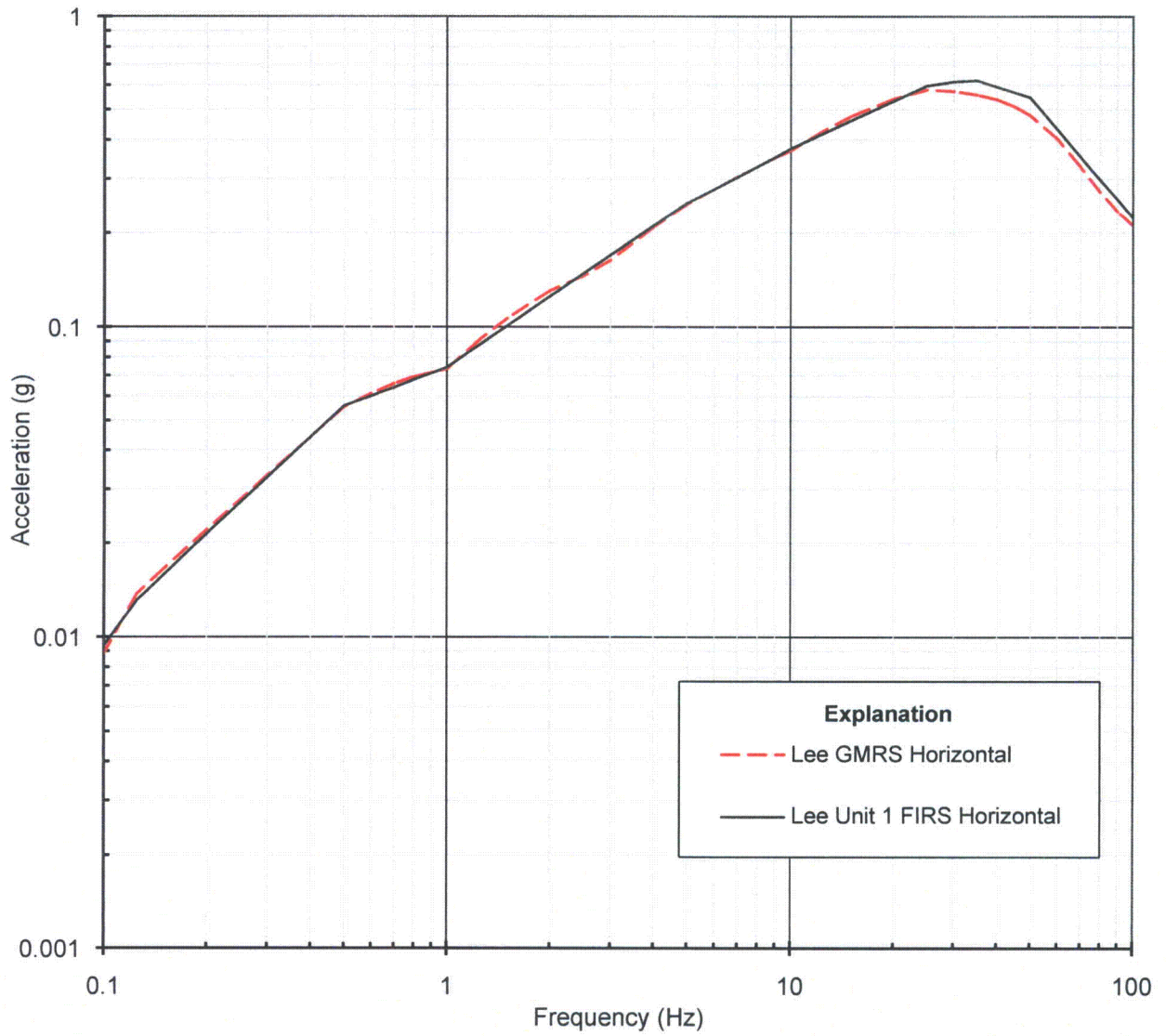
AMPLIFICATION (H), UNIT 1 FIRS

WLS COL 2.5-2

WILLIAM STATES LEE III
NUCLEAR STATION UNITS 1 & 2

Amplification Factors for M 5.1, Single-Corner
Source Model, Unit 1 FIRS Computed Using
Spectral Shapes as Control Motions

FIGURE 2.5.2-241 Rev



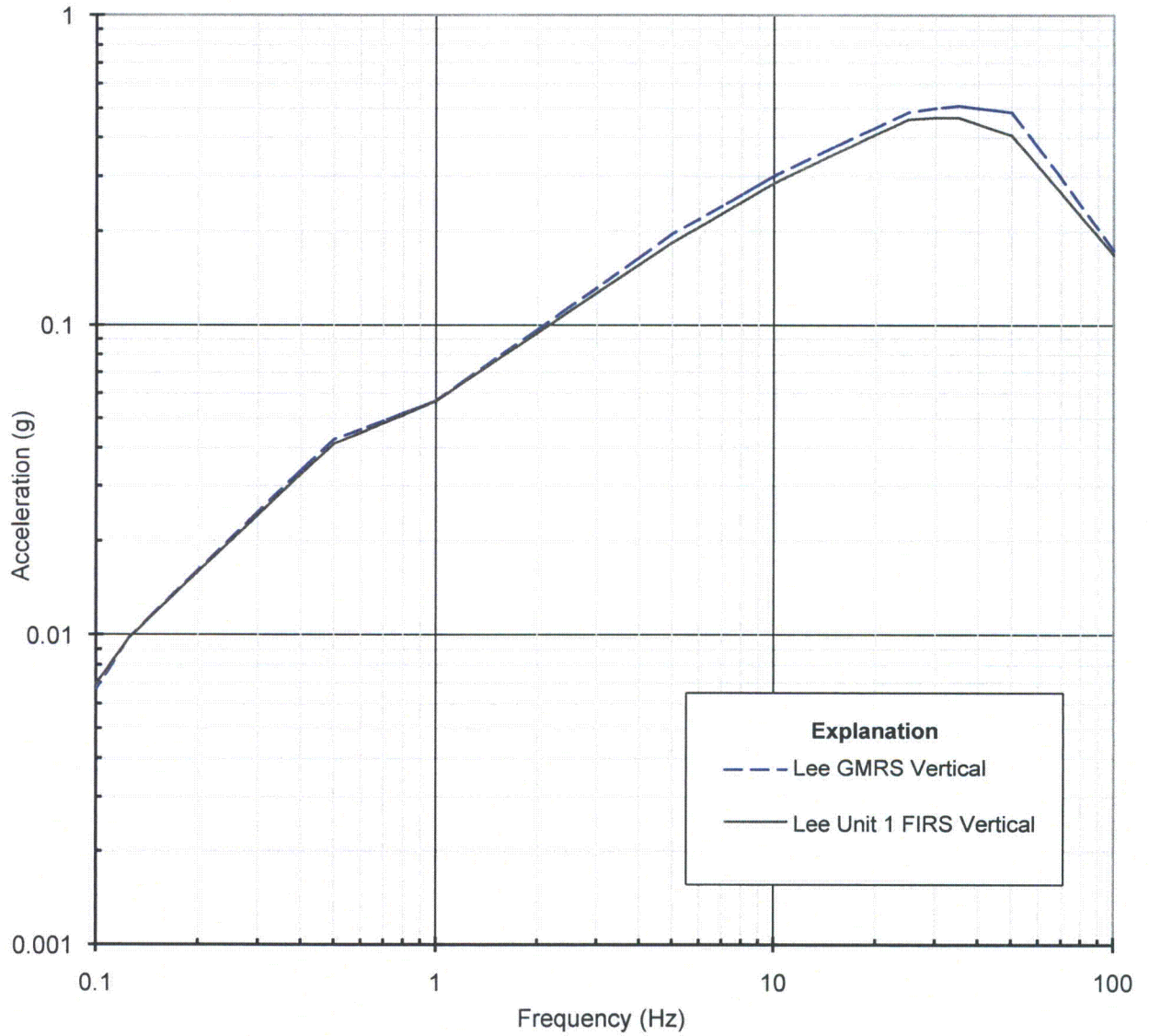
WLS COL 2.5-2

**WILLIAM STATES LEE III
NUCLEAR STATION UNITS 1 & 2**

Horizontal Component Unit 1 FIRS
Compared to the GMRS

FIGURE 2.5.2-244

Rev



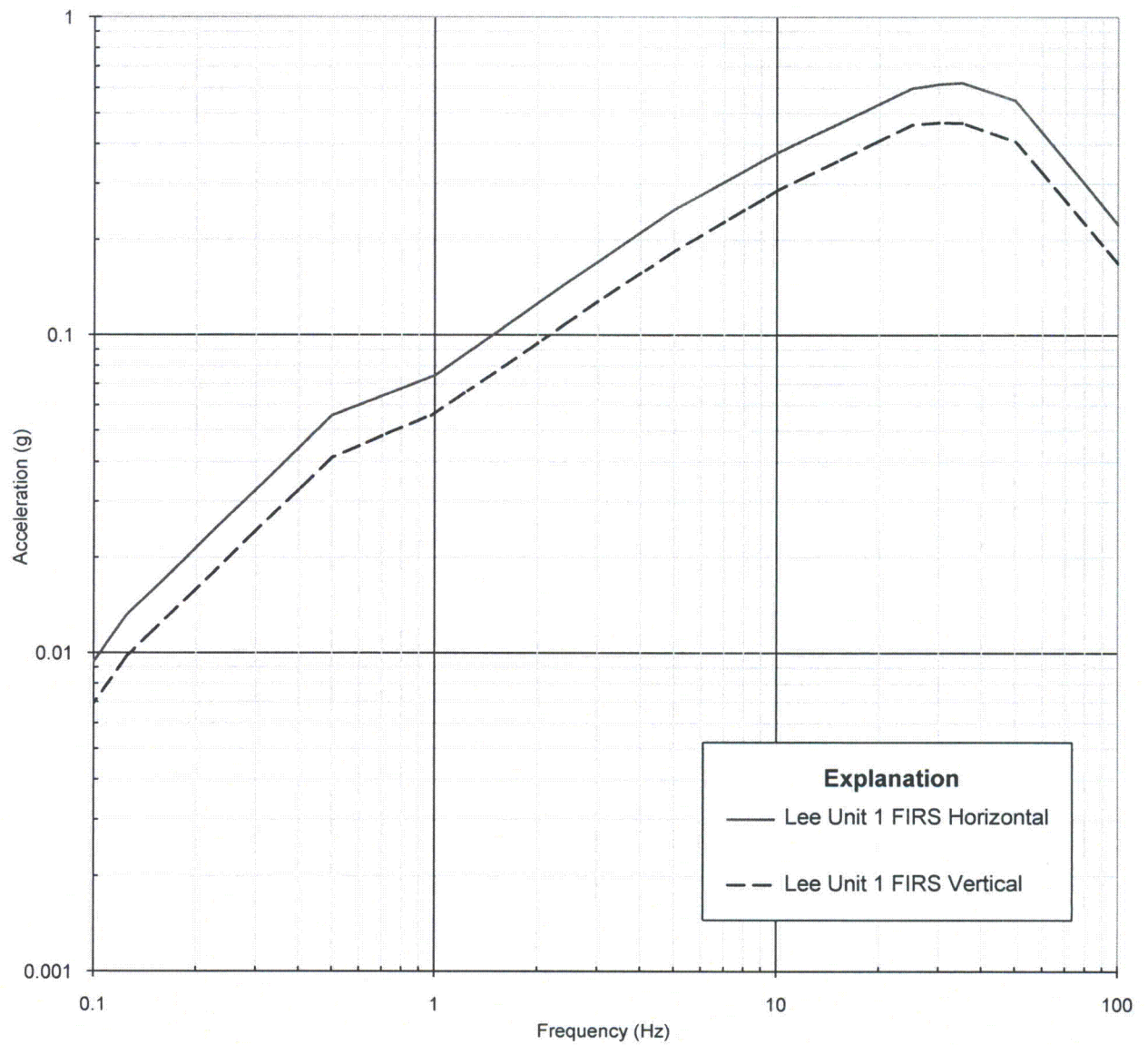
WLS COL 2.5-2

**WILLIAM STATES LEE III
NUCLEAR STATION UNITS 1 & 2**

Vertical Component Unit 1 FIRS
Compared to the GMRS

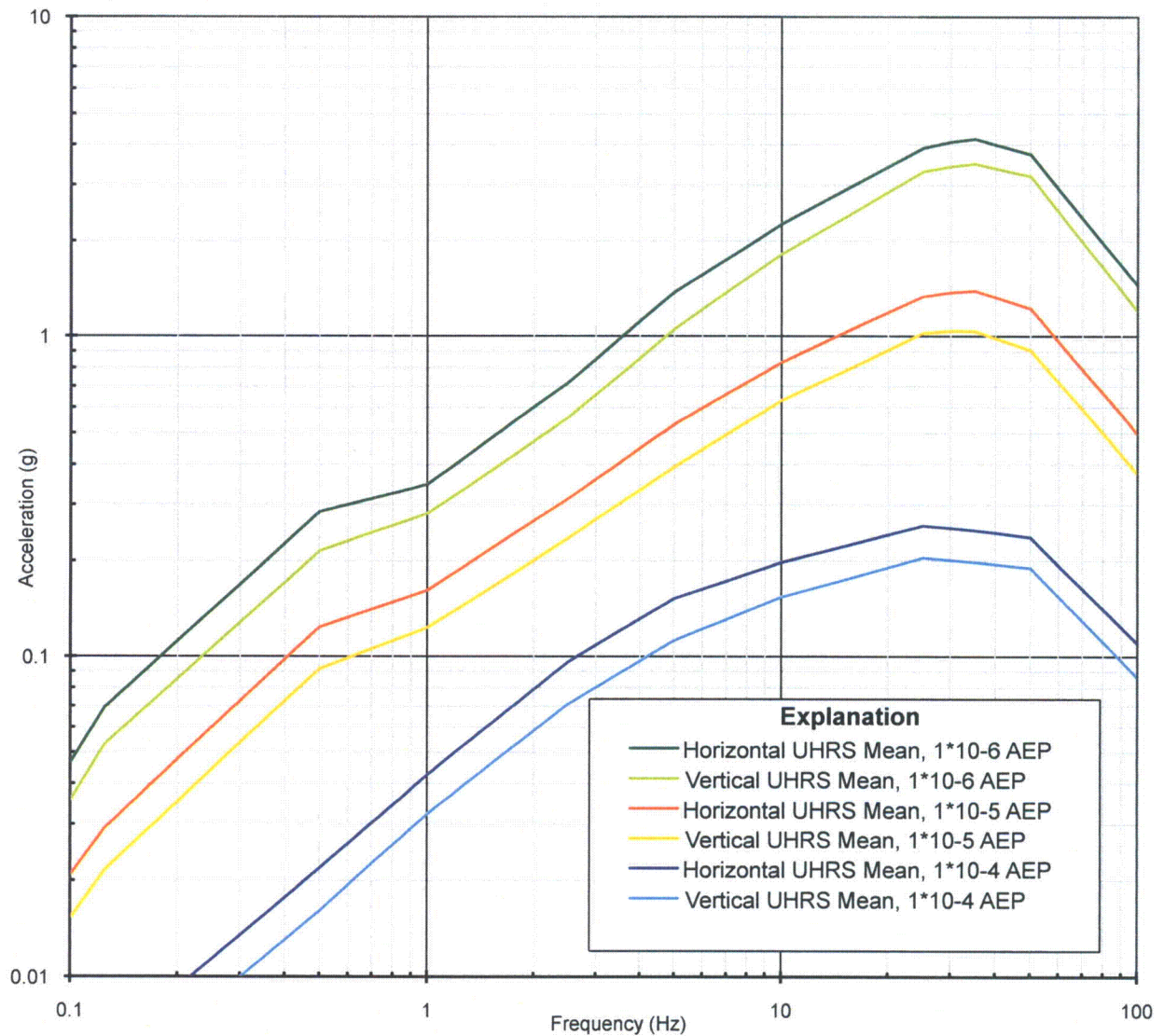
FIGURE 2.5.2-245

Rev



WLS COL 2.5-2

WILLIAM STATES LEE III NUCLEAR STATION UNITS 1 & 2
Comparison of Horizontal and Vertical FIRS A1
FIGURE 2.5.2-246 Rev

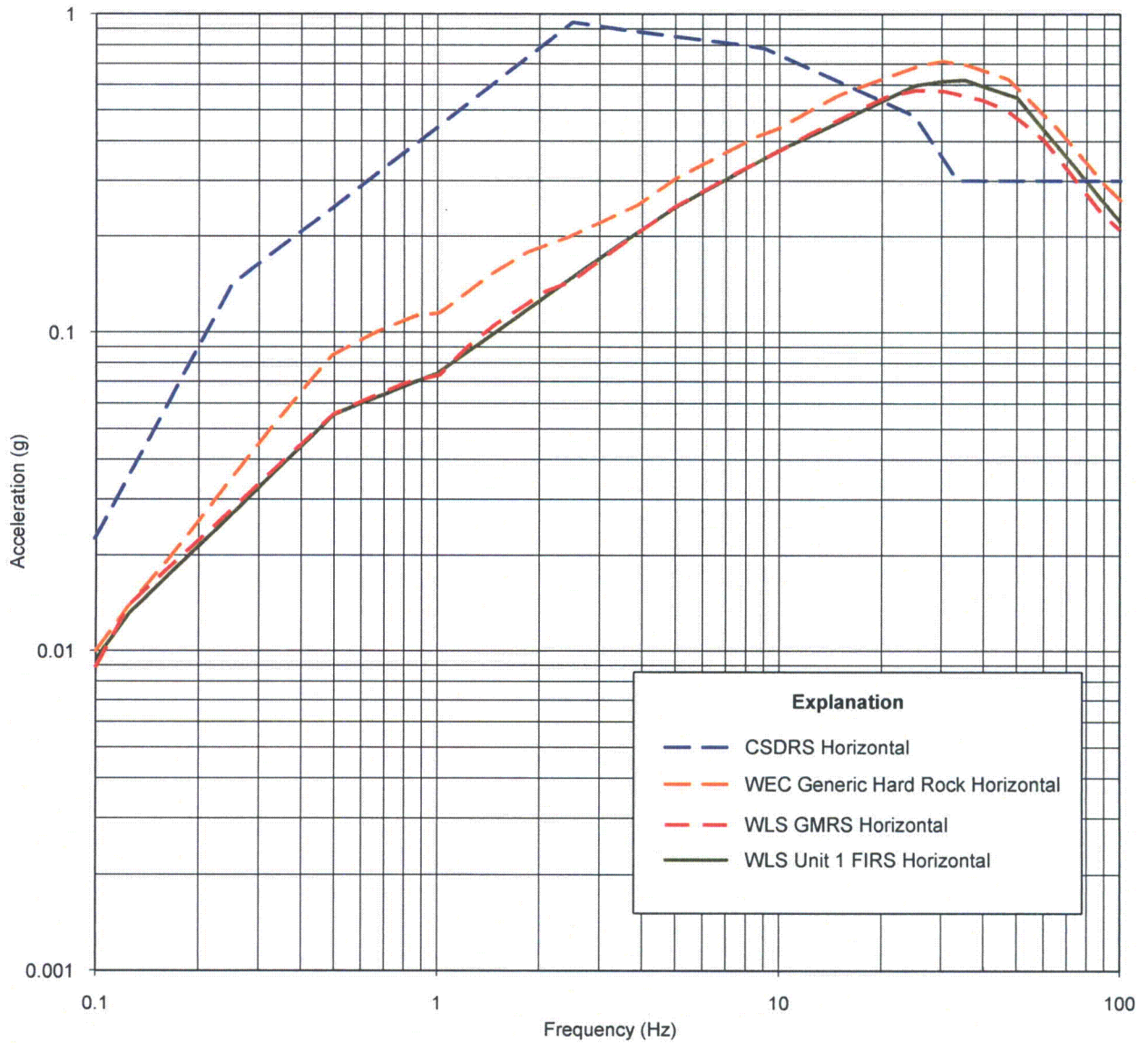


WLS COL 2.5-2

**WILLIAM STATES LEE III
 NUCLEAR STATION UNITS 1 & 2**

Unit 1 FIRS Horizontal and Vertical
 Component UHRS at Annual Exceedence
 Probabilities 10⁻⁴, 10⁻⁵, and 10⁻⁶ yr⁻¹

FIGURE 2.5.2-247 Rev

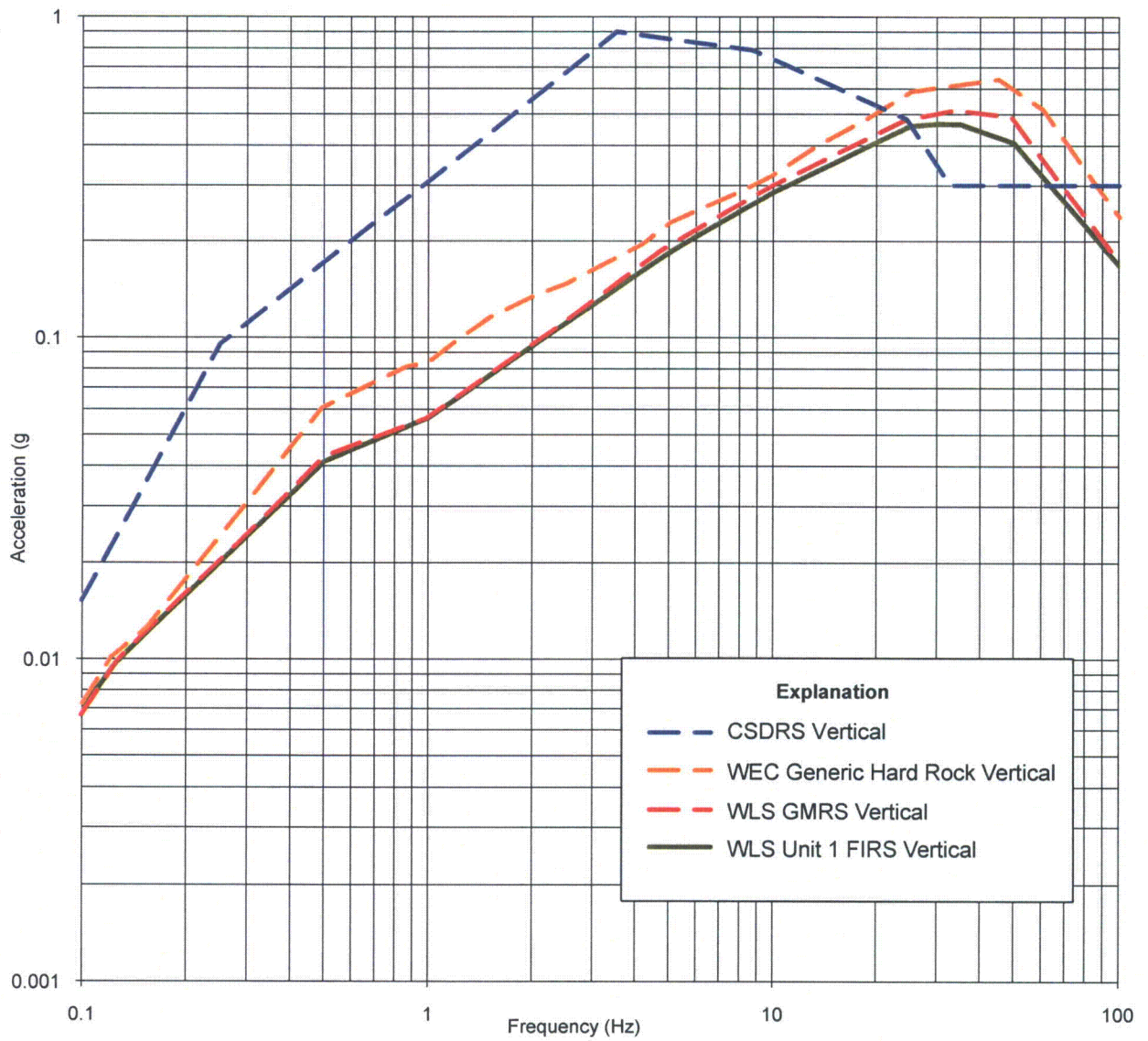


WLS SUP 3.7-3

WILLIAM STATES LEE III
NUCLEAR STATION UNITS 1 & 2

Design Ground Motion
Response Spectra - Horizontal

FIGURE 3.7-201 Rev



WLS SUP 3.7-3

WILLIAM STATES LEE III
NUCLEAR STATION UNITS 1 & 2

Design Ground Motion
Response Spectra - Vertical

FIGURE 3.7-202

Rev

Rev. 3

For

WILLIAM STATES LEE III NUCLEAR STATION

COMBINED CONSTRUCTION PERMIT AND OPERATING LICENSE COL PROJECT

DEVELOPMENT OF HORIZONTAL AND VERTICAL SITE-SPECIFIC HAZARD

CONSISTENT UNIFORM HAZARD RESPONSE SPECTRA AT

THE LEE NUCLEAR STATION UNIT 1

LEFT INTENTIONALLY BLANK

ACRONYMS

The definitions of acronyms used in this technical report are listed below.

1D - One Dimensional
AEF - Annual Exceedance Frequency
CCDF - complementary cumulative distribution function
CENA - Central and Eastern North America
COV - coefficient of variability
D - distance in kilometers or miles
EPRI - Electric Power Research Institute
FAS - Fourier Amplitude Spectra
FIRS - Foundation Input Response Spectra
fps - feet per second
FSAR - Final Safety Analysis Report
g - acceleration unit
GMPE - Ground Motion Prediction Equation
GMRS - Ground Motion Response Spectra
Hz - Hertz
km - kilometers
M - Moment Magnitude
P - compressional wave
PSD - Power Spectral Density
PSHA - Probabilistic Seismic Hazard Analysis
RMS - Root Mean Square
RVT - Random Vibration Theory
SDF - Single Degree of Freedom
SV - vertically polarized shear wave
UHRS - Uniform Hazard Response Spectra
V/H - Vertical-to-Horizontal Ratio
Vp - compressional wave velocity
Vs - shear wave velocity
WNA - Western North America
km/sec - kilometers per second
> - Greater than
< - Less than
≤ - Equal to or less than
≥ - Greater than or equal to
% - Percent

Table of Contents

Cover Sheet.....	1
Blank Page	2
Acronyms.....	3
Table of Contents.....	4
List of Tables.....	4
List of Figures.....	4
List of Appendices.....	5
REPORT OVERVIEW.....	6
1.0 INTRODUCTION.....	6
2.0 IMPLEMENTATION OF RANDOM VIBRATION THEORY (RVT) FOR SITE RESPONSE ANALYSES.....	7
2.1 RVT Durations.....	8
2.2 RVT-Based Equivalent-Linear Site-Response.....	9
3.0 APPROACHES TO DEVELOP SITE-SPECIFIC HAZARD.....	17
3.1 Description of Approaches.....	17
3.2 Approach 3 – Full Integration Method.....	19
3.3 Approach 3 – Approximate Method.....	20
3.4 Implementation of Approach 3.....	22
4.0 APPLICATION TO VERTICAL HAZARD.....	27
4.1 Hazard Deaggregation For The William States Lee III Nuclear Station.....	27
4.2 Development of V/H Ratios.....	28
4.3 Implementation of V/H Ratios In Developing Vertical Hazard.....	31
5.0 CONCLUSIONS.....	33
6.0 REFERENCES.....	34
7.0 TABLES AND FIGURES.....	38
8.0 Appendices.....	68

List of Tables

Cover Page.....	39
Table 1 Definitions of Locations for Motions in Site-Response Analyses.....	40
Table 2 Hard Rock Expected Horizontal Peak Acceleration Levels, Point Source Distances, and Durations.....	41
Table 3 Sample Size Required For Percent Error In The Standard Deviation For A Normal Distribution.....	42
Table 4 Moment Magnitude.....	43

List of Figures

Cover Page.....	44
Figure 1 Comparison of median RVT and SDF (computed from acceleration time histories) 5% damped response spectra.....	45
Figure 2 Lee Nuclear Station Unit 1 amplification factors (5% damping) at a suite of Source distances.....	46
Figure 3 Example of median and ± 1 sigma estimates of amplification factors computed for deep a soil site in the CENA.....	47
Figure 4 Test case illustrating the effect of magnitude on median amplification factors computed for a deep soil site in the CENA.....	49
Figure 5 Test case illustrating the effect of single-verses double-corner source spectra on median amplification factors computed for a deep soil site in the CENA.....	51
Figure 6 Test case illustrating the effect of magnitude on median amplification factors and sigma values (σ_n) computed for a deep soil site in the CENA.....	53
Figure 7 Test case illustrating the effect of single-verses double-corner source	

spectra on median amplification factors and sigma values (σ_n) computed for a deep soil site in the CENA.....	54
Figure 8 Median spectral acceleration (S_a) and sigma estimates computed for numbers of realizations from 15 to 240 using five different random seeds for a deep soil site in the CENA.....	55
Figure 9 Test case illustrating Approach 3 using a simple bilinear reference site hazard curve (dotted line, slope = 3, 6).....	56
Figure 10 Test case illustrating Approach 3 using a simple bilinear reference site hazard curve (dotted line, slope = 3, 6).....	57
Figure 11 Test case illustrating Approach 3 using a realistic (WNA) reference site hazard curve (solid line).....	58
Figure 12 Test case illustrating Approach 3 using a realistic (WNA) reference site hazard curve (solid line).....	59
Figure 13 Lee Nuclear Site hard rock horizontal hazard curve for peak acceleration (Duke Energy Carolinas, LLC, 2007).....	60
Figure 14 Lee Nuclear Station Unit 1 AEF 10^{-4} horizontal UHRS.....	61
Figure 15 Lee Nuclear Station Unit 1 AEF 10^{-5} horizontal UHRS.....	62
Figure 16 High-frequency (≥ 5 Hz) and low-frequency (≤ 2.5 Hz) hard rock hazard deaggregation for the Lee Nuclear Site (Duke Energy Carolinas, LLC, 2007).....	63
Figure 17 Site-specific median V/H ratios computed for the Lee Nuclear Station Unit 1 for M 5.1 at a suite of distances.....	64
Figure 18 Empirical WNA soft rock median V/H ratios.....	65
Figure 19 Site-specific median and ± 1 sigma V/H ratios computed for the Lee Nuclear Station Unit 1 for M 5.1 at a distances of 80 km.....	66
Figure 20 Horizontal and vertical component UHRS at annual exceedance probabilities 10^{-4} , 10^{-5} , 10^{-6} yr $^{-1}$	67

List of Appendices

- Appendix A – Modification of Herrmann's Duration Formula
- Appendix B – Criteria for Adjusting Kappa
- Appendix C – Limitations of Stochastic Point-source Modeling

REPORT OVERVIEW

This report presents and describes the detailed methodology used to develop horizontal and vertical hazard consistent site-specific uniform hazard response spectra (UHRS) at the Duke Energy William States Lee III Nuclear Station Unit 1. The information presented in this technical report provides a detailed presentation of analysis methodology, specifically addressing calculation approaches using random vibration theory (RVT), location-specific uniform hazard response spectra using Approach 3 (described in NUREG/CR-6728), and incorporation of site-specific aleatory and epistemic variabilities in dynamic material properties. This document supplements the analysis results presented in Subsection 2.5.2 of the Final Safety Analysis Report (FSAR).

The site-specific UHRS are computed as free-field motions at the ground surface, although other elevations or locations within a profile may be specified. In the case of the William States Lee III Unit 1, site-specific UHRS were calculated at the base of the Unit 1 nuclear island structure. As described in the FSAR Subsection 2.5.4, the William States Lee III Unit 1 foundation is supported on new and previously placed concrete materials positioned directly over continuous hard rock with shear wave velocity dominantly over 9,200 feet per second (fps). To address this configuration, location-specific UHRS were developed for the Unit 1 nuclear island. The UHRS analysis goal is to achieve site-specific response spectra which reflect the desired exceedance frequencies, or stated another way, preserve the reference site hazard level and result in full site-specific hazard curves for William States Lee III Unit 1. The analyses described in this report apply to the development of horizontal and vertical uniform hazard spectra for William States Lee III Unit 1.

1.0 INTRODUCTION

In developing site-specific response spectra, the usual approach involves, as a first step, a Probabilistic Seismic Hazard Analysis (PSHA) reflecting an outcropping reference site condition. The reference site condition is usually rock and, for central and eastern North America (CENA), reflects a theoretical shear-wave velocity over the top 1 km of the crust of 2.83 km/sec with a shallow crustal damping kappa value of 0.006 sec (EPRI, 1993). The shear-wave velocity is based on the empirical Mid-continent compressional-wave velocity model of Pakiser and Mooney (1989), taken by EPRI (1993) to represent the CENA, and an assumed Poisson ratio of 0.25. Since the 2.83 km/sec is but a single assigned rock shear-wave velocity, a realistic range of velocities and depths, as well as kappa values, could be developed to define a realistic range in hard rock site conditions for which hard rock attenuation relations and resulting hazard directly apply.

The kappa value, which controls high frequency motions, is empirical and based on examining motions recorded at hard rock sites (e.g. Silva and Darragh, 1995). Subsequent to the reference site condition PSHA, adjustments are made to the resulting reference site UHRS to compensate for any significant differences in dynamic material properties that may exist between the local site (Table 1) and the reference site. Table 1 describes the definitions of locations for motions in site-response analyses used in this technical report. In applying the adjustments, the goal or objective is to achieve site-specific response spectra which reflect the desired exceedance frequencies, that is, preserve the reference site annual exceedance frequency (AEF) thereby maintaining hazard consistency. The site-specific UHRS are usually computed as free-field motions at the ground surface, although other elevations or locations within a profile may be specified (Table 1).

* Site condition reflected in the attenuation relations used in the PSHA

The development of horizontal and vertical hazard consistent site-specific UHRS may be considered as involving two independent analyses. The first or initial computation is the development of relative amplification factors (5% damped response spectra) between the site of interest and the reference site ($S_a^{site}(f)/S_a^{reference}(f)$) that accommodates linear or nonlinear site response. Currently the state-of-practice approach involves vertically propagating shear-waves and approximations using equivalent-linear analysis using either a time domain method (e.g. SHAKE) or a more computationally efficient frequency domain random vibration theory (RVT) method.

Subsequent to the development of the amplification factors, site-specific motions are computed by scaling the reference site motions with the transfer functions. In the past, purely deterministic methods have been used but these generally result in site-specific motions that reflect higher probability than desired. More recently, semi-deterministic methods have been developed to conservatively achieve desired hazard levels, still using a fundamentally deterministic method (NUREG/CR-6728). Along with these semi-deterministic methods, fully probabilistic methods were also developed that accurately preserve the reference site hazard level and result in full site-specific hazard curves. The fully probabilistic approaches represent a viable and preferred mechanism to properly incorporate parametric aleatory and epistemic variabilities and achieve desired hazard levels and performance goals.

This report is intended to present an illustration of the two components used in the development of hazard consistent site-specific UHRS: RVT equivalent-linear site-response and fully probabilistic site-specific hazard analyses.

2.0 IMPLEMENTATION OF RANDOM VIBRATION THEORY (RVT) FOR SITE RESPONSE ANALYSES

RVT reflects a classical engineering method for estimating population mean peak time domain values based on a single root mean square (RMS) estimate of the response of a system, provided the system excitation reflects stationary random noise. The advantage of using the RVT formulation is that a large number of time domain analyses are not required to obtain stable estimates of mean response. The entire response analysis can be done in the frequency domain through the use of Parseval's relation (Boore, 1983). This relation is a direct correspondence between the Fourier amplitude spectra (FAS) or power spectral density (PSD) and the time domain root-mean-square (RMS) response for any system parameter (acceleration, particle velocity, shear-strain, factor of safety against liquefaction, etc.).

The combination of RVT and Parseval's relation then permits a single linear system analysis in the frequency (power spectral) domain resulting in an estimate of time domain response that reflects a mean response over the entire population of time histories whose FAS match that of the system demand or load function. In other words, for a linear system, one which admits a frequency domain analysis and spectral superposition is appropriate (no transfer of energy between frequencies), RVT results in a peak time domain response for the entire population of phase spectra which can be associated with the PSD of the load function. In principle the load function must reflect random noise whose statistics do not vary with time (remain stationary). In applications to strong ground motions, e.g. acceleration or velocity time histories, clearly this does not appear to be the case as typical records show changes in amplitude and perhaps frequency content with time. However the randomness constraint is, fortunately, a weak constraint and extensive testing (e.g. Boore, 1983; Boore and Joyner,

1984; EPRI 1993; Silva et al., 1997; Boore, 2003) has shown the application to strong ground motion in terms of response spectra, peak acceleration, peak particle velocity, and peak shear-strains to be quite robust.

For applications to site response and strong motion, RVT is generally used in two distinct places: 1) in estimating response spectra (oscillator time domain peak values) and peak particle velocities given a ground motion FAS and duration, and 2) estimating peak shear-strain time domain values given a shear-strain FAS and duration.

2.1 RVT Durations

For both applications, i.e. estimating spectral accelerations and peak particle velocities as well as peak shear-strains, durations are taken as the inverse of the source corner frequency (Boore, 1983) with a distance dependent term to accommodate the increase in duration due to wave scattering (modified from Herrmann, 1985 as discussed in Appendix A). For the Lee Nuclear Station Unit 1, Table 2 lists the point-source model parameters and durations used in developing site-specific V/H ratios (Section 4.2.1).

2.1.1 Peak-to-RMS Ratio

Several relations exist between the time domain RMS, estimated by integrating the PSD over frequency, and the corresponding peak time domain values (Boore, 1983; 2003). These relations reflect varying degrees of approximation in the peak-to-RMS ratio, increasing in complexity and accuracy as the number of extrema over the duration decreases. Boore (1983) illustrates a range in RVT ground motion parameter estimates computed using different approximations. The maximum range is about 10% for the extreme case of only 2 extrema ($M = 3.0$; Boore, 1983) over the source duration. Based on extensive comparisons of response spectra computed from time histories (referred to as single degree of freedom (SDF) spectra) with RVT estimates, Pacific Engineering typically implements an intermediate approximation. The intermediate approximation is an asymptote expression for the peak-to-RMS ratio (Equation 24; Boore, 1983) and was used in the Lee Nuclear Station Unit 1 analyses.

To integrate the PSD, numerical integration is performed rather than analytical integration, as the PSD includes site response in addition to the FAS of the simple point-source model. Because the PSD is reasonably smooth, a simple and rapid Simpson's three-point scheme is implemented but with a very dense sampling to fully accommodate the presence of peaks and troughs. Typically (e.g. Lee Nuclear Station Unit 1) 25,000 points are used from 0.007 Hz (about 150 sec) to 150 Hz. The wide integration range is to ensure inclusion of potential high- and low-frequency amplification. Additionally, the RMS is sensitive to the integration over low-frequency so it is prudent to extend its range to at-least an order of magnitude below the lowest frequency of interest, 0.1 Hz for nuclear applications (e.g. Lee Nuclear Station Unit 1). For application to other types of structures (e.g. long-span bridges, liquid natural gas facilities, etc) requiring estimates of motions to lower frequency, the integration range in FAS is extended from 0.0001 Hz to 150 Hz.

2.1.2 Computation of RVT Response-Spectra

A number of procedures (equations) exist for computing response spectra (peak time domain oscillator amplitude). These equations accommodate the increasing non-stationarity of oscillatory time histories as oscillator frequency decreases. Non-stationarity becomes critical as oscillator frequency becomes lower than the source corner frequency. Under these conditions, the oscillator duration exceeds the source duration, severely violating the weak assumption of stationarity. For these cases, various correction procedures have been developed for RVT that reflect a range in computed response spectra of about 10%. Boore (2003) gives an excellent illustration of two very different correction procedures showing their similarity for both small and large magnitude earthquake sources. For applications to transfer functions, horizontal amplification factors and vertical-to-horizontal (V/H) ratios, differences in response spectra due to different corrections at low-frequency are cancelled through taking ratios, as long as the corrections are applied consistently.

In typical Western North America (WNA) and CENA, source durations (inverse corner frequency) scale with moment magnitude (M) such that for M 5, 6, and 7, durations are approximately 1, 3, and 9 seconds respectively. As a result, corrections only become important for oscillator periods longer than 1, 3, or 9 seconds, depending on the magnitude used in generating the transfer functions.

Figure 1 shows an example comparison using 30 time histories from a finite fault simulation reflecting randomly selected model parameters (e.g. slip model, nucleation point, shear-wave velocity profiles etc.). Figure 1 compares median response spectra computed from time histories with RVT response spectra computed from the corresponding PSDs. In general, over the entire frequency range, the RVT spectrum agrees quite well with the SDF, reflecting a slightly smoother version. At low-frequency, the RVT spectrum is slightly above the SDF spectrum.

For the Lee Nuclear Station Unit 1, because the site response is linear and therefore magnitude independent and the maximum response is at high frequencies, the dominant source with M of 5.1 (based on deaggregations, Section 4.1) was used (Table 2). Since the maximum site response occurs at very high frequencies (> 50 Hz), RVT correction procedures are not an issue. An appreciation that the correction effects are not an issue, as their impacts are cancelled in the ratios, is seen in the Unit 1 amplification factors at low frequency (Figure 2). The amplification factors remain unity down to 0.1 Hz, nearly a factor of 10 lower than the source corner frequency for an M 5.1 source (Table 2). As is apparent from Figure 2, distances are not those listed in Table 2. The suite listed in Table 2 reflects the suite used for Lee Nuclear Station Unit 1 Foundation Input Response Spectra (FIRS) analyses, which included concrete fill over hard rock as well as computation of V/H ratios for Unit 1, both of which require a reasonably dense grid of reference site motions. The motivation for the distances used in Figure 2 is discussed in Section 3.4.2.3.

2.2 RVT-Based Equivalent-Linear Site-Response

The RVT site-response computational formulation that has been most widely employed to evaluate 1D site response assumes vertically-propagating plane shear-waves (S-waves). Departures of soil response from a linear constitutive relation are treated in an approximate manner through the use of the equivalent-linear formulation. The equivalent-linear formulation, in its present form, was introduced by Idriss and Seed (1968). A stepwise iterative analysis approach was formalized into a 1D, vertically propagating S-wave code

called SHAKE (Schnabel *et al.*, 1972). Subsequently, this code has become the most widely used and validated analysis package for 1D site response calculations.

Careful validation exercises between equivalent-linear and fully nonlinear formulations using recorded motions (peak horizontal acceleration) from 0.05 to 0.5g showed little difference in results for response spectral ordinates (EPRI, 1993). Both formulations compared favorably to recorded motions suggesting both the adequacies of the vertically-propagating S-wave model and the approximate equivalent-linear formulation. While the assumptions of vertically propagating S-waves and equivalent-linear soil response represent approximations to actual conditions, their combination has achieved demonstrated success in modeling observations of site effects and represent a stable, mature, and reliable means of estimating the effects of site conditions on strong ground motions (Schnabel *et al.*, 1972; EPRI, 1988; Schneider *et al.*, 1993; Silva *et al.*, 1997).

The vertically propagating shear-wave approach cannot successfully model amplitudes to arbitrarily long periods at deep soil sites at large source distances, as this formulation does not consider horizontally propagating surface waves. It is not clear, however, under what circumstances (profile depth, source size and distance, and structural frequency) the 1D vertically propagating shear-wave model would result in unconservative motions. Validation exercises consisting of modeling recorded motions using the 1D approximation at deep soil sites in tectonically active regions suggest the simple model performs well in terms of spectral amplitudes to periods of at least several seconds (EPRI, 1993; Silva *et al.*, 1997; Hartzell *et al.*, 1999), periods long enough to accommodate nuclear facilities.

A clear advantage of the equivalent-linear vertically propagating shear-wave model is its simplicity, resulting ease of implementation, and transparency. Due to its computational efficiency, the modeling approach is easily able to accommodate site-specific aleatory and epistemic variabilities in dynamic material properties in ground motions. This is accomplished by varying input parameters and computing the resulting motions. Unfortunately, to develop stable estimates of computed motions for each suite of parameters, multiple time histories (e.g. 5 to 15), each matched to the control motion response or Fourier amplitude spectra, must be analyzed. This is the case as peaks and troughs in response spectra as well as peak shear-strains are sensitive to the phase spectra of the control motion. For the traditional equivalent-linear formulation (e.g. SHAKE), since peak time domain shear-strains are used to iterate or soften the system (approximate nonlinear response), each time history results in somewhat different response, with the same dynamic material properties. The stacking (averaging) of responses necessary to achieve stability over multiple input time histories (all matched to the same control motion spectrum) renders the time domain (SHAKE) approach difficult to properly develop fully probabilistic response spectra.

As a practical alternative for the computation of site-response, the RVT based equivalent-linear approach (RASCALS) was developed (EPRI, 1988, 1993) and thoroughly validated (EPRI, 1993; Silva *et al.*, 1997). In this approach, which propagates an outcrop (control motion) power spectral density through a 1D soil column, RVT is used to predict peak time domain values of shear strain based upon the shear-strain power spectrum. The control motion power spectrum is propagated through the 1D rock/soil profile using the plane-wave propagators of Silva (1976). Using RVT to provide an estimate of peak time domain shear-strains results in estimates that reflect, in a single run, the mean over the entire population of control motion phase spectra, which is conditional on a single control motion power or Fourier amplitude spectrum (FAS). The computational efficiency of the RVT approach then easily

allows the large number of site response analyses required to develop fully probabilistic hazard consistent response spectra as it eliminates the need for multiple time histories. For each suite of dynamic material properties, only a single site-response analysis is necessary, resulting in a mean system response over the population of phase spectra associated with the control motion PSD. Additionally, for amplification factors computed with any time domain site-response analysis procedure, the frequency-to-frequency and record-to-record variability in the computed soil response due to the time history propagation introduces additional variability. This additional variability reflects a double counting as frequency-to-frequency and record-to-record variability has already been accommodated in the aleatory variability in the attenuation relations used in developing the reference PSHA. Employment of an RVT approach, because the control motion reflects a smooth spectrum, properly neglects the frequency-to-frequency and record-to-record variability in response spectra computed from real or realistic time histories and avoids double counting of frequency-to-frequency and record-to-record variability in the computed site response.

In the RVT implementation for peak shear-strains, the simple asymptotic expression of Equation 24 in Boore (1983) is used (Section 2.2). Based on extensive validations, this simple approach adequately reflects peak shear-strains through the soil column resulting in close comparisons between SHAKE, nonlinear codes, and recorded motions (EPRI, 1993). Careful validation exercises in modeling motions recorded from 19 earthquakes at over 500 sites quantified the accuracy of the RVT equivalent-linear approach along with the use of a point-source model to characterize control motions (EPRI, 1993; Silva et al., 1997).

2.2.1 Amplification Factors

To generate amplification factors (site-specific soil S_a /reference S_a) which properly accommodate site-specific aleatory variability, a randomization process of dynamic material properties is typically implemented about a base-case profile (EPRI, 1993). In this process, layer thickness and shear-wave velocity are randomized based on a correlation model resulting from an analysis of variance on over 500 measured shear-wave velocity profiles (EPRI, 1993). In this model, velocities are represented by a distribution at a given depth coupled to a correlation with depth, to prevent unrealistic random velocity excursions above and below a given layer. The layer thickness model is also based on measured profiles and replicates the overall observed decrease in velocity fluctuations as depth increases. This realistic trend is accommodated through increasing layer thicknesses with increasing depth. The correlation and layering model prevents unconservative profile realizations with uncorrelated velocity fluctuations over depth resulting in increased effective overall damping due to wave scattering at impedance boundaries (scattering κ). This condition is exacerbated at high loading levels due to nonlinearity, concentrating shear strains in low velocity layers. As a check on this possibility it is important to compare the median response spectrum over multiple realizations with that from a single analysis with base-case properties, at low (linear) loading levels. If the median spectrum falls below that computed using the base-case dynamic material properties at high frequency by more than about 5%, a significant amount of scattering κ has been added in the velocity randomization, resulting in an overall larger κ value than desired and unconservative high-frequency motions at low loading levels. This should then be compensated by appropriately lowering the κ value in the control motions, another advantage of using a point-source model to generate control motions as it is not an unambiguous endeavor to adjust control motions developed from attenuation relations or spectral shapes (NUREG/CR-6728) for lower (or larger) κ values. For the point-source model, the process of adjusting κ , illustrating typical sizes of the reduction in κ and its impact on the median spectra is discussed in Appendix B.

In addition to velocity and layer thickness variations, depth to basement material is also commonly randomized to cover the anticipated range over the site. For large impedance contrasts at the base of the soil, this variability smoothes the fundamental column resonance which may not be stable over multiple earthquakes (Silva et al., 1986) suggesting some degree of smoothing may be appropriate.

It is also essential to consider aleatory variability in nonlinear dynamic material properties both laterally across the site as well as vertically (where the same base-case properties are employed over a depth range). This variability in modulus reduction and damping curves is accommodated by assuming a log-normal distribution at a strain value where the curves are changing rapidly, 0.03%, randomly sampling a distribution and applying this perturbation to the base-case curves. The perturbation is tapered approaching the ends of the curves to preserve the shape of the base-case curves. Empirical sigma values, based on laboratory test of materials of the same general type (e.g. gravely sands) such that the G/G_{max} and hysteretic damping curves would be applied over depth ranges which boring logs or laboratory index property tests indicate appropriate, are 0.15 (σ_{in}) and 0.30 (σ_{in}) for modulus reduction and hysteretic damping respectively.

The G/G_{max} and hysteretic damping curves are randomized independently. Intuitively one may expect a random excursion to a more linear modulus reduction curve would be accommodated with a higher probability of a damping curves reflecting less damping. However, such intuition may be more properly associated with mean curves rather than random excursions about mean properties. Additionally, extensive tests with negatively correlated curves showed very little difference in the variability of computed motions. This is easy to understand as hysteretic damping has a much less significant impact on computed motions than does modulus reduction. A given percentage change in G/G_{max} results in a much larger impact on computed motions than a similar percentage change in hysteretic damping. Shear-wave velocity affects both amplification as well as energy loss through wave damping while hysteretic damping affects only energy loss. The overwhelming sensitivity of equivalent-linear site response is in the modulus reduction curves (Silva, 1992).

2.2.2 Control Motions

Control motions* (PSD) may be generated by use of the single-corner (and double-corner for the CENA) point-source model reflecting the magnitude contribution to the hazard. With this approach motions are generated for reference site-conditions as well as local site-conditions by propagation from the source to the site (EPRI, 1993). Implicit in this approach is the validity of the point-source ground motion model in terms of spectral shape. Validations of the point-source model (EPRI, 1993; Silva et al., 1997; Boore, 2003) have shown the model produces realistic response spectra for a wide range in M , distance, and site-conditions. These validation exercises have demonstrated the appropriateness of the model to serve as control motions for site-response analyses and resulted in the use of the model in developing hard rock response spectral shapes and V/H ratios for the CENA (NUREG/CR-6728). A limitation of the model is its demonstrated overprediction of low-frequency response spectra at large M ($M \geq 7.0$) and at close distances (≤ 20 km) in the WNA (Silva et al., 1997). This observation led Atkinson and Silva (1997) to introduce a double-corner source model for large M WNA earthquakes. Another potential limitation of the point-source model is an

* Control Motion: Motion used as input to site response analyses. This can be reflected in time histories matched or scaled to a response spectrum or, in the case of RVT, a PSD.

underprediction of absolute spectral levels at intermediate frequency for large magnitude ($M \geq 6.5$) and distances greater than about 100 km (Silva et al., 1996). However, an intermediate frequency underprediction in an absolute sense does not reflect a serious limitation of the model in developing relative amplification factors. For such applications the model is used in a relative sense, generating both site-specific motions as well as reference site motions with the amplification computed as the spectral ratio. In this application, reference site distances are adjusted to produce a range in loading levels through a suite of reference site expected peak accelerations (Section 2.2.2.1). As a result, the model is implemented in a relative sense and, in this context, the critical issue for a control motion to provide realistic loading of the site-specific profile across structural frequency is an appropriate spectral shape which varies correctly with both magnitude as well as distance. To assess the appropriateness of the point-source model in terms of spectral shape, Appendix C shows a favorable comparison between spectral shapes computed with the recently developed empirical Next Generation Attenuation Models (NGA) (PEER, 2008), Ground Motion Prediction Equations (GMPEs), and those of the point-source model. In this comparison the point-source model produces rock site shapes in good agreement with the empirical shapes with varying magnitude as well as both close and large distance, indicating its appropriateness for use in developing amplification factors.

For the CENA, the appropriateness of the single- or double-corner source models remains an unresolved issue with most CENA attenuation relations based on the point-source model (EPRI, 2004). For reference site conditions consisting of hard rock in the CENA, the single- and double-corner source model spectral shapes presented in NUREG/CR-6728 may also be used as control motions. Uncertainty in single- versus double-corner models results in the recommendation of computation of amplification factors using both models and combining the resulting hazard curves with the same relative weights as used in developing the reference (e.g. hard rock) PSHA.

For applications to the WNA, rock control motions may be generated using empirical attenuation relations or spectral shapes presented in NUREG/CR-6728, after adjusting the surface outcrop motions to base-of-soil conditions (NUREG/CR-6728). Alternatively, the point-source single-corner frequency model may be used with M limited to about $M 7.0$ for deep soil sites to avoid overdriving the soil column at low-frequency (< 1 Hz). Alternatively or in conjunction, the WNA double-corner source model (Atkinson and Silva, 1997) may be used as control motions. Use of the point-source models reflects computational efficiency as it avoids the intermediate step of spectral matching to the empirical spectra, which are not well constrained for all M at distances exceeding about 100 km.

2.2.2.1 Effects of Spectral Shape

In the development of amplification factors, the shape of the control motion spectrum plays an important role due to nonlinearity in the site-response. The three factors which control spectral shape, apart from site effects include: magnitude (through the source corner frequency), single- versus double-corner source spectra, and distance (through depletion of high-frequency energy as distance increases) (Silva et al., 1997). In principle all three dependencies in control motion spectral shape should be accommodated in developing amplification factors. Accommodating these potential dependencies on control motion spectral shape would result in development of hundreds of mean amplification factors at a fine discrete grid of values for M , e.g. every 0.1 unit in M , and in distance, e.g. every 1 to 2 km in distance over the ranges of contributions to the reference hazard. For the CENA, separate suites of amplification factors computed for both single- and double-corner source models

would be required as well. However, the actual dependencies have been examined through sensitivity analyses, resulting in general guidelines in magnitude and distance dependencies that produce significant ($\geq 10\%$) differences in mean amplification factors.

For deterministic approaches in developing site-specific UHRS (Section 3.1, Approaches 1 and 2), typically only two magnitudes and associated distances are used reflecting the high-frequency (5 Hz to 10 Hz, 5 Hz and above) and low-frequency (1 Hz to 2.5 Hz, 2.5 Hz and below) contributions to the reference hazard (NUREG/CR-6728). However, for the fully probabilistic approach to developing site-specific UHRS (Section 3.1, Approach 3), a wide range in levels of reference site spectra is required as the entire reference (e.g. hard rock) hazard curve has contributions to each point (exceedance frequency) on the site-specific (e.g. soil) hazard curve. Typically the range in levels of reference site spectra is accommodated through a suite of expected reference site peak acceleration values, conditional on M , generated by varying source distances (Table 2). This approach then naturally accommodates any dependence on distance in the amplification factors due to the effects of distance on control motion spectral shape.

To illustrate effects of control motion loading level on amplification factors, Figure 3 shows median and ± 1 sigma estimates computed for a generic deep soil site in the CENA using a single-corner frequency M 7.0 point source model. Reference (hard rock, Table 2) expected peak accelerations range from 0.01g to 1.50g at 11 discrete values with distances ranging from about 300 km to 0 km (several km depth). As Figure 3 clearly shows, at frequencies exceeding about 2 Hz, amplification decreases as loading levels increase. Also apparent, at high frequency, is the increase in sigma with increasing loading levels. This is due to the inclusion of aleatory variability through the randomization of modulus reduction and hysteretic damping curves. As loading levels increase, nonlinearity becomes more important, appropriately reflecting a larger total aleatory variability. Also apparent in Figure 3 is the large deamplification at very high loading levels reaching a minimum for the median at about 30 Hz near 0.2. Based on empirical attenuation relations (e.g. Abrahamson and Shedlock, 1997), the minimum for observations available through 1997 is about 0.5. The minimum value shown in Figure 3 of about 0.2 may be a result of the equivalent-linear approximation, using a single value of shear-wave velocity and damping at all frequencies. As a result, a minimum amplification of 0.5 is implemented, based on observations.

To illustrate the effect of magnitude on amplification factors, Figure 4 shows median amplification factors computed for M 5, 6, and 7 for the same generic profile using single-corner-frequency point-source models. At low levels of motion, 0.01g to 0.10g, there is a strong M dependency at high-frequency (≥ 20 Hz). This is principally due to distance effects, depleting the larger M high-frequency control motion. This observation is due to the increased width of the oscillator transfer function as oscillator frequency increases. At the large distances for M 6 and M 7 (beyond 200 km and 300 km respectively), the Fourier amplitude spectrum is severely depleted. As a result, the high-frequency oscillators reach back to low-frequency for energy such that the amplification factors reflect lower frequency values. This is precisely the same phenomenon which causes response spectral acceleration to saturate to peak acceleration at high frequency. While these M dependencies due to distance are quite large at high-frequency, they become insignificant at frequencies of interest (≤ 30 Hz) for loading levels of concern (above 10%g). This observation also points out a possible limitation of the CENA spectral shapes in NUREG/CR-6728. For consistency with

* Median estimates

the empirical WNA shapes, the CENA shapes were defined only to a distance of 200 km. Use of these shapes for larger distances will likely result in too much high-frequency energy and unconservative amplification factors at low levels of motions and at high-frequency. For the case of the Lee Nuclear Station Unit 1, the similarity of the amplifications, median and sigma estimates, over the distance range of 1 km to 200 km (Figure 2) indicates this observation is not an issue. This is the case as the fundamental resonance for the Lee Nuclear Station Unit 1 is near 90 Hz (Section 3.4.2.3), well beyond the peak in the hard rock spectral shapes (NUREG/CR-6728). As a result, even at a distance of 1 km, the Fourier amplitude spectrum is depleted.

Of significance for the development of UHRS for nuclear facilities is the range in median amplification over the 1 Hz to 20 Hz range for M 5, 6, and 7 shown in Figure 4. In general, for loading levels up to about 0.75g, which covers the range of interest for AEF of 10^{-4} and 10^{-5} over most of the CENA, the range in amplification is about 20% for a unit change in magnitude. Based on sensitivity analyses such as these as well as the observation of Bazzurro and Cornell (2004) of an even weaker magnitude dependency, from analyses with recorded motions, a conservative guideline for accommodation of magnitude dependencies in the reference hazard deaggregation is about one half magnitude unit. That is, one should maintain the model magnitudes as a function of structural as well as exceedance frequency from the reference deaggregation to a precision of about one half magnitude unit. This approximation recognizes both the magnitude dependency of amplification factors as well as the range in magnitudes contributing to the reference hazard at a given structural and exceedance frequency. Use of the mode is clearly more appropriate than the mean, even though there is rarely a single peak over magnitude.

These results point out the inappropriateness of simply scaling control motions up and down to reflect either different magnitude sources or different distances, conditional on magnitude.

To illustrate the potential effects of source processes in the CENA in terms of single- versus double-corner source spectra, Figure 5 shows a comparison of median amplification factors computed for the same suite of expected horizontal hard rock (reference) peak acceleration values. As with the magnitude dependencies shown in the low loading levels in Figure 4, the differences between the amplification factors computed with the two source models at 0.01g are, in reality, due to differences in distances (317 km and 340 km for the single- and double-corner source models respectively). Of more relevance and significance are the differences in median amplification factors at higher loading levels ($\geq 0.20g$) in the 1 Hz to 20 Hz frequency range. In this frequency range, the differences steadily increase from about 5% to 10% at 0.2g to over 20% at 0.75g with the amplification factors computed with the two-corner model exceeding those computed with the single-corner source model. The converse is true below the fundamental column resonance near 0.2 Hz. These trends are a result of lower intermediate frequency source spectra for the double-corner source model compared to the single-corner model (NUREG/CR-6728). This results in lower loading levels, more linear response, for the double-corner source model, leading to larger intermediate frequency amplification and less of a shift the fundamental column resonance to lower frequency. It is important to point out this effect would be greater for larger magnitudes as well as less for smaller magnitudes, becoming insignificant for magnitude less than about 5.25. This can be appreciated by comparing response spectral shapes illustrated in NUREG/CR-6728 as the spectral sag of the double-corner source model largely disappears at M 5.0.

To provide a further illustration of the impacts of magnitude and source processes on median amplification factors as well as their associated aleatory variabilities, Figures 6 and 7 show results plotted versus reference (hard rock) response spectra for selected frequencies (100 Hz, 10 Hz, and 1.0 Hz). These plots display the factors and standard deviations in the manner of which they are implemented in the fully probabilistic approach to developing site-specific UHRS (Section 3.0). Figure 6 shows the effects of control motion magnitude on median amplification factors and their aleatory variabilities conditional on the reference spectral acceleration. The range in loading level (0.01g to 1.50g) is seen in the frame for 100 Hz (peak acceleration by definition). The corresponding ranges in 10 Hz and 1 Hz hard rock response spectra are displayed in the corresponding frames. Figure 6 illustrates the smooth nature of the factors and their aleatory variabilities as well as the clear magnitude and loading level dependencies. The overall smoothness of the amplification factors and standard deviations is significant as linear (log scale) interpolation is used to develop estimates between the discrete loading levels (e.g. Table 2).

As previously mentioned, the positive slope of the sigma values reflects the important impact of the aleatory variability in the randomization of the G/G_{max} and hysteretic damping curves. As loading level increases, nonlinear dynamic material properties exert more of an influence (become more important) on computed motions. As expected, peak acceleration has the lowest variability. Empirically, peak acceleration is the most stable and therefore most accurately known strong ground motion parameter (Abrahamson and Shedlock, 1997). The decrease in variability with increasing magnitude and increasing loading level is also expected. Larger magnitude sources are statistically stable (stationary) for longer durations and, as loading level increases, nonlinearity tends to buffer or reduce fluctuations or variability in response. At low levels of loading, doubling control motions may double soil peak acceleration while at high loading levels, due to nonlinearity, doubling control motions increases soil motions by a smaller degree.

Completing the illustration, Figure 7 shows a similar comparison between single- and double-corner source models for M 7.0. As with Figure 6, similar trends are shown for the double-corner source model, smooth variation of median amplification and aleatory variability with variations in loading levels.

Alternatively, in lieu of the point-source model, the spectral shapes (NUREG/CR-6728) may be used as hard (CENA, single- and double-corner) rock or soft (WNA) rock (adjusted for base-of-soil conditions, NUREG/CR-6728) control motions. For use in the RVT equivalent-linear analyses, an RVT spectral match is performed generating a FAS whose RVT response spectrum matches the target or appropriate NRC spectral shape (NUREG/CR-6728). As another alternative for control motions, the attenuation relations used in developing the reference PSHA may be used, provided the reference site condition is rock and for soft outcropping rock, the resulting rock spectra are adjusted for base-of-soil conditions (NUREG/CR-6728). With this approach, separate amplification factors should be developed using spectra computed for each attenuation relation as control motions to accommodate potential epistemic variability in site-response due to the differences in spectral shape among the attenuation relations. The resulting amplification factors should then be combined with the same relative weights as used in developing the reference PSHA. Additionally, for the CENA, amplification factors computed for the single- and double-corner source models should be combined with the same relative weights as used in developing the reference PSHA.

3.0 APPROACHES TO DEVELOP SITE-SPECIFIC HAZARD

In developing site-specific UHRS or hazard there are two goals which must be met to achieve desired risk levels:

- 1) Preserve the hazard level (AEF) of the reference site PSHA across structural frequency to achieve hazard consistency and,
- 2) Incorporate site-specific aleatory (randomness) and epistemic (uncertainty) variabilities of dynamic material properties in the hazard.

3.1 Description of Approaches

In general, there are four fairly distinct approaches intended to accomplish the stated goals. The approaches range from the simplest and least accurate (Approach 1), which scales the reference site UHRS on the basis of a site-response analysis using a broad-band control motion to the most complex and most accurate, a PSHA computed using attenuation relations, median estimates and standard deviations, developed for the specific-site (Approach 4).

Approach 1: This approach is fundamentally deterministic and involves, for a rock reference site, use of the outcrop UHRS to drive the site-specific column(s). By definition it assumes a rock outcrop UHRS has similar characteristics as rock beneath soil, not generally a valid assumption for soft rock (NUREG/CR-6728), and has no mechanism to conserve the outcrop AEF. For cases where the hazard is dominated by earthquakes with significantly different M at low (e.g. ≤ 1 Hz to 2.5 Hz) and high (e.g. ≥ 5 Hz to 10 Hz) structural frequencies, the outcrop UHRS may be quite broad, unlike any single earthquake, resulting in unconservative high-frequency motions (too nonlinear in site response). Even if only a single earthquake is the major contributor at all structural frequencies, variabilities incorporated in the hazard analysis may result in a broad spectrum, again unlike any single earthquake. For these reasons, this approach is discouraged and Approach 2, an alternative semi-deterministic method may be used.

Approach 2: This approach is also fundamentally deterministic and is intended to avoid the broad-band control motion of Approach 1. For a rock reference site, Approach 2 uses low- and high-frequency (and intermediate if necessary) deterministic spectra computed from the attenuation relations used in the PSHA, or suitable spectral shapes (NUREG/CR-6728) reflecting expected rock conditions beneath the local soils, scaled to the UHRS at the appropriate frequencies (e.g., RG 1.165). These scaled motions, computed for the modal deaggregation M and D are then used as control motions to develop multiple (typically 2 to 3) mean transfer functions based on randomized soil columns. If the control motions are developed from the attenuation relations used in the reference PSHA, the generic site condition they reflect must be appropriate for the rock beneath the local soils. Additionally, separate control motions should be developed for each attenuation relation to include the effects of spectral shape uncertainty (epistemic) on soil response. The resulting mean transfer functions would then be combined using the same relative weights as in the reference PSHA. The mean transfer functions are then enveloped with the resulting transfer function applied to the outcrop (rock or soil) UHRS. This method was termed Approach 2A in NUREG/CR-6728. The use of mean (rather than median) transfer functions followed by enveloping is an empirical procedure to conservatively maintain the outcrop exceedance probability (NUREG/CR-6728 and - 6769), as this fundamentally deterministic approach does not include the contributions to soil spectra from the entire range in rock or reference site

hazard (Bazzurro and Cornell, 2004). The motivation for this "empirical" procedure is discussed in Section 3.3 (Approach 3 – Approximate Method).

For cases where there may be a wide magnitude range contributing to the hazard at low- or high-frequency and/or the site has highly nonlinear dynamic material properties, low, medium, and high M control motion spectra may be developed at each frequency of interest. A weighted mean transfer function (e.g., with weight of 0.2, 0.6, 0.2 reflecting 5%, mean, 95% M contributions) is then developed at each structural frequency of interest. Following Approach 2A, the weighted mean transfer functions for each frequency of interest are then enveloped with the resultant applied to the outcrop UHRS. This more detailed analysis procedure was termed Approach 2B in NUREG/CR-6728.

Approach 3: This approach is a fully probabilistic analysis procedure, which moves the site response, in an approximate way, into the hazard integral. The approach is described by Bazzurro and Cornell (2004) and NUREG/CR-6769. In this approach, the hazard at the soil surface is computed by integrating the site-specific hazard curve at the bedrock level with the probability distribution of the amplification factors (Lee *et al.*, 1998; 1999). The site-specific amplification, relative to CENA rock (in the case of the Lee Nuclear Station Unit 1), is characterized by a suite of frequency-dependent amplification factors that can account for nonlinearity in soil response. Approach 3 involves approximations to the hazard integration using suites of transfer functions, which result in complete hazard curves at the ground surface, or any other location, for specific ground motion parameters (e.g., spectral accelerations) and a range of frequencies.

The basis for Approach 3 is a modification of the standard PSHA integration:

$$P[A_S > z] = \iiint P \left[AF > \frac{z}{a} \mid m, r, a \right] f_{M,R|A}(m, r; a) f_A(a) dm dr da \quad (1)$$

where A_S is the random ground motion amplitude on soil at a certain natural frequency, z is a specific level of A_S , m is earthquake magnitude, r is distance, a is an amplitude level of the random reference site (e.g. hard rock) ground motion, A , at the same frequency as A_S , $f_A(a)$ is derived from the rock hazard curve for this frequency (namely it is the absolute value of its derivative), and $f_{M,R|A}$ is the deaggregated hazard (i.e., the joint distribution of M and R , given that the rock amplitude is level a). AF is an amplification factor defined as:

$$AF = A_S/a \quad (2)$$

where AF is a random variable with a distribution that can be a function of m , r , and a . To accommodate epistemic uncertainties in site dynamic material properties, multiple suites of AF may be used and the resulting hazard curves combined with weights to properly reflect mean hazard and fractiles.

Soil response, in terms of site amplification ($S_a(\text{site})/S_a(\text{reference})$), is controlled primarily by the amplitude of rock motion and m , so Equation 1 can be approximated by:

$$P[A_S > z] = \iint P \left[AF > \frac{z}{a} \mid (m, a) \right] f_{M|A}(m; a) f_A(a) dm da \quad (3)$$

where r is dropped because it has an insignificant effect in most applications. To implement Equation 3, only the conditional magnitude distribution for relevant amplitudes of a is needed. $f_{M|A}(m; a)$ can be represented (with successively less accuracy) by a continuous function, with three discrete values or with a single point, (e.g., $m^1(a)$, the model magnitude given a). With the latter, Equation 3 can be simplified to:

$$P[A > z] = \int \int P[AF > \frac{z}{a} | a, m^1(a)] f_A(a) da \quad (4)$$

where, $f_{M|A}(m; a)$ has been replaced with m^1 derived from deaggregation. With this equation, one can integrate over the rock acceleration, a , to calculate $P[A_S > z]$ for a range of soil amplitudes, z .

It is important to note there are two ways to implement Approach 3: the full integration method described below, or by simply modifying the attenuation relation ground motion value during the hazard analysis with a suite of transfer functions (Cramer, 2003). Both implementations result in very similar site-specific hazards (Cramer, 2003) and both will tend to double count site aleatory variability, once in the suite of transfer function realizations and again in the aleatory variability about each median attenuation relation. The full integration method tends to lessen any potential impacts of the large total site aleatory variability (Bazzurro and Cornell, 2004). Approximate corrections for the site component of aleatory variability, may be made by implementing the approximate technique (Equation 7, Section 3.3) with $C = 0$, $AF = 1$, and a negative exponential, where a_{ip} = the soil amplitude and σ the component of variability that is removed. For the typical aleatory variability of the amplification factors ($\sigma_{ln} \approx 0.1-0.3$ e.g. Figures 5 and 6) and typical hazard curve slopes in the CENA ($\kappa \approx 2-3$, Figure 13), the reduction in motion is about 5% to 10%.

Approach 4: Approach 4 entails the development and use of site-specific attenuation relationships, median estimates, and aleatory variabilities, developed specifically for the site of interest which incorporate the site response characteristics of the site. The PSHA is performed using these site-specific relationships for the specified AEF. This approach is considered the most accurate as it is intended to accommodate the appropriate amounts of aleatory variability into site and region specific attenuation relations. Epistemic variability is appropriately captured through the use of multiple attenuation relations. Approach 3 is considered a fully probabilistic approximation to Approach 4.

3.2 Approach 3 – Full Integration Method

The site-specific hazard curve can be calculated using the discretized form of Equation 3 from Bazzurro and Cornell (2004).

$$G_z(z) = \sum_{all x_j} P\left[Y \geq \frac{z}{x_j} \mid x_j\right] p_X(x_j) = \sum_{all x_j} G_{Y|X}\left(\frac{z}{x_j} \mid x_j\right) p_X(x_j) \quad (5)$$

where $G_z(z)$ is the sought hazard curve for $S_a^s(f)$, that is, the annual probability of exceeding level z .

$$G_{Y|X}\left(\frac{z}{x}\right) = \hat{\Phi}\left(\frac{\ln\left[\frac{z}{x}\right] - \ln\left[\hat{m}_{Y|X}(x)\right]}{\sigma_{\ln Y|X}}\right) \quad (6)$$

where $G_{Y|X}$ is the complementary cumulative distribution function of (CCDF) $Y = AF(f)$, conditional on a rock amplitude x . This is simply the CCDF of the site amplification factors as a function of control motion (e.g. rock or reference site) loading level.

$\hat{\Phi} = 1 - \Phi$ - the widely tabulated complementary standard Gaussian cumulative distribution function.

$\hat{m}_{Y|X}$ - the conditional median of Y (the amplification factor).

$\sigma_{\ln Y|X}$ - the conditional standard deviation of the natural logarithm of Y (aleatory variability of the amplification factor).

$p_X(x_j)$ - the probability that the rock or reference site control motion level is equal to (or better, in the neighborhood of) x_j .

Equation 5 is the essence of Approach 3 and simply states that the soil hazard curve is computed as the product of the soil amplification (specifically its CCDF), conditional on a reference (rock) amplitude x , times the probability of obtaining that reference amplitude, summed over all reference amplitudes.

The soil amplifications, median and σ_{\ln} estimates are all that are required, and are generated by driving the soil column with a suite of reference site motions (Section 2.2). At each reference motion, multiple realizations of randomized dynamic material properties are developed followed by site response analyses to generate a suite, typically 30 to 100 (Section 3.4.1), of amplification factors. From that suite, a median and σ_{\ln} is computed, generally assuming a log-normal distribution.

The probability of obtaining a reference motion is the derivative of the reference (e.g. rock) hazard curve obtained from the PSHA. This is done numerically and is a stable process as the hazard curves are quite smooth. Equation 5 can quite easily be entered into an EXCEL spread sheet. Approach 3 is indeed, one simple equation.

3.3 Approach 3 – Approximate Method

An alternative solution to Equation 4 can also be calculated using Equation (7) from Bazzurro and Cornell (2004). This is a closed form approximation of the integration of the amplification factor over a range of rock amplitudes.

$$z_{rp} = a_{rp} \overline{AF}_{rp} \exp\left(\frac{\sigma_s^2}{2} \frac{\kappa}{1-C}\right) \quad (7)$$

where z_{rp} is soil amplitude z associated with return period r_p ; a_{rp} is the reference spectral acceleration a associated with return period r_p ; \overline{AF}_{rp} is the geometric mean (mean log) amplification factor for the reference (e.g. rock) motions with return period r_p ; κ is the log-log

slope of the reference hazard curve that is calculated at each point from the reference hazard curve and ranges from about 2 to 3 for CENA and possibly as large as 6 for WNA. C is the log-log slope (absolute value) of the amplification factor with respect to the reference motion that is calculated at each point from the amplification factors, AF and is a measure of the degree of soil nonlinearity. If $C = 0$, the response is linear and highly nonlinear for C approaching 1, where the approximation breaks down (Bazzurro and Cornell, 2004). As previously mentioned, C ranges from about 0.1 to about 0.8 (Bazzurro and Cornell, 2004). σ_s is the log standard deviation of the AF and is around 0.3 (σ_{ln}) or less (Figures 6 and 7). In other words, at a given AEF or point on the reference site hazard curve, the corresponding soil amplitude is given as the median soil amplification times the rock or reference site amplitude plus an exponential factor.

The exponential factor is necessary to maintain the reference AEF and accommodates both the aleatory variability as well as the degree of nonlinearity of the site amplification. The slope of the reference hazard curve is a weighting factor that includes the contributions to the soil amplitude for all reference hazard levels. Equation 7 clearly demonstrates the additional factors needed over median amplification to preserve the hazard level (AEF) of the reference motion. This Equation shows that in order to preserve the reference site (e.g. rock) hazard level, multiplying the reference motion by the median soil amplification requires an additional exponential term. This additional term includes the aleatory variability of the soil or amplification factor, the slope of the reference site hazard curve, as well as the slope of the amplification factors (e.g. with varying reference motion). This exponential factor accommodates the potential contributions to a given soil motion by the entire range in reference site motions due to soil nonlinearity. That is, a given soil motion may have the same value at low levels of reference loading (relatively linear response) and at high loading levels (relatively nonlinear response). To preserve the reference site exceedance frequency, all the contributions to a given soil motions over the entire range in reference loading levels must be included in the soil hazard. These contributions are not explicitly considered in the deterministic Approach 2 method. Additionally, the effects of aleatory variability in the soil amplification due to lateral variability in velocities and depth to basement as well as randomness in G/G_{max} and hysteretic damping curves are included in the exponential term. For a linear site, C is zero so it is easy to see the exponential term then accommodates the effects of profile variability in the soil hazard. The reference hazard curve slope (κ in Equation 7) is present to accommodate the impacts of the soil variability and nonlinear amplification over the entire reference site motion or hazard curve. In the case $C = 0$ and for a reference hazard slope near 1, the median amplification times the exponential term simply reflects the mean, for a lognormal distribution. This was the motivation for using mean, rather than median amplification factors in Approach 2. However, for more realistic reference site hazard curve slopes, use of the mean amplification alone will result in motions that are too low for the assumed AEF. The difference or underestimation increases as soil nonlinearity, characterized through C , becomes larger for a given aleatory variability in the amplification factors. This was the motivation for the "empirical" correction in Approach 2 of enveloping the low- and high-frequency transfer functions. The high-frequency transfer function will typically have lower high-frequency amplification than the low-frequency amplification factor as it reflects higher loading levels, resulting in a higher degree of nonlinearity, and a greater value of C . Use of mean amplification alone may then depart significantly from Equation 7 resulting in higher probability motions than would be consistent with the reference hazard level, depending on the value of C and the slope of the reference hazard curve. Using an

envelop of the low-frequency amplification, which typically does not reflect nearly as high loading levels at high-frequency, and the high-frequency amplification was an ad-hoc manner of conservatively achieving the desired AEF using deterministic analyses.

It is important to point out that a similar issue, though less significant, can occur at low-frequency. In this case the high-frequency amplification has larger low-frequency amplification than the low-frequency amplification. The envelope at low-frequency is then controlled by the high-frequency amplification, compensating for the neglect of the complete exponential in the low-frequency mean amplification (NUREG/CR-6728).

3.4 Implementation of Approach 3

Approach 3 is implemented using the full integration method which consists simply of coding Equation 5. The soil (or rock) amplification distributions relative to the reference site condition are developed by driving the site-specific column at a suite of distances generated on a grid of expected reference site peak accelerations (Table 2), to accommodate nonlinear soil response. At each distance, or reference site expected peak acceleration, random suites of dynamic material properties are generated resulting in a distribution of structural frequency dependent amplification factors ($S_a(\text{site})/S_a(\text{reference})$). For a given structural frequency (e.g. 1 Hz), this process results in median and sigma estimates, for each loading level, from which a CCDF is produced using standard asymptotic expressions, typically accurate to the fourth decimal place. For each loading level, reference S_a at 1 Hz, the amplification CCDF is then available to integrate over the entire reference 1 Hz hazard curve. This is precisely the motivation for the wide range in reference peak accelerations, 0.01g to 1.50g (Table 2), to cover the entire reference hazard curve for each structural frequency. For reference site motion outside the range, the closest values are used. To minimize any error in interpolation (log) for reference site motions between grid points (Table 2), a dense sampling of typically 11 values of expected reference site peak accelerations is used. The array of peak accelerations is sampled more densely over the range in values contributing most to the hazard, usually 0.2g to 0.5g. Since the amplification factors are smooth (e.g. Figures 6 and 7 and Bazzurro and Cornell, 2004; Silva et al., 1999), interpolation is not a significant issue and the 11 point grid listed in Table 2 is adequate to capture site nonlinearity.

To compute the probability of reference motions ($P(x)$ in Equation 5), the reference motion hazard curve is numerically differentiated using central differences. Although hazard curves are smooth so differencing is a stable process, the curves are interpolated to 100 points to maximize the integration accuracy of Equation 5. The use of 100 points was established by increasing the number of points until stability (no change in derived soil hazard) was achieved to an AEF of about 10^{-10} . Using this approach, stability usually occurred at about 50 points so 100 points has been adopted as a conservative value for integration.

It is important to point out that because multiple levels of reference motions contribute to the soil or site-specific hazard, a wider range in reference hazard than soil hazard is necessary to achieve accuracy in the soil hazard. Extensive tests have shown that a conservative range over which to integrate the reference hazard is a factor of 10 in AEF beyond that desired for the soil or site-specific AEF. In other words, if site-specific hazard is desired to 10^{-6} AEF, reference hazard is required to an AEF of 10^{-7} . Additionally, the same consideration applies at high exceedance frequencies as well. In this case, if site-specific hazard is desired at 10^{-2} AEF, reference hazard is conservatively required to an AEF of 10^{-1} .

Approach 3 is also appropriate for computing site-specific vertical hazard from horizontal site-specific hazard curves, producing vertical UHRS at the same AEF as the horizontal UHRS. Resulting horizontal and vertical GMRS and FIRS then both achieve the same target performance goals. As with the horizontal site-specific hazard, regarding the range in the reference site hazard, accuracy in the vertical hazard requires a wide integration range over the site-specific horizontal hazard. As a result, to achieve an AEF of 10^{-6} for the vertical site-specific hazard requires the reference site hazard to an AEF of 10^{-8} .

3.4.1 Optimum Number of Realizations

Ideally the objective of the randomization process is to develop statistically stable estimates of median values and standard deviations with as few analyses as possible. Bazzuro and Cornell (2004) suggest that as few as 10 realizations are sufficient for application of Approach 3. As Table 3 suggests, simple statistics indicates stability is a slowly varying function of sample size, particularly for standard deviations. For a tolerance of the statistical sample being within 20% of the population standard deviation at the 90% confidence level, the number of samples is 30 and naturally less for median estimates. Because σ_{in} is less than 1, typically around 0.1 to 0.4, and it enters as σ_{in}^2 (e.g. Equation 7), its impacts are generally not large. As Table 3 indicates, improving the accuracy in the aleatory variability to 10% requires a four-fold increase in sample size to 130 realizations at the 90% confidence level. These trends are reflected in Figure 8, which shows the range in median and sigma estimates computed for various sample sizes with five different random seeds. In general, neither median nor sigma estimates are truly stable for fewer than about 200 realizations. Such observations led to 300 realizations to achieve less than a 10% error in sigma estimates in NUREG/CR-6728. In that research exercise, high accuracy was desired as comparisons were made between Approaches 2, 3, and 4. Achievement of similar accuracy in development of hazard consistent UHRS is simply not warranted in view of the impact on computed transfer functions. As both the simple statistics and Figure 8 show, doubling the number of realizations from 30 to 60 does not generally result in a significant improvement in accuracy. Increasing the number of samples beyond 100, as Figure 8 illustrates, is required to achieve highly stable results.

However, it is really the desired accuracy in the computed hazard which should inform the number of samples required. Based on Equation 7 (Section 3.3), for a given percent accuracy in amplitude, the required accuracy in the standard deviation depends on the slope of the reference hazard curve as well as the degree of nonlinearity through the slope of the amplification factors C . For the Lee Nuclear Station Unit 1 profile, since it is linear, C becomes zero and from Figure 13, the slope of the reference (hard rock) hazard curve is a bit less than 2, and the σ_{in} is about 0.1. In this case, the exponential term containing σ_{in} in Equation 7 has a value of about 1.01. A 100% increase in σ_{in} results in a value of about 1.04, or a 3% change. At the 90% confidence level, fewer than 5 realizations are required (30 were run for the Lee Nuclear Station Unit 1 analyses), increasing to fewer than 13 at the 99% confidence level and of course fewer still for estimates of the mean. Conversely, for a σ_{in} near 0.5, a steep hazard curve slope near 4, and over a highly nonlinear loading level (e.g. over 1g at 10 Hz in Figure 6) with C near 0.5, the exponential term is about 2.7. In this case a 10% increase in σ_{in} results in an exponential value of about 3.4, or about a 20% increase in amplitude, which is significant. For cases such as these, to achieve a 10% accuracy in amplitude requires better than a 5% accuracy in σ_{in} . From Table 3 the number of samples increases from fewer than 5 to 550 at the 90% confidence level to over 1,000 at the 99% confidence level. Clearly, for application of fully probabilistic approaches to developing site-

specific hazard, the number of realizations should be case specific and determined with preliminary analyses. For the deterministic approach, since the mean is given by the median times an exponential of σ_{in}^2 divided by 2, to achieve a 10% accuracy in the mean requires only about a 30% accuracy in σ_{in} , or about 15 realizations at the 90% confidence limit, 35 samples at the 99% confidence limit.

3.4.2 Example Illustrations

A straightforward way to illustrate the fully probabilistic Approach 3 is through comparisons with the Approximate method (Equation 7) as well as a fully deterministic method using a median amplification. As previously discussed, the approximation renders the full integration quite transparent and it is easy to illustrate the impacts of median amplification, slope of the reference site hazard curve, and amplification variability (σ_{in}) with simple cases.

3.4.2.1 Illustration Using a Horizontal or Vertical Mock Reference Hazard Curve

To clearly demonstrate Approach 3, the results of the simplest case of a linear (i.e. $C = 0$ in Equation 7) reference hazard curve and a linear median amplification or V/H ratio of 2.0 is considered in Figure 9. The aleatory variability of the amplification is taken as 0.2 (σ_{in}) and the slope of the reference hazard curve is 3 (log-log) initially then increased to an extreme value of 6. Figure 9 compares three derived hazard curves obtained using: Approach 3 full integration (Equation 5), Approach 3 Approximate (Equation 7), and simply median amplification or V/H ratio (2.0) times the reference hazard. For horizontal components, this latter (deterministic) curve effectively reflects Approach 2, which would use the mean amplification. However for this example, the mean is only 2% larger than the median. In general, it is clear that for a slope near 3, there is little difference between the deterministic and fully probabilistic results. The Approach 3, full integration method, results in the largest motions for a given AEF with the results using the approximate fully probabilistic method very slightly lower. For the steeper slope, it is easy to see from Equation 7 the expected impacts of Approach 3. The exponential term in Equation 7 becomes larger for the steeper (by a factor of 2) slope, resulting in the difference between the median deterministic amplification and fully probabilistic Approach 3 becoming significant, approaching 15 to 20%.

Increasing the amplification variability to 0.4 (σ_{in}) (Figure 10), now shows a substantial difference between deterministic and fully probabilistic results: a difference near 25% for a slope of 3 and nearly 70% for an extreme case with a slope of 6. Use of the mean amplification would only increase the corresponding soil hazard curve by about 8%, leaving it a full 15% below the fully probabilistic Approach 3, illustrating the recommendation in NUREG/CR-6728 for enveloping high- and low-frequency mean amplification factors as an empirical means of conservatively maintaining the desired hazard level.

This simple example also serves to illustrate the inherent stability of the Approach 3 full integration method. In both Figures 9 and 10, near the discontinuity in slope of the reference site hazard curve (going from a slope of 3 to a slope of 6), the derivative of the reference hazard curve is undefined (very large), causing the observed bulge in the hazard curve computed using the approximate Approach 3 method. The full integration method simply integrates through the singularity, resulting in a gradual change in slope of the resulting soil hazard curve. Because real hazard curves can not have such discontinuities, this extreme case illustrates the appropriateness of the numerical differentiation (e.g. density of points in the hazard reference site hazard curve) as well as the numerical integration scheme employed.

Also apparent in Figures 9 and 10 is the breakdown of the Approach 3 full integration method near the limits of the reference site (input) hazard curve. At low AEF (10^{-10}), the reference hazard curve extends to 10^{-11} AEF so the Approach 3 full integration hazard is correct to an AEF of 10^{-10} , as is evident in Figures 9 and 10. However, at high exceedance frequency, the reference site hazard curve extends to an AEF of 10^{-1} . Near this AEF, the Approach 3 full integration hazard shows a decreasing slope and convergence to the reference site hazard. The full integration method simply reflects decreasing contributions to the integral (sum, Equation 5) as the limit of the reference site hazard curve is approached.

3.4.2.2 Illustration Using a Horizontal or Vertical Realistic Reference Hazard Curve

While the previous simplified example case gave a clear illustration of using the full integration and approximate Approach 3 through examining the differences between deterministic and fully probabilistic approaches to developing UHRS, further insights can be provided by a more realistic case. For this example, a real WNA reference site hazard curve for peak acceleration was used and serves to illustrate the impact of increasing slope of the reference site hazard curve on developing fully probabilistic site-specific motions. As can be seen in Figure 11, the reference site hazard curve has a slope which increases significantly with decreasing AEF. As with the previous example, median amplification or V/H ratio is set at 2.0 and is taken as linear (again $C = 0$ in Equation 7). Figure 11 illustrates the effect of increasing slope of the reference site hazard curve as the AEF decreases for a range in amplification aleatory variability ($\sigma_{in} = 0.1$ to 0.4). From Figure 11 it is easy to appreciate the impacts of the exponential term in Equation 7, the increase in motion for a fully probabilistic analysis compared to a deterministic approach, as both the slope and σ_{in} increase. For a typical σ_{in} in the range of 0.3, accommodating aleatory variability in velocities, depth to basement, and modulus reduction and hysteretic damping curves across a site, the difference between the median deterministic soil hazard curve and the fully probabilistic hazard curve is about 25% near the AEF of 10^{-4} . Recall that this example, as well as the last one, assumes linear response in order to provide a more transparent illustration. Consequently the exponential term in Equation 7 is a minimum, resulting in a minimum difference between deterministic and fully probabilistic methods.

Figure 12 illustrates the comparison between deterministic and fully probabilistic analysis results including the approximate Approach 3 method. A typical σ_{in} value of 0.3 is considered and the results illustrated in Figure 12 shows good agreement between the full integration and approximate methods to an AEF of about 2×10^{-5} . Below this exceedance frequency the approximate method breaks down in this example as the exponential term is becoming too large (Bazzurro and Cornell, 2004).

This example also provides a check on the implementation of the full integration method in terms of differencing the reference site hazard curve (density of points) as well as the numerical integration procedure (Simpson's Rule). The full integration method agrees quite well with the approximate result over AEF where it is expected to do so. At high probability, the reference site hazard curve slope is quite small so the deterministic and fully probabilistic approaches should agree (see Equation 7).

3.4.2.3 Illustration for The Lee Nuclear Station Unit 1 Horizontal UHRS

The Lee Nuclear Station Unit 1 has approximately 20 ft of concrete ($V_s = 7,500$ ft/sec) overlying CENA generic rock ($V_s \approx 9,300$ ft/sec). In developing the amplification factors for

Unit 1, the thickness in the concrete was varied $20 \text{ ft} \pm 3 \text{ ft}$ and velocities were randomly varied using a typical concrete coefficient of variability (COV) of 0.1. Due to the profile stiffness, a linear analysis was used in developing the amplification factors (Figure 2). Also, due to the linear analysis, the typical dense grid of expected reference site peak accelerations (Table 2) was not needed. Instead, to examine any potential impacts of spectral shape on 5% damped response spectra and thereby amplification factors due to crustal damping at large distances ($> 100 \text{ km}$), a coarse distance grid spanning 1 km to 400 km was used (Figure 2). While the expected amplification due to the concrete fill is well above 50 Hz (resonance near 90 Hz), some amplification may propagate to frequencies of potential structural concern, below 50 Hz. This may be due not only to the variability, randomness in dynamic material properties, but also the smoothing aspect of 5% damped response spectra. Recall that at high-frequency, response spectra, being a constant damping smoothing operator, reflect transfer functions or resonances that are extremely wide. Depletion of reference site energy at high-frequency due to crustal damping at large distance ($> 100 \text{ km}$) may cause the amplification factor resonance to shift to lower frequency.

Figure 2 reveals this is not an issue of concern as there is only a very minor difference between the amplification factors computed at 1 and 400 km. As a result, any of the suite of amplification factors may be used.

Also, for the Lee Nuclear Station Unit 1, because of the linear response, the amplification factors are, by definition, independent of reference site spectral shape due to magnitude as well as single- or double-corner source spectral shapes. For this case, Approaches 1 and 2 are identical.

As a result, based on our previous examples, Approach 3 (without the correction factors, Section 3) as applied to the Lee Nuclear Station Unit 1 becomes trivial and reflects an excellent illustration case. An additional benefit in transparency of Approach 3 applied to the Lee Nuclear Station Unit 1 is the unusually small aleatory variability due to the typical uniformity of concrete properties (COV = 0.1). The resulting σ_{in} is about 0.1 giving a mean to median ratio of only 1.005. This result indicates that the mean amplification over the median amplification (Figure 11) is only about 0.5%, virtually the same. As a consequence a fully probabilistic method, Approach 3 analysis, due to linear site response ($C = 0$ in Equation 7) and a very small aleatory variability ($\sigma_{in} \approx 0.1$, see Figure 11) should give results very similar to a deterministic method (Approaches 1 and 2 in this case), provided the hard rock hazard curve does not have a steep slope.

To illustrate the deterministic and probabilistic approaches applied to the Lee Nuclear Station Unit 1, Figure 13 shows the hard rock (reference site) mean hazard curve computed for peak acceleration. Over the AEFs of interest in the integration, 10^{-3} to 10^{-6} , to define the site UHRS at AEFs of 10^{-4} and 10^{-5} , the slope of the hazard curve is about 2, or slightly less. Comparing the "deterministic UHRS" computed by multiplying the median amplification factor at 1 km (Figure 2) times the hard rock AEF 10^{-4} mean UHRS with the fully probabilistic Approach 3 method, Figure 14 shows the expected equivalence. The two approaches yield very nearly identical results, as expected for a linear analysis, small σ_{in} , and gently sloping reference site hazard curve. Figure 15 shows similar results computed for an AEF of 10^{-5} .

In summary, the Lee Nuclear Station Unit 1 reflects a clear and transparent application of the fully probabilistic Approach 3 method to achieve hazard consistent horizontal and vertical

UHRS. The Unit 1 site properties are such that the fully probabilistic method reduced to a classical deterministic method is well illustrated by the approximate Approach 3 method in the previous test cases.

4.0 APPLICATION TO VERTICAL HAZARD

Typically the vertical UHRS is developed by a deterministic application of V/H ratios applied to the horizontal UHRS. Since V/H ratios vary with both magnitude and distance for sites with nonlinear response and with distance for linear sites (e.g. hard rock) (Silva, 1997; NUREG/CR-6728), it is essential to capture these dependencies, identified through model deaggregations, in developing the vertical UHRS. For the deterministic approach, paralleling Approach 2 for the horizontal motions (Section 3.0), conservative estimates of appropriate V/H ratios must be used to ensure achievement of the same hazard levels and target performance goals as the horizontal UHRS. Additionally, V/H ratios reflect epistemic variability as is evidenced by WNA empirical soft rock and deep firm soil V/H ratios (Abrahamson and Shedlock, 1997), further pointing out the necessity of conservatism in a deterministic approach to developing vertical UHRS. As previously discussed in the context of Approach 2 for the horizontal UHRS, incorporation of epistemic variability in a deterministic framework is not unambiguous as one can not simply average over suites of motions or transfer functions which reflect epistemic variability. This process will not generally achieve desired hazard levels and reliance on conservatism in V/H ratios remains the most reliable option. These considerations, along with a desire for easy implementation as a function of expected horizontal peak acceleration, led to the purposeful incorporation of conservatism in development of the CENA hard rock V/H ratios (NUREG/CR-6728).

To accurately achieve desired hazard levels as well as performance goals, a fully probabilistic approach is used, directly paralleling that for the horizontal hazard. Implementation of the full integration Approach 3 (Section 3.2) for vertical hazard simply substitutes V/H ratios for horizontal amplification factors. In this case, the distribution of V/H ratios are integrated with the horizontal site-specific hazard curves (presumably developed using Approach 3). As with the horizontal case, Approach 3 then admits the proper and unambiguous incorporation of both aleatory and epistemic variabilities in V/H ratios, achieving desired hazard levels. Again, in parallel with development of the horizontal hazard, model deaggregations are used but, as previously stated, in addition to magnitude, source distance is required as V/H ratios depend on distance as well as magnitude for soil or soft rock site conditions.

4.1 Hazard Deaggregation For The William States Lee III Nuclear Station

Figure 16 shows the source contributions in magnitude and distance for the Lee Nuclear Station. In general there are three controlling sources: background sources with M near 5 and within about 20 to 40 km, the Charleston, South Carolina source zone with M near 7 around 250 km distance, and the New Madrid source zone over 400 km distance and with M around 8. For high-frequencies, 5 Hz to 10 Hz and above, as AEF decreases from 10^{-4} to 10^{-5} and 10^{-6} , the background source becomes much more dominant and concentrates within about 20 km of the site at an AEF of 10^{-6} . At low frequency, 1 Hz to 2.5 Hz, distance sources dominate at AEF of 10^{-4} to 10^{-5} . At 10^{-6} AEF and at 1 Hz to 2.5 Hz, the background source within 20 to 40 km becomes more significant, controlling the peak in the deaggregation, although distant source have significant contributions.

It is these general trends that are intended to be captured in applying the magnitude and distance dependent V/H ratios to the horizontal hazard.

4.2 Development of V/H Ratios

In the following sections the development of site-specific ratios and the motivation for inclusion of empirical V/H ratios is presented.

4.2.1 Site-Specific V/H Ratios

To develop site-specific vertical motions, incident inclined P-SV waves are modeled from the source to the site using the plane-wave propagators of Silva et al. (1976) assuming a shear-wave point-source spectrum (Boore; 1983, 2003). The point-source model is used to accommodate the effects of source distance and source depth on V/H ratios. For consistency, both the horizontal and vertical motions are modeled using the same source and path parameters (Table 2). The horizontal motions are modeled as vertically propagating shear-waves. For the vertical motions, the angles of incidence are computed by two-point ray tracing through the crust and site-specific profile. To model site response, the near-surface V_P and V_S profiles are placed on top of the crustal structure, the incident P-SV wavefield is propagated to the surface assuming a linear analysis, and the vertical motions are computed. For the Lee Nuclear Station Unit 1 with 20 ft of concrete over hard rock (Table 2), the base-case shear- and compressional-wave velocities are 7,500 ft/sec and 14,000 ft/sec respectively.

For typical crustal structures without strong near-surface V_P gradients and at close distances, the predominant motion on the vertical component is principally due to the SV wavefield. In a soil column (particularly deep profiles), however, because there is usually a large V_P gradient (larger for P-waves than for S-waves as Poisson ratios generally decrease with increasing depth), the vertical component is usually controlled by the compressional wavefield at high frequency (Silva, 1997; Amirbekian and Bolt, 1998; Beresnev et al., 2002).

In the implementation of the equivalent-linear approach to estimate V/H response spectral ratios, the horizontal component analyses are performed for vertically propagating shear-waves. To compute the vertical motions, a linear analysis is performed for incident inclined P-SV waves using low-strain V_P and V_S derived from the base-case profiles. The P-wave damping is assumed to be equal to the low strain S-wave damping (Johnson and Silva, 1981). The horizontal component and vertical component analyses are assumed to be independent.

The approximations of linear analysis for the vertical component and uncoupled vertical and horizontal components have been validated in two ways. Fully nonlinear modeling using a 3-D soil model shows that the assumption of largely independent horizontal and vertical motions for loading levels up to about 0.5g (soil surface, horizontal component) for moderately stiff profiles is appropriate (EPRI, 1993). Additionally, validation exercises with recorded motions have been conducted at over 50 sites that recorded the 1989 M 6.9 Loma Prieta earthquake (EPRI, 1993). These validations show the overall bias and variability is acceptably low for engineering applications but is higher than that for horizontal motions. The vertical model does not perform as well as the model for horizontal motions (EPRI, 1993; Silva, 1997). An indirect validation was also performed by comparing V/H ratios from WNA empirical attenuation relations with model predictions over a wide range in loading conditions (Silva, 1997). The results show a favorable comparison with the model exceeding the empirical V/H ratios at high frequency, particularly at high loading levels. In the V/H comparisons with empirical relations, the model also shows a small under prediction at low frequency (≤ 1 Hz) and at large distance (≥ 20 km).

For the vertical analyses, a hard rock kappa value of 0.003 sec, half that of the horizontal, is used. This factor of 50% is based on observations of kappa at strong motion sites (Anderson and Hough, 1984), validation exercises (EPRI, 1993), as well as the observation that the peak in the vertical spectral acceleration (5% damped) for WNA rock and soil sites is generally near 10 to 12 Hz compared to the horizontal motion peak that occurs at about 5 Hz, conditional on M 6.5 at a distance of about 10 to 30 km (Abrahamson and Silva 1997; Campbell 1997; Campbell and Bozorgnia 2003). This difference of about 2 in peak frequency is directly attributable to differences in kappa of about 2. Similar trends are seen in CENA hard rock spectra with the vertical component peaking at higher frequencies than the horizontal component.

The site-specific V/H ratios are shown in Figure 17 and reflect median estimates computed with the stochastic model for M 5.1. As previously discussed, due to the stiffness of the Unit 1 profile, linear analyses were performed for the horizontal component resulting in magnitude independent amplification factors and V/H ratios. For M 5.1, the distances range from 80 to 0 km (Table 2) with expected horizontal hard rock peak accelerations ranging from 0.01 to 0.50g. As Figure 17 shows, the V/H ratios for the shallow concrete profile of Unit 1 are nearly constant with frequency and increase rapidly as distance decreases, within about a 15 km source distance. For distances beyond 10 to 15 km, the V/H ratio is about 0.5 and increases rapidly to about 0.9 within about 5 km. The peak near 60 Hz is likely due to the peak in the vertical spectra. The multiple peaks beginning near 1 Hz reflect deep crustal resonances (structure below a depth of 1 km, Table 2) and would be smoothed if the crustal model were randomized and discrete layers replaced with steep velocity gradients to reflect lateral variability and a more realistic crustal structure. The distance ranges more than adequately accommodate the hazard deaggregation.

As previously discussed, the model predictions of V/H ratios at low-frequency may be slightly unconservative and at high frequency they may be conservative. While it is important to include site-specific effects on the vertical hazard, potential model deficiencies may be compensated with inclusion of empirical V/H ratios computed from WNA generic rock attenuation relations (Section 4.2.2). Additionally, empirical V/H ratios of Fourier amplitude spectra based on CENA recordings at hard rock sites for small magnitudes and at very large distances have median values near about 0.8 and vary slowly with frequency (Gupta and McLaughlin, 1987; Atkinson, 1993). To accommodate potential model deficiencies as well as the large uncertainty in hard and firm rock V/H ratios for CENA, a minimum value of 0.7 is adopted, the average of the empirical CENA and site-specific V/H ratios at large distance (> 20 km).

4.2.2 Empirical V/H Ratios

Empirical western North America V/H ratios for soft rock are included in the development of vertical motions in addition to site-specific point-source simulations. The use of WNA empirical V/H ratios implicitly assumes similarity in shear- and compression-wave profiles and nonlinear dynamic material properties between site condition in WNA and the Lee Nuclear Station Unit 1 column (Silva et al., 1999). Whereas this may not be the case for the average WNA rock site profile (Silva, 1997), the range in site conditions sampled by the WNA empirical generic rock relations likely accommodates site-specific conditions. The relative weights listed in Table 4 reflect the assumed appropriateness of WNA soft rock empirical V/H ratios for Unit 1. Additionally, because the model for vertical motions is not as thoroughly validated as the model for horizontal motions (EPRI, 1993), inclusion of empirical models is

warranted. The additional epistemic variability introduced by inclusion of both analytical and empirical models also appropriately reflects the difficulty and lack of consensus regarding the modeling of site-specific vertical motions (EPRI, 1993). In the implementation of Approach 3 to develop vertical hazard curves, the epistemic variability is properly accommodated in the vertical mean UHRS, reflecting a weighted average over multiple vertical hazard curves computed for Unit 1 using multiple models. The vertical FIRS (and UHRS) then maintain the desired risk and hazard levels, consistent with the horizontal UHRS.

For the empirical V/H ratios, both Abrahamson and Silva (1997) and Campbell and Bozorgnia (2003); Bozorgnia, and Campbell (2004) soft rock WNA relations are used with equal weights (Table 4). As an example, Figure 18 shows the Campbell and Bozorgnia V/H ratios computed for M 5.1 and M 8.0. Distance bins differ between the empirical and analytical V/H ratios because the empirical ratios use a generic suite of distances used on several projects while the analytical V/H ratios are region specific. For distances beyond 57 km, the empirical V/H ratios are nearly constant with increasing distance. Additionally, for the smaller M ($M < 5.5$), there are few strong motion data available at larger distances (Campbell and Bozorgnia, 2003). Because the ratios vary slowly with distance, the differences in distances are not significant. The empirical WNA soft rock ratios show more distance (loading level) dependence than the site-specific analytical ratios (Figure 17), perhaps due to nonlinearity in the horizontal soft rock motion (Silva, 1997). These trends, with the M independence of V/H ratios, are expected for firm rock conditions. That is, as the profile becomes stiffer, nonlinearity decreases, and for distances within about 10 to 15 km, distance becomes the dominant controlling factor in V/H ratios (Silva, 1997).

The empirical soft rock V/H ratios show a clear dependency on magnitude, although it is not particularly strong as the comparison is over magnitude 5.1 and 8.0. The distance dependency for the empirical V/H ratios shown in Figure 18 clearly illustrates epistemic variability having significantly different trends with distance between those of Abrahamson and Silva (1997) and Campbell and Bozorgnia (2003). As an example, at 20 Hz and for M 5.1, Abramson and Silva (1997) show little distance dependency with a value near 0.7 while Campbell and Bozorgnia (2003) show a range varying from about 0.6 to about 1.0, about a 70% change, over the distance range of 57 km to 1 km. The converse is apparent for M 8.0. Such differences between relations generally considered reliable illustrate the significant epistemic variability inherent in developing vertical hazard and the necessity for its statistically proper inclusion through the use of multiple models, within the context of Approach 3 (Section 3.0).

It is important to note the site-specific and generic V/H ratios peak at very different frequencies, about 60 Hz and about 10 to 20 Hz, respectively, with the site-specific having generally higher V/H ratios, particularly at close distances. Use of an empirical V/H ratio alone may underestimate the vertical hazard at high frequency, provided the model predictions are reasonably accurate.

For the empirical V/H ratios, to fully accommodate the hazard deaggregation (Section 4.1, Figure 16), V/H ratios for magnitude 7.0 were also computed and used (Table 4) in developing the vertical hazard (Section 4.3).

4.2.3 Aleatory Variability In V/H Ratios

In addition to the epistemic variability accommodated through the use of multiple models for V/H ratios, aleatory variability due to randomness of dynamic material properties varying

vertically and laterally across the site should be accommodated as well. However, in developing the vertical hazard, since site-specific aleatory variability has been incorporated in developing the horizontal site-specific hazard curves, it is advisable to constrain the sigma of the site-specific V/H ratios to values less than about 0.15 to 0.20 (σ_{in}). This range is to accommodate the observation of slightly larger variability about median attenuation relations in the vertical component compared to the horizontal component (Abrahamson and Silva, 1997). An example of aleatory variability in site-specific V/H ratios computed for the Lee Nuclear Station Unit 1 is shown in Figure 17 for a suite of distances and in Figure 19 for a distance of 80km. For the Unit 1 site conditions and hard rock in general, the aleatory variability is quite small, less than about 0.1 (σ_{in}) due to the COV of 0.1 for shear-wave velocity within the concrete. However for less uniform materials, the standard deviation can be significantly larger; as a result, limiting its value avoids potential double counting site-specific aleatory variability in developing vertical hazard. It should be noted that for the computation of site-specific V/H ratios, the denominator (horizontal component) should be taken as the median (i.e. not varied) and multiple realizations of the vertical component taken to form the basis for the aleatory variability in the V/H ratios. This approach is intended to properly isolate the variability in the V/H ratios to that of the verticals, recognizing the variability in the horizontal component has already been accommodated in the randomization of shear-wave dynamic material properties.

The occasion to limit the V/H ratio variability may arise due to the randomization process incorporated in the model for the vertical motions. For simplicity, the randomization of the compressional-wave velocities fixes the Poisson ratios in the profile at the values of the base-case shear- and compressional-wave velocities. The profile randomization scheme (Section 2.2.1), based on shear-wave velocities and layer thickness, produces realizations of shear-wave velocities with corresponding compressional-wave velocities using the original Poisson ratios. This process results in a suite of random shear- and compressional-wave profiles, all with the same Poisson ratios (verses depth). It may very well be the case this simplifying assumption results in too large a range in compressional-wave velocities, perhaps due to a coupling between shear-wave velocity and Poisson ratio. Obviously, because horizontal components and consequently shear-waves are of major concern and because there are many more measured shear-wave velocity profiles than both shear- and compressional-wave velocity profiles, the profile randomization scheme has concentrated on shear-waves. Additionally, a more statistically correct compressional-wave randomization scheme would have little impact as a 20% to 30% change in the aleatory variability, if small, has a very minor impact (3% to 4%) on the vertical hazard for typical ranges in the slope (κ) of the horizontal hazard curve (2 to 6) and slope of the V/H ratios with loading level (distance), as illustrated in Equation 7.

Returning to the empirical V/H ratios, Figure 18, as only median estimates are available through horizontal and vertical attenuation relations (Abrahamson and Silva, 1997; Campbell and Bozorgnia, 1997, 2003), in application of Approach 3 which requires aleatory variability (e.g. Equation 7) in the V/H ratios, a value of 0.15 (σ_{in}) is used.

4.3 Implementation of V/H Ratios In Developing Vertical Hazard

In assigning the V/H ratios in the Approach 3 analysis, the source M and D change significantly with structural frequency as exceedance frequency changes (Section 4.1, Figure 16). To accommodate the deaggregation in (contributing sources) integrating the horizontal hazard with the distributions of V/H ratios, the M and D selection follows that listed in Table 4. The magnitudes selected are intended to capture the dominant sources: M 5.1 for close-in

sources and M 7.0 and M 8.0 for the Charleston, South Carolina and New Madrid, Missouri sources, respectively, both at distances well beyond 100 km. The distances used for the V/H ratios (Table 4) reflect the distance sensitivity, or lack of sensitivity beyond about 10 to 15 km for the site-specific ratios and beyond about 50 km for the empirical ratios, considering the contributing source distances. The weights listed in Table 4 are intended to approximate the relative contributions of the three sources across structural frequency and exceedance probability. Because the V/H ratios vary slowly with distance, only a smooth approximation to the hazard deaggregation is necessary. To adequately capture the change in M and D with AEF, only a few distance bins are required: 5 and 57 km for the empirical V/H ratios and 0, 7, and 28 km for the analytical V/H ratios (Table 4).

To illustrate the vertical hazard computed using Approach 3 with the empirical and site-specific V/H ratios, Figure 20 shows horizontal and vertical UHRS computed for the Lee Nuclear Station Unit 1 profile for AEF 10^{-4} , 10^{-5} , and 10^{-6} . The magnitude and distance deaggregation (Figure 16, Section 4.1) is seen to be captured in the apparent V/H ratios (vertical UHRS divided by the horizontal UHRS). As the AEF decreases and both the high- and low-frequency source contributions move closer to the site (Table 4, Figure 16), higher weight is placed on the closer empirical and site-specific V/H ratios resulting in larger apparent V/H ratios. The fully probabilistic approach then results in hazard consistent vertical UHRS that properly accommodate site-specific aleatory and epistemic variability as well as the effect of magnitude and distance on vertical motions. This is especially the case at high-frequency and low AEF at 10^{-6} .

4.3.1 UHRS Interpolation and Extrapolation

Because the reference (hard rock) hazard is computed at only seven frequencies, namely 0.5, 1.0, 2.5, 5.0, 10.0, 25.0, and 100.0 Hz (taken as peak acceleration), the site-specific hazard has been both extrapolated to 0.1 Hz and at high-frequency, the reference hazard curves were interpolated at 34 and 50 Hz, as these are the critical frequencies to define the Unit 1 UHRS shapes beyond 25 Hz. The interpolation is performed by using the deterministic shapes (NUREG/CR-6728) for the appropriate M to interpolate the hard rock UHRS at AEF of 10^{-4} , 10^{-5} , and 10^{-6} yr⁻¹, resulting in three points on 34 and 50 Hz hazard curves. The adjacent hazard curves at 25 and 100 Hz are then used as shapes to extrapolate to lower and higher exceedance probabilities, resulting in approximate hard rock hazard curves. Approach 3 is then applied to develop site-specific horizontal and vertical UHRS at the same exceedance frequency as the 25 Hz and 100 Hz hard rock hazard curves. Approach 3 (full integration method) is then applied to develop site-specific horizontal and vertical UHRS at the same exceedance probability as the 25 and 100 Hz hard rock hazard. For the vertical component, because the site-specific V/H ratios peak at very high-frequency (beyond 50 Hz), it is important to maintain the appropriate hazard levels between 25 and 50 Hz.

Below 0.5 Hz, because the aleatory variability in attenuation relations increases with period (Abrahamson and Shedlock, 1997; EPRI, 2004), use of a median spectral shape (NUREG/CR-6728) to extrapolate at low-frequency may be inappropriate and result in potentially unconservative hazard or higher probability than desired. To address this uncertainty, a conservative approach is adopted by extrapolating the 0.5 Hz 10^{-4} , 10^{-5} , and 10^{-6} hard rock UHRS, assuming a constant slope in spectral velocity (+1 slope in pseudo-absolute spectral acceleration) (BSSC, 2004). The extrapolation is extended at low-frequency to the earthquake source corner frequency, where the slope is increased to a constant spectral displacement. Since the source corner frequency, or transition from approximately constant spectral velocity to spectral displacement, depends on magnitude, an

average representative magnitude of M 7.2 is assumed to apply for frequencies below 0.5 Hz, based on the low-frequency deaggregation (Figure 16). Application of the empirical relation

$$\text{Log } T = -1.25 + 0.3 M \quad (8)$$

(BSSC, 2004) results in a corner period (T) of approximately 8 sec (0.125 Hz). To accommodate this expected change in slope, the extrapolations are performed at 0.125 and 0.1 Hz, assuming constant spectral velocity from 0.5 to 0.125 Hz and constant spectral displacement for frequencies below 0.125 Hz.

5.0 CONCLUSIONS

For the Lee Nuclear Station Unit 1, a fully probabilistic methodology (Approach 3) was used to develop the site-specific UHRS (NUREG/CR-6728 and 6769). As part of this approach, site-specific amplification factors as well as V/H ratios were developed using RVT (NUREG/CR-6728), rather than time domain analyses (e.g. SHAKE).

As part of the acceptance review of the William States Lee III Nuclear Station Combined License Application, the NRC indicated that FSAR Section 2.5.2 did not provide a sufficient level of detail describing the Approach 3 methodology and how the methodology was used with RVT to develop the final site ground motions. To address these comments, this document presents a full and complete development of both RVT, in applications to site response and V/H ratios, as well as both deterministic (Approaches 1 and 2) and probabilistic (Approaches 3 and 4) methods to developing site-specific UHRS.

Regarding site response, the two areas where RVT is used directly in estimating response spectra and peak shear strains for equivalent-linear analyses have been presented and discussed. Other related considerations in site response such as choice of control motion, effects of control motion spectral shape, and incorporation of aleatory variabilities in dynamic material properties have been presented and discussed in terms of potential impacts to the development of site-specific UHRS. Additionally, general guidelines for implementing RVT in terms of site response have been presented and discussed.

All four methodologies for developing site-specific ground motions (Approaches 1 to 4) have been presented and discussed in order of increasing accuracy and complexity. The fully probabilistic approach used in computing the Lee Nuclear Station Unit 1 UHRS (Approach 3) was developed through the derivation of basic equations, illustrating the various simplifications as well as assumptions. Also presented and discussed are implementation limitations of Approach 3 as well as the other approaches, and how these limitations are addressed to preserve accuracy, or conservatism in the case of deterministic approaches, in computing site-specific hazard curves. Sensitivities of the fully probabilistic approach to various parameters have also been explored to illustrate the essential elements in the methodology, which enables the approach to achieve hazard consistency. Also presented is a discussion of the optimum number of site response realizations, in terms of confidence levels, to achieve a given accuracy in ground motion at a given hazard level for implementation of the fully probabilistic approach.

Finally, Lee Nuclear Station Unit 1 specific parameter values and results have been presented for the horizontal and vertical UHRS.

6.0 REFERENCES

- Abrahamson, N.A. and W.J. Silva (1997). "Empirical response spectral attenuation relations for shallow crustal earthquakes." *Seismological Research Letters*, 68(1), 94-127.
- Abrahamson, N.A. and K.M. Shedlock (1997). "Overview." *Seismological Research Letters*, 68(1), 9-23.
- Amirbekian, R.V. and Bolt, B.A. (1998). "Spectral comparison of vertical and horizontal seismic strong ground motions in alluvial basins." *Earthquake Spectra*, 14(4), 573-595.
- Anderson, J. G. and S. Hough (1984). A Model for the shape of the Fourier amplitude spectrum of acceleration at high frequencies: *Bulletin Seismological Society of America*, 74(5), 1969-1993.
- Atkinson, G.M. and W.J. Silva (1997). "An empirical study of earthquake source spectra for California earthquakes." *Bulletin of Seismological Society of America*, 87(1), 97-113.
- Atkinson, G.M. (1993). "Notes on ground motion parameters for eastern North America: duration and H/V ratio." *Bulletin of Seismological Society of America*, 83(2), 587-596.
- Bazzurro, Paolo and C.A. Cornell (2004). "Nonlinear soil-site effects in probabilistic seismic-hazard analysis." *Bulletin of Seismological Society of America*, 94(6), 2110-2123.
- Beresnev, I.A, Nightengale, A.M. Silva, W.J. (2002). "Properties of vertical ground motions." *Bulletin of the Seismological Society of America*, 92(2), 3152-3164.
- Bozorgnia, Y. and Campbell, K. (2004). "The vertical-to-horizontal response spectral ratio and tentative procedures for developing simplified V/H and vertical design spectra" *Journal of Earthquake Engineering*, 8(2), 175-207.
- Boore, D.M. (2003) "Simulation of ground motions using the stochastic method" *Pure and Applied Geophysics*, 160, 635-676.
- Boore, D.M. and Joyner, W.B. (1984). "A note on the use of random vibration theory to predict peak amplitudes of transient signals." *Bulletin of Seismological Society of America*, 74, 2035-2039.
- Boore, D.M. (1983). "Strong-motion seismology." *Reviews of Geophysics*, 21, 1308-1318.
- Building Seismic Safety Council (BSSC) (2004). "National Earthquake Hazards Reduction Program (NEHRP), Recommended Provisions for Seismic Regulations for New Buildings and Other Structures (FEMA 450), Report prepared for the Federal Emergency Management Agency (FEMA).
- Campbell, K W. (1997). "Empirical near-source attenuation relationships for horizontal and vertical components of peak ground acceleration, peak ground velocity, and

- pseudo-absolute acceleration response spectra." *Seismological Society of America*, 68(1), 154-176.
- Campbell, K.W. and Y. Bozorgnia (1994). "Near-source attenuation of peak horizontal acceleration from worldwide accelerograms recorded from 1957 to 1993." in *Proceedings, Fifth U.S. National Conference on Earthquake Engineering*. Chicago, Illinois. vol. III, p.283-292.
- Campbell, K.W. and Y. Bozorgnia (2003). "Updated Near-Source Ground Motion (Attenuation) Relations for the Horizontal and Vertical Components of Peak Ground Acceleration and Acceleration Response Spectra," *Bulletin of the Seismological Society of America*, 93 (1):314-331
- Cramer, C. H. (2003) "Site-specific seismic hazard analysis that is completely probabilistic." *Bulletin of Seismological Society of America*, 93, 1841-1846.
- Duke Energy Carolinas, LLC (2007), William States Lee III Nuclear Station – Project 724, Application for Combined License for William States Lee III Nuclear Station Units 1 and 2.
- Electric Power Research Institute (2004). "CEUS Ground Motion Project Final Report." EPRI, Palo Alto, CA, Dominion Energy, Glen Allen, VA, Entergy Nuclear, Jackson, MS, and Exelon Generation Company, Kennett Square, PA: 2004. 1009684.
- Electric Power Research Institute (1993). "Guidelines for determining design basis ground motions." Palo Alto, California: Electric Power Research Institute, vol. 1-5, EPRI TR-102293.
- Electric Power Research Institute. (1988). "Engineering model of earthquake ground motion for eastern North America." Palo Alto, California: Electric Power Research Institute, EPRI NP-6074.
- Gupta, I.N. and K.L. McLaughlin (1987). "Attenuation of ground motion in the Eastern United States." *Bulletin of Seismological Society of America*, 77, 366-383.
- Hartzell, S., S. Harmsen, A. Frankel, and S. Larsen (1999). "Calculation of broadband time histories of ground motion: Comparison of methods and validation using strong-ground motion from the 1994 Northridge Earthquake." *Bulletin of Seismological Society of America*, 89(6), 1484-1504.
- Herrmann, R.B. (1985). "An extension of random vibration theory estimates of strong ground motion to large distance." *Bulletin of Seismological Society of America*, 75, 1447-1453.
- Idriss, I. M. and H.B. Seed (1968) "Seismic response of horizontal soil layers." *Journal of Soil Mechanics and Foundation Engineering*, *Proceedings of ASCE*, Vol. 94, No. 4, pp. 1003-1031.

- Johnson, L.R., and W.J Silva (1981). "The effects of unconsolidated sediments upon the ground motion during local earthquakes." *Bulletin of Seismological Society of America*, 71, 127-142.
- Lee, R., M. E. Maryak, and J. Kimball (1999). "A methodology to estimate site-specific seismic hazard for critical facilities on soil or soft-rock sites." *Seismological Research Letters*, 70, 230.
- Lee, R., W.J. Silva, and C. A. Cornell (1998). "Alternatives in evaluating soil- and rock-site seismic hazard." *Seismological Research Letters*, 69, 81.
- McGuire, R.K., W.J. Silva and C.J. Costantino (2001). "Technical basis for revision of regulatory guidance on design ground motions: hazard- and risk-consistent ground motions spectra guidelines." Prepared for Division of Engineering Technology, Washington, DC, NUREG/CR-6728.
- McGuire, R.K., W.J. Silva and C.J. Costantino (2002). "Technical Basis for Revision of Regulatory Guidance on Design Ground Motions: Development of Hazard- and Risk-consistent Seismic Spectra for Two Sites." NUREG/CR-6729.
- Pacific Engineering Research Center (PEER) (2008), Next Generation of Ground Motion Attenuation Models (NGA), "Special issue on the next generation attenuation project," Technical editors, J. Stewart, R. Archuleta, M. Power, *Earthquake Spectra*, vol. 24(1).
- Pakiser, L.C. and W. D. Mooney (1989). "Geophysical Framework of the Continental United States." *Geological Society of America Memoir* 172.
- Schnabel, P.B., Lysmer, J., and Seed, H.B. (1972). SHAKE: a Computer Program for Earthquake Response Analysis of Horizontally Layered Sites. Earthquake Engineering Research Center (EEEC), University of California at Berkeley, EERC 72-12.
- Schneider, J.F., W.J. Silva, and C.L. Stark (1993). Ground motion model for the 1989 M 6.9 Loma Prieta earthquake including effects of source, path and site. *Earthquake Spectra*, 9(2), 251-287.
- Silva, W. J., S. Li, B. Darragh, and N. Gregor (1999). "Surface geology based strong motion amplification factors for the San Francisco Bay and Los Angeles Areas." A PEARL report to PG&E/CEC/Caltrans, Award No. SA2120-59652.
- Silva, W.J., N. Abrahamson, G. Toro, C. Costantino (1997). "Description and validation of the stochastic ground motion model." Report Submitted to Brookhaven National Laboratory, Associated Universities, Inc. Upton, New York.
- Silva, W.J. and R. Darragh (1995). "Engineering characterization of earthquake strong ground motion recorded at rock sites." Palo Alto, California: Electric Power Research Institute, TR-102261.

- Silva, W.J. (1992). "Factors controlling strong ground motions and their associated uncertainties." Seismic and Dynamic Analysis and Design Considerations for High Level Nuclear Waste Repositories, ASCE 132-161.
- Silva, W.J., T. Turcotte and Y. Moriwaki (1986). "Soil response to earthquake ground motions." Palo Alto, Calif.: Electric Power Research Institute, EPRI Research Project RP 2556-07.
- Silva, W.J. (1997). Characteristics of vertical strong ground motions for applications to engineering design, in Proc. FHWA/NCEER Workshop on the National Representation of Seismic Ground Motion for New and Existing Highway Facilities, Technical Report, NCEER-97-0010, National Center for Earthquake Engineering Research, Buffalo, New York.
- Silva, W.J. (1976). "Body Waves in a Layered Anelastic solid." Bulletin of Seismological Society of America, vol. 66(5), 1539-1554.

7.0 TABLES AND FIGURES

TABLES

Table 1

Definitions of Locations for Motions in Site-Response Analyses

1. **Outcrop:** May be specified at the surface or at any depth within a profile.
 - A. **Surface Outcrop:** All material above the outcrop location is removed. Motion comprised as the sum of upgoing and downgoing waves. For vertically propagating waves (shear or compressional) the free surface effect results in an amplification of exactly 2 over upgoing waves (incident wavefield).
 - B. **At-Depth Outcrop:** Material above the outcrop location remains in place. Motion comprised of upgoing wavefields only. However the upgoing wavefields at the outcrop location may contain wavefields which propagated above the outcrop location, reflected from impedance contrasts and the free surface, and propagated down past the outcrop location. If there are significant impedance contrasts below the outcrop location, these reflected wavefields contribute to the upgoing wavefields at the outcrop location and may increase or decrease the upgoing wavefield.
2. **At Depth In-Column or Total Motions:** As with the Outcrop-At-Depth, material above the location of the computed motions remains in place. Motions are comprised of upgoing and downgoing wavefields (total motion) and reflect motions experienced by a buried instrument (e.g. vertical array).
3. **Free-Field:** Surface or At-Depth motions unaffected to a significant degree ($\leq 10\%$) by the built environment. For recording instruments, this is generally achieved at a foundation dimension away from structures. For in-structure motions, this is achieved at ground level and light structures of two stories or fewer.
4. **Site:** In this document the term site is used in its classical sense to reflect a single geographical point, rather than the area occupied by a nuclear station.

Table 2 Hard Rock Expected Horizontal Peak Acceleration Levels, Point Source Distances, and Durations					
M 5.1, single-corner					
G(g)	Distance (km)	Depth (km)	T _{source} (sec)	T _{path} (sec)	T _{total} (sec)
1.50	0	2	0.96	0.04	1.00
1.25	0	2	0.96	0.06	1.02
1.00	0	3	0.96	0.08	1.04
0.75	0	4	0.96	0.12	1.08
0.50	0	5	0.96	0.20	1.16
0.40	0	6	0.96	0.25	1.21
0.30	0	8	0.96	0.34	1.30
0.20	7	8	0.96	0.47	1.43
0.10	16	8	0.96	0.84	1.80
0.05	28	8	0.96	1.43	2.39
0.01	80	8	0.96	3.97	4.93

Notes: Additional parameters used in the point-source model are:

$$Q = 670 f^{0.33}$$

$$\Delta\sigma(1c) = 110 \text{ bars}$$

$$\kappa = 0.006 \text{ sec, hard rock}$$

$$\rho = 2.71 \text{ cgs}$$

$$\beta = 3.52 \text{ km/sec}$$

$$R_c = 60 \text{ km, crossover hypocentral distance to } R^{-0.5} \text{ geometrical attenuation}$$

$$T = 1/fc + 0.05 (R-1)^*, R > 1; \text{ RVT duration, } R = \text{hypocentral distance (km)}$$

CENA Generic Hard Rock Crustal Model			
Thickness (km)	Vs (km/sec)	Vp (km/sec)	ρ (cgs)
1	2.83	4.90	2.52
11	3.52	6.10	2.71
28	3.75	6.50	2.78
[infinite]	4.62	8.00	3.35

* See Appendix A for a discussion on the distance dependency of duration for CENA and WNA.

Table 3			
Sample Size Required For Percent Error In The Standard Deviation For A Normal Distribution			
% Error	Confidence Levels (%)		
	90	95	99
	Sample Size		
50	5	7	13
30	15	21	35
20	30	46	80
10	130	200	300
5	550	700	>1000

Table 4 Moment Magnitude						
Empirical V/H Ratio Weights						
AEF (yr ⁻¹)	High-Frequency ≥ 5.0 Hz			Low-Frequency ≤ 2.5 Hz		
	Magnitude (M)			Magnitude (M)		
	5.1	7.0	8.0	5.1	7.0	8.0
	Weights			Weights		
10 ⁻⁴	0.37	0.37	0.26	0.20	0.40	0.40
10 ⁻⁵	1.00	0.	0.	0.25	0.25	0.50
10 ⁻⁶	1.00	0.	0.	0.43	0.14	0.43

Empirical V/H Ratio Distances	
Magnitude (M)	Distance (km)
5.1	5
7.0	57
8.0	57

Model V/H Ratio Weights						
AEF (yr ⁻¹)	High-Frequency ≥ 5.0 Hz			Low-Frequency ≤ 2.5 Hz		
	Distance (km)			Distance (km)		
	28	7	0	28	7	0
	Weights			Weights		
10 ⁻⁴	0.6	0.2	0.2	0.8	0.1	0.1
10 ⁻⁵	0.3	0.7	0.0	0.8	0.1	0.1
10 ⁻⁶	0.1	0.6	0.3	0.4	0.3	0.3

Profile	Weighting		Empirical Relation Weights		Site Condition Weights	
	Empirical	Model	A&S (1997)	C&B (2003)	Soft Rock	Soil
Unit 1	0.2	0.8	0.5	0.5	1.0	0.0

Notes:
 A&S (1997) = Abrahamson and Silva (1997)
 C&B (2003) = Campbell and Bozorgnia (2003)

FIGURES

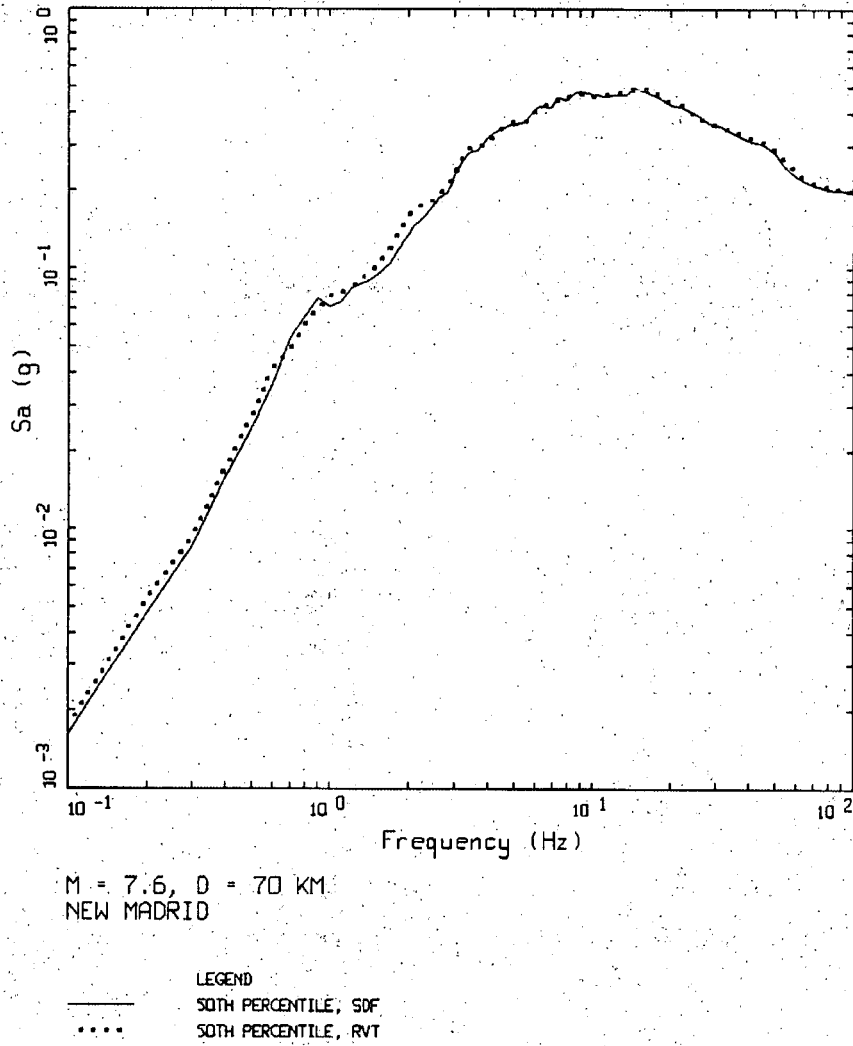


Figure 1. Comparison of median RVT and SDF (computed from acceleration time histories) 5% damped response spectra. Medians computed over 30 realizations.

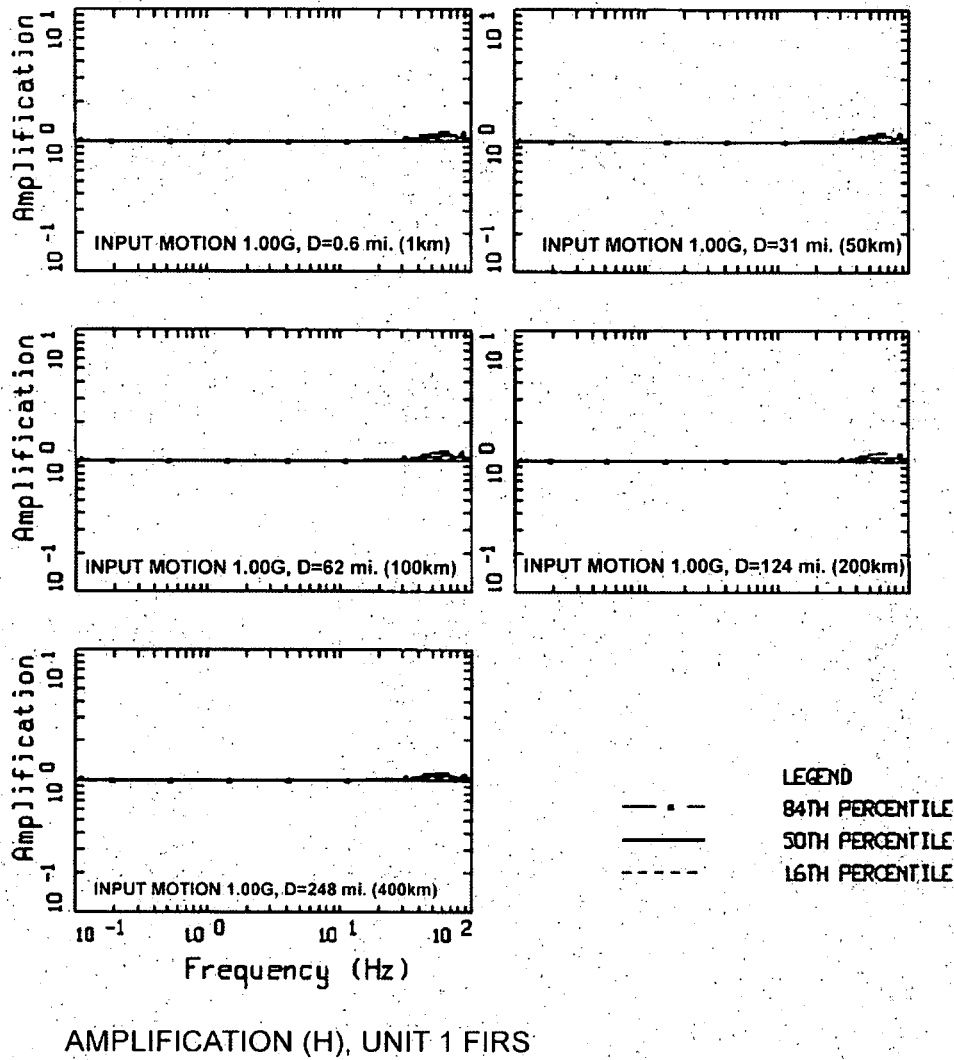
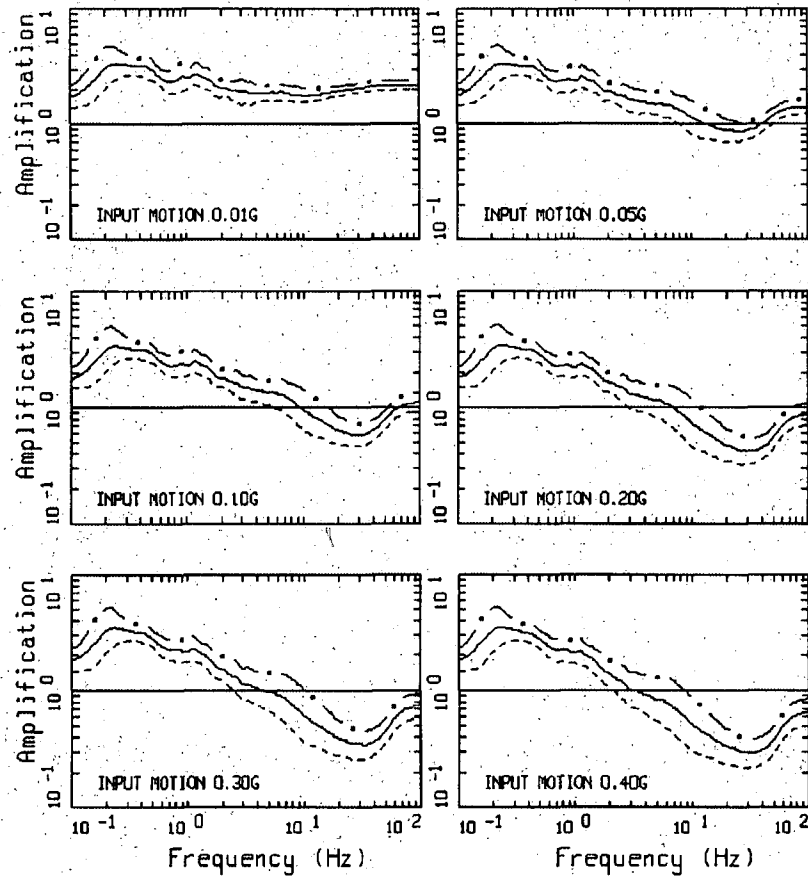
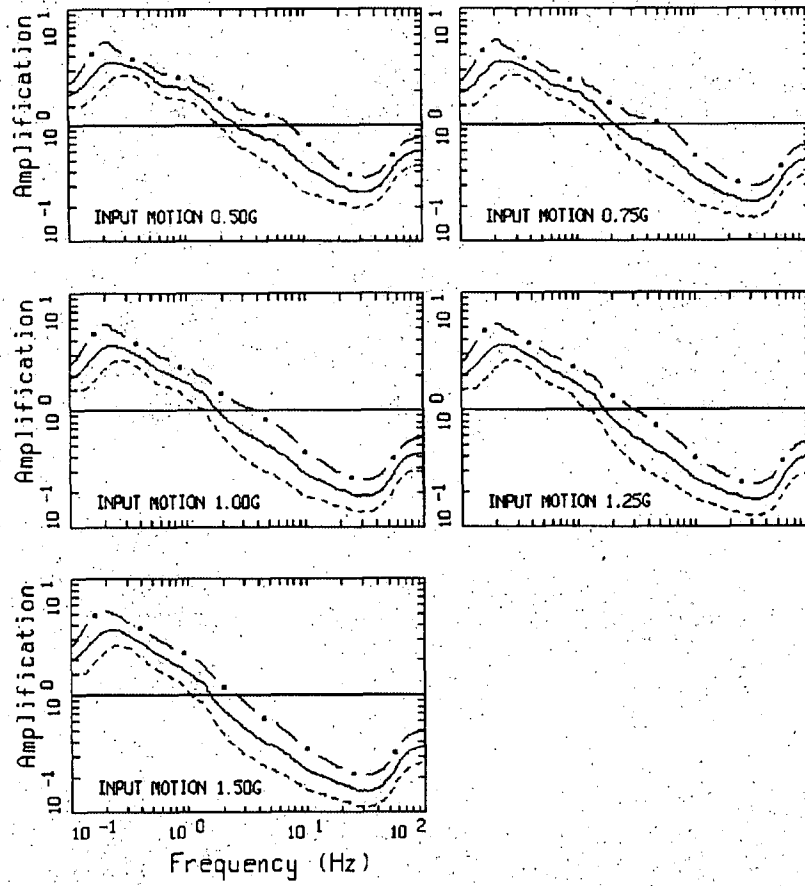


Figure 2. Lee Nuclear Station Unit 1 amplification factors (5% damping) at a suite of source distances. Mean properties: 20 ft concrete with a shear-wave velocity of 7,500 ft/sec over hard rock ($V_S = 9,300$ ft/sec). Due to the stiffness of the concrete, linear site response analyses were performed. Although M 5.1 was used, based on high frequency deaggregations, response is independent of M due to linearity of the concrete under transient loading.



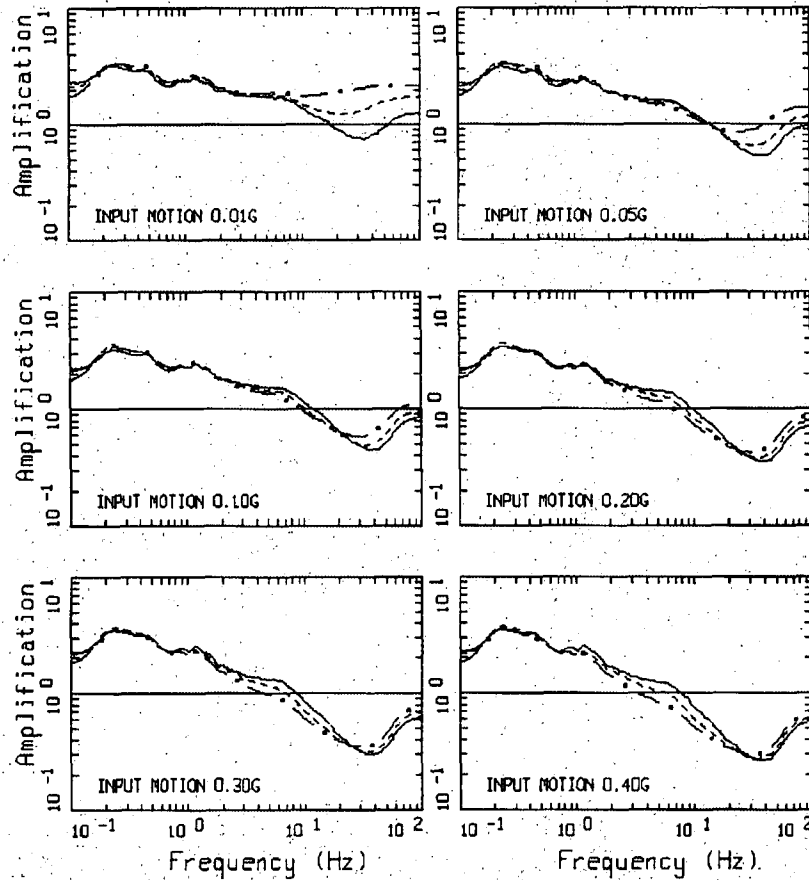
AMPLIFICATION, M = 7.00, 1 CORNER
PAGE 1 OF 2

Figure 3. Example of median and ± 1 sigma estimates of amplification factors computed for deep a soil site in the CENA. Hard rock reference expected peak acceleration ranges from 0.01g to 1.50g. Distances were adjusted to obtain target (input) median peak acceleration values. Single-corner point-source magnitude is 7.0.



AMPLIFICATION, M = 7.00, 1 CORNER
PAGE 2 OF 2

Figure 3 (cont.)

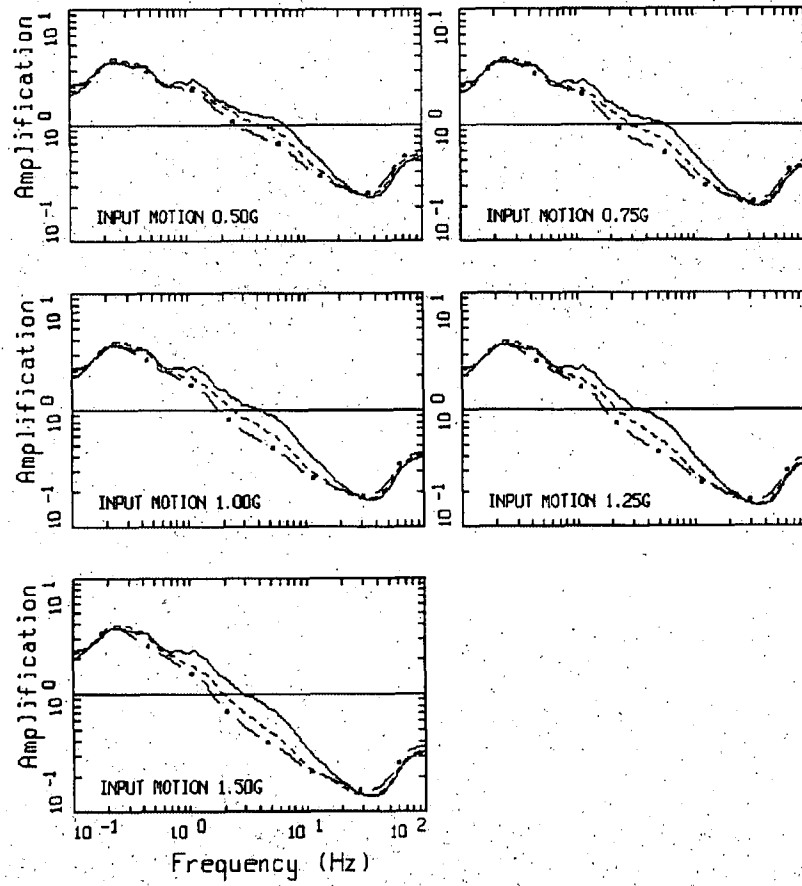


AMPLIFICATION

PAGE 1 OF 2

LEGEND	
—	M = 5.0, 1 CORNER
- - -	M = 6.0, 1 CORNER
- . - .	M = 7.0, 1 CORNER
—	UNITY LINE

Figure 4. Test case illustrating the effect of magnitude on median amplification factors computed for a deep soil site in the CENA. Distances were adjusted to obtain the target hard rock (input) median peak acceleration values. Plotted versus structural frequency.



AMPLIFICATION
PAGE 2 OF 2

LEGEND
— M = 5.0, 1 CORNER
- - - M = 6.0, 1 CORNER
- · - M = 7.0, 1 CORNER
— UNITY LINE

Figure 4 (cont.)

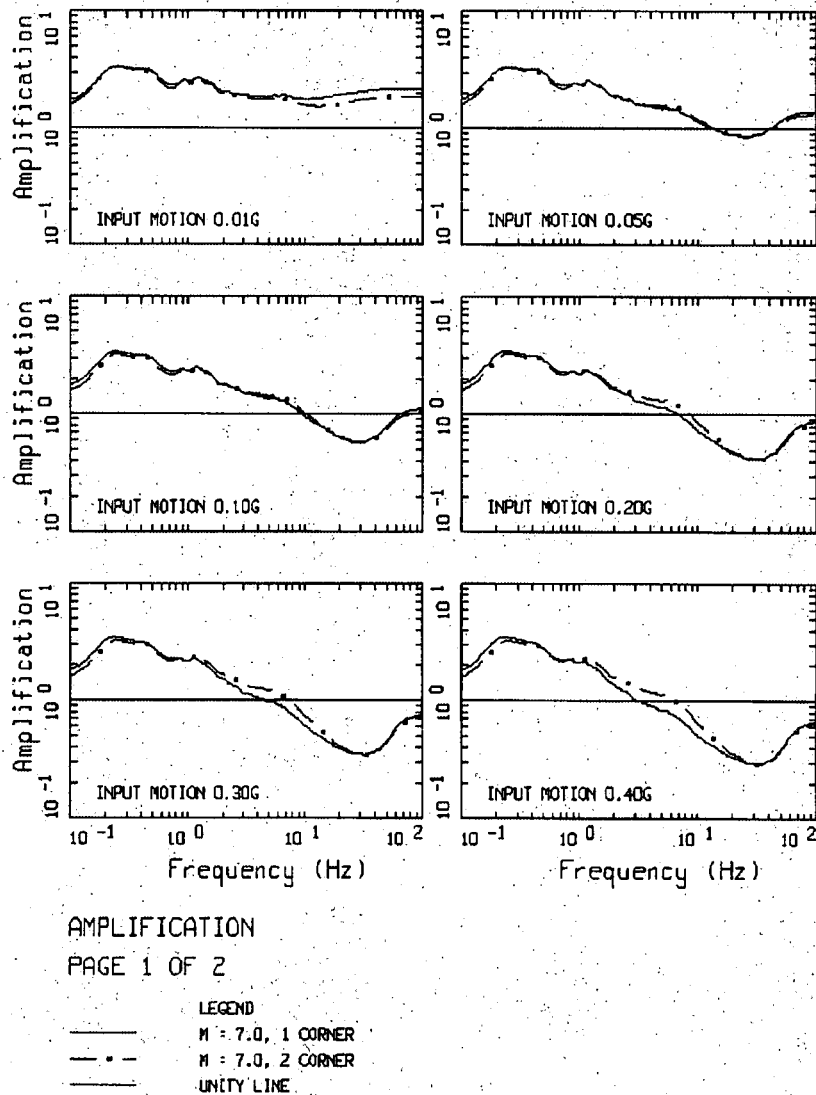
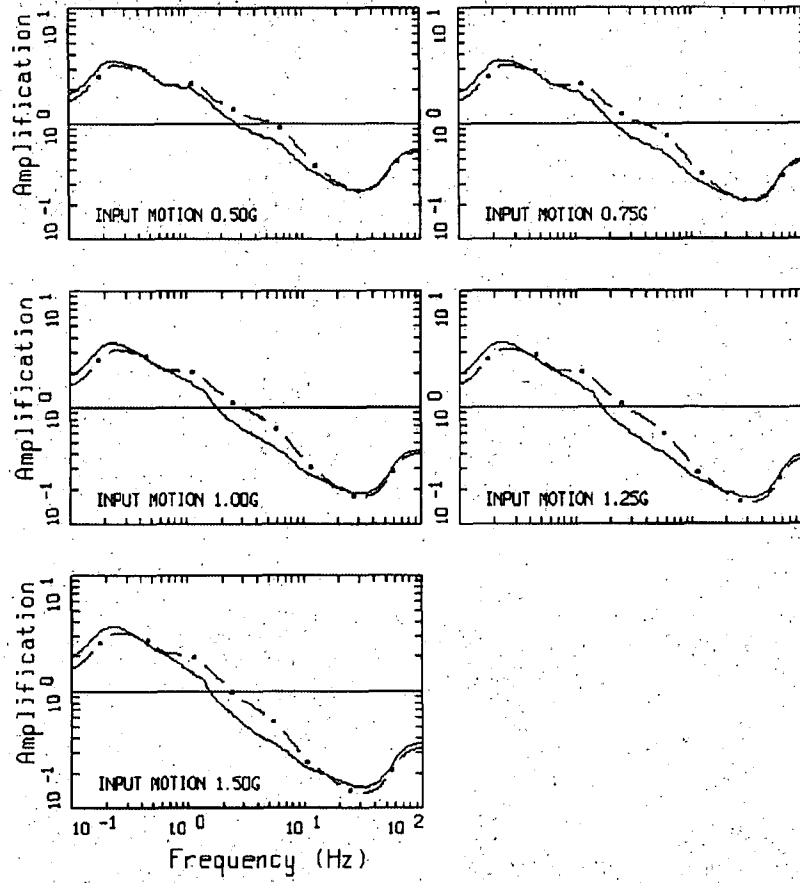


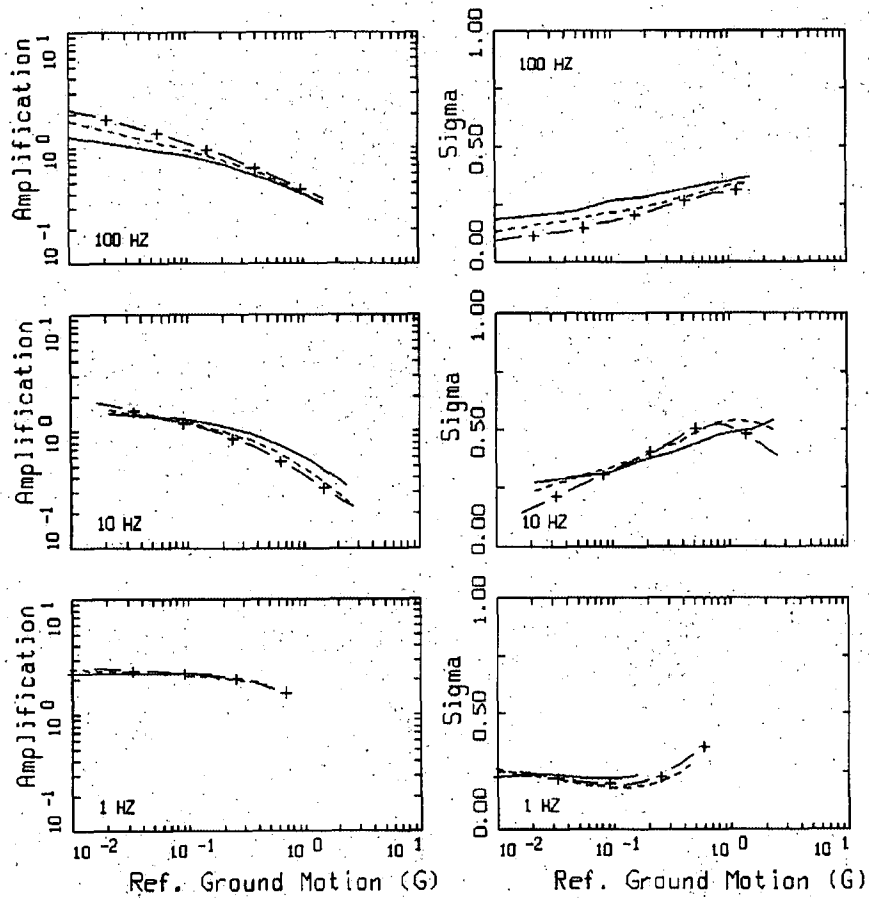
Figure 5. Test case illustrating the effect of single-versus double-corner source spectra on median amplification factors computed for a deep soil site in the CENA. Distances were adjusted to obtain the target hard rock (input) median peak acceleration values. Plotted versus structural frequency.



AMPLIFICATION
PAGE 2 OF 2

LEGEND
— M = 7.0, 1 CORNER
- - - M = 7.0, 2 CORNER
— UNITY LINE

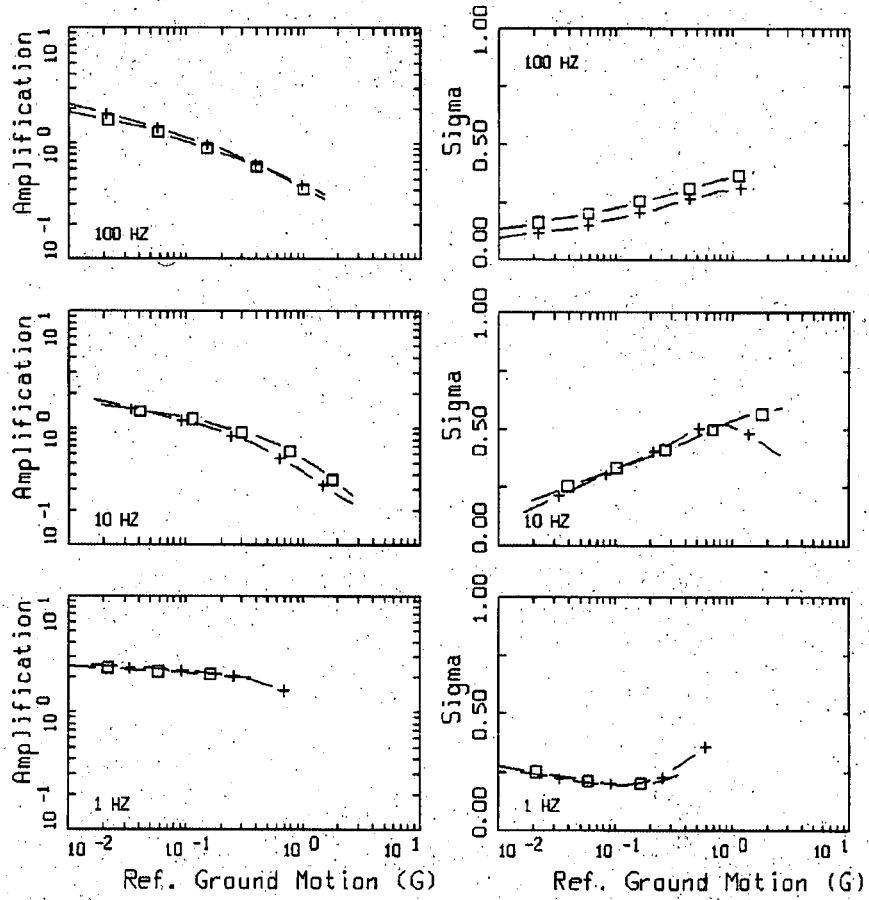
Figure 5 (cont.)



MEDIAN AMPLIFICATION AND SIGMA

LEGEND	
—	M5.0, 1 CORNER
- - -	M6.0, 1 CORNER
- + -	M7.0, 1 CORNER

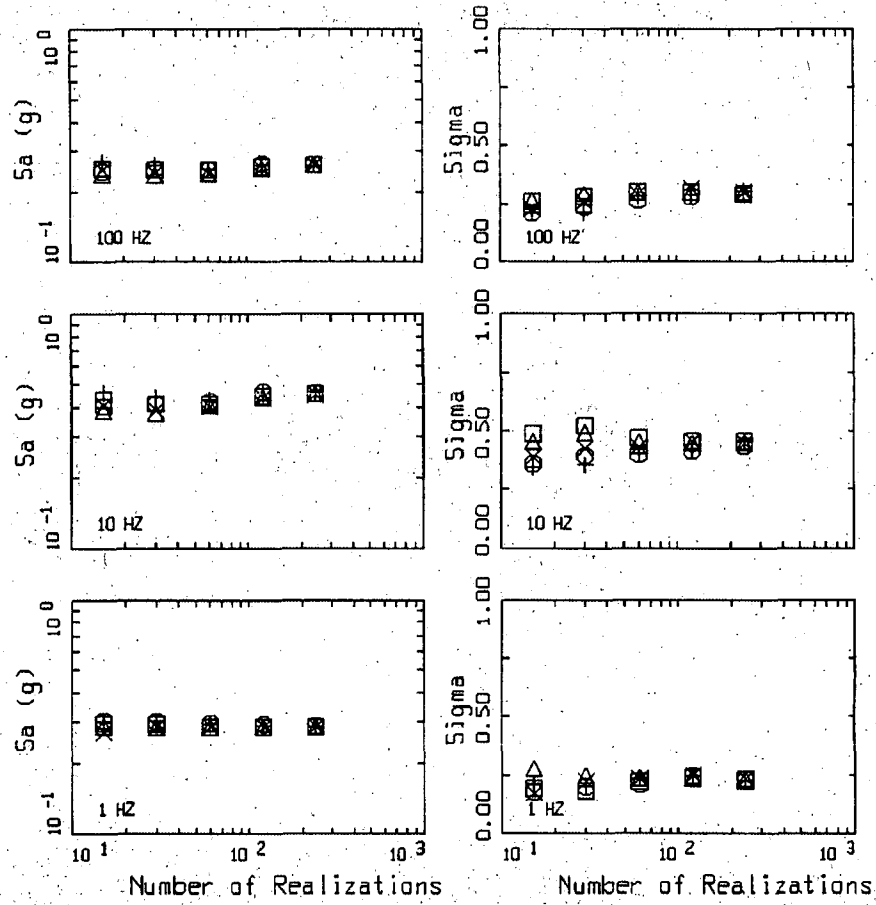
Figure 6. Test case illustrating the effect of magnitude on median amplification factors and sigma values (σ_n) computed for a deep soil site in the CENA. Plotted versus reference site ground motion (5% damped S_a) at three structural frequencies.



MEDIAN AMPLIFICATION AND SIGMA

LEGEND
 — + — M7.0, 1 CORNER
 — □ — M7.0, 2 CORNER

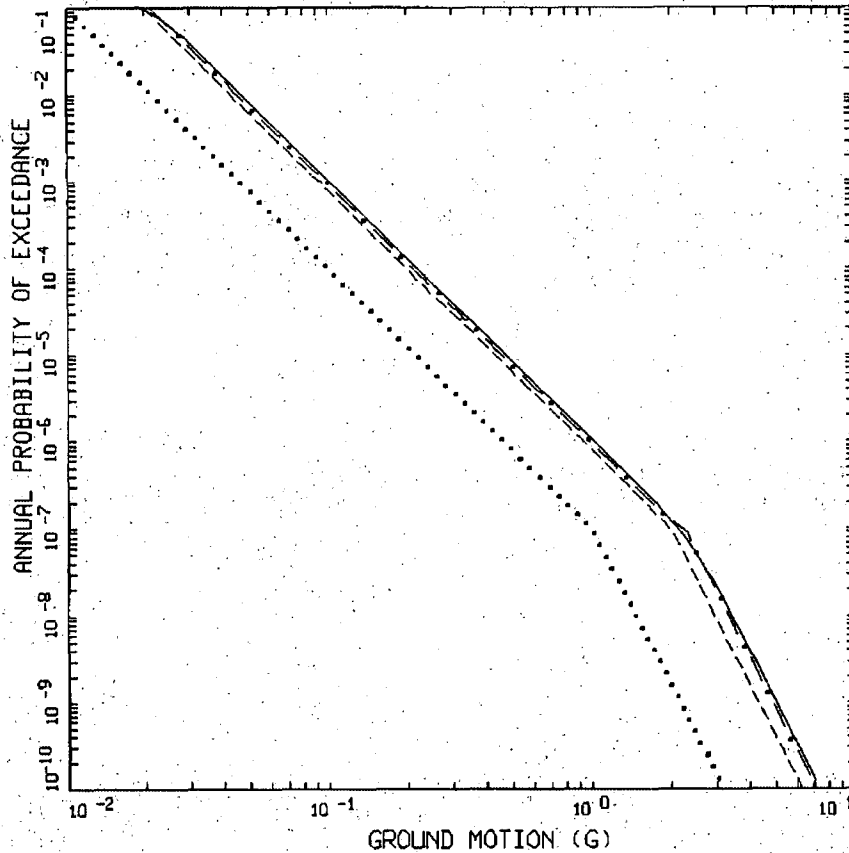
Figure 7: Test case illustrating the effect of single-verses double-corner source spectra on median amplification factors and sigma values (σ_m) computed for a deep soil site in the CENA. Plotted verses reference site ground motion (5% damped S_a) at three structural frequencies.



SPECTRAL ACCELERATION AND SIGMA

LEGEND	
□	S1
×	S2
△	S3
○	S4
+	S5

Figure 8. Median spectral acceleration (Sa) and sigma estimates computed for numbers of realizations from 15 to 240 using five different random seeds for a deep soil site in the CENA.

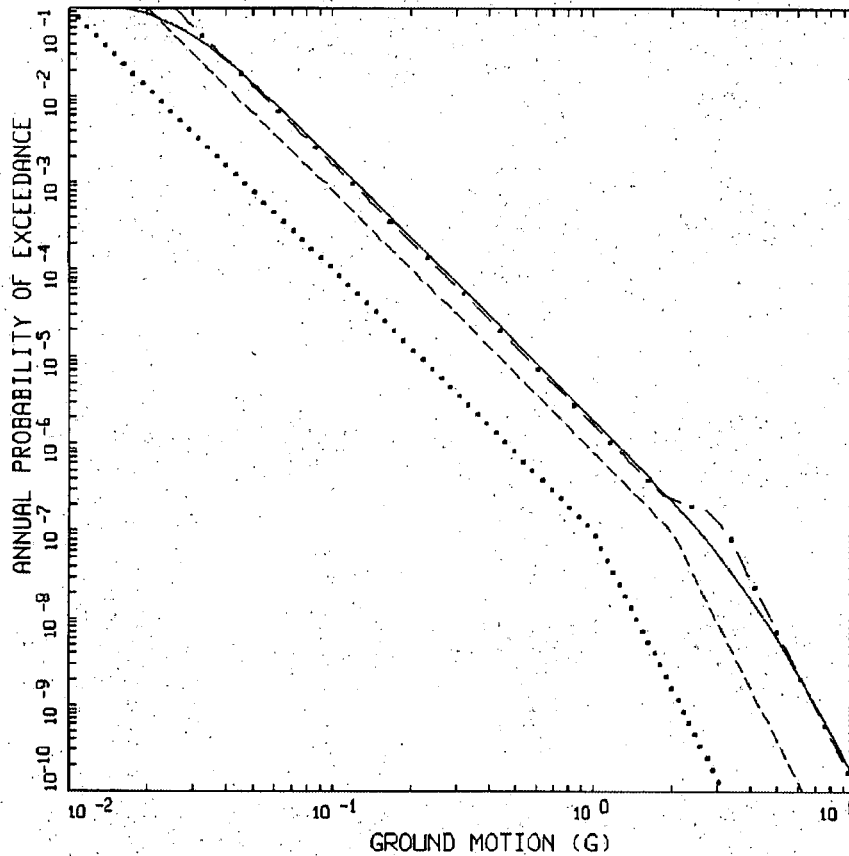


TEST EXAMPLE
 AMP=2.0, SIGMA AMP=0.20

- LEGEND
- INPUT ROCK HAZARD CURVE, SLOPES=3,6
 - INPUT ROCK HAZARD CURVE MULTIPLIED BY AMP=2.0
 - . - . - . OUTPUT SOIL HAZARD CURVE: APPROACH 3 APPROXIMATE
 - OUTPUT SOIL HAZARD CURVE: APPROACH 3 FULL INTEGRATION

Figure 9. Test case illustrating Approach 3 using a simple bilinear reference site hazard curve (dotted line, slope = 3, 6). Median amplification factor is 2.0, $\sigma_{in} = 0.2$. Dashed line, reference hazard times median amplification, very close to Approach 2

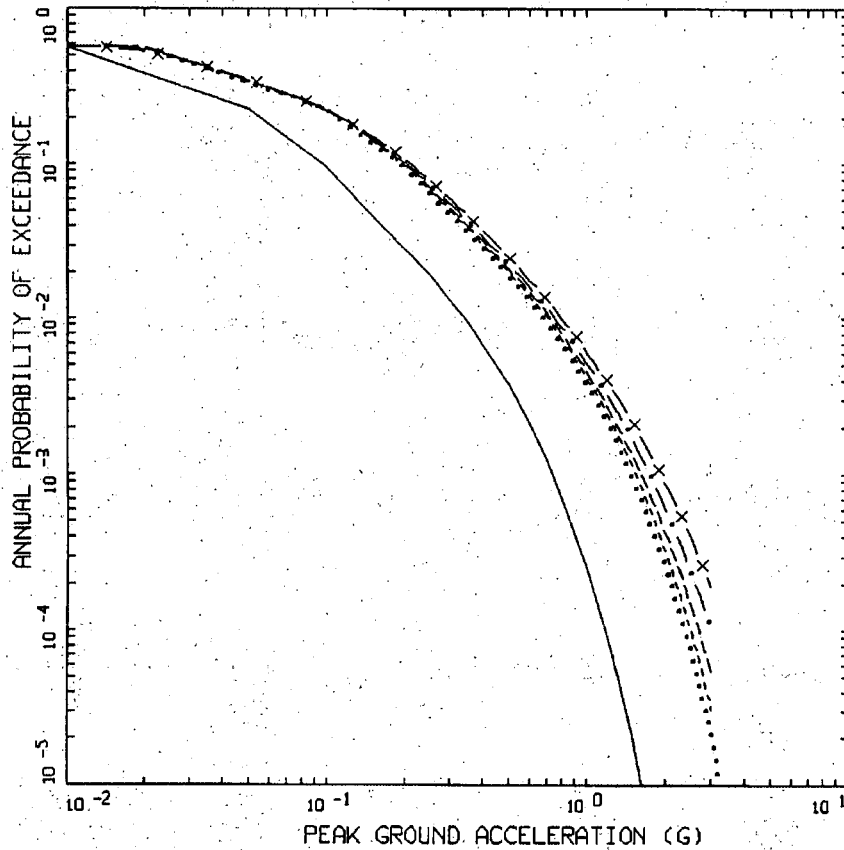
which uses mean amplification (mean = median $e^{\frac{\sigma^2}{2}}$). Dashed-dot line represents approximate Approach 3 (Equation 7), solid line is full integration Approach 3 (Equation 5). Note the impact of the reference hazard curve slope on the difference between Approaches 2 and 3.



TEST EXAMPLE
AMP=2.0, SIGMA AMP=0.40

- LEGEND
- INPUT ROCK HAZARD CURVE, SLOPES=3,6
 - INPUT ROCK HAZARD CURVE MULTIPLIED BY AMP=2.0
 - . - . - . OUTPUT SOIL HAZARD CURVE: APPROACH 3 APPROXIMATE
 - OUTPUT SOIL HAZARD CURVE: APPROACH 3 FULL INTEGRATION

Figure 10. Test case illustrating Approach 3 using a simple bilinear reference site hazard curve (dotted line, slope = 3, 6). Median amplification factor is 2.0, $\sigma_{ln} = 0.4$. Dashed-line, reference hazard times median amplification, very close to Approach 2 which uses mean amplification (mean = median $e^{\frac{\sigma^2}{2}}$). Dashed-dot line represents approximate Approach 3 (Equation 7), solid line is full integration Approach 3 (Equation 5). Note the impact of the reference hazard curve slope on the difference between Approaches 2 and 3.

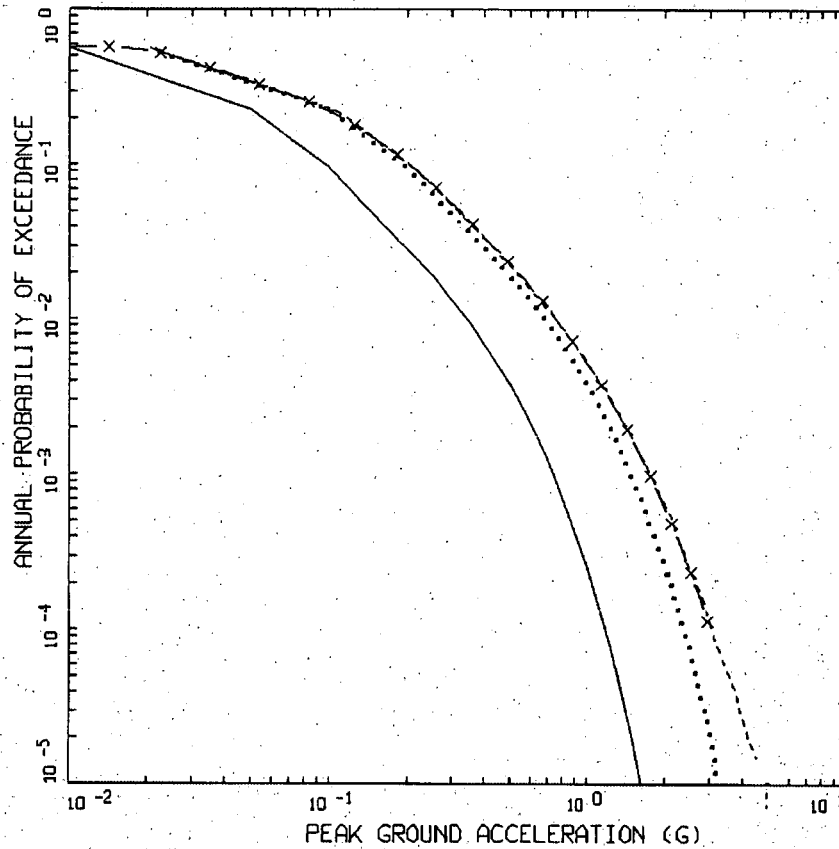


TEST EXAMPLE: PGA HAZARD CURVE
AMP FACTOR = 2.0

- LEGEND
- INPUT HAZARD CURVE
 - INPUT HAZARD CURVE SCALED BY AMP=2.0
 - - - - APPROACH 3 FULL INTEGRATION: SIGMA = 0.10
 - . - . APPROACH 3 FULL INTEGRATION: SIGMA = 0.20
 - - - - APPROACH 3 FULL INTEGRATION: SIGMA = 0.30
 - X - APPROACH 3 FULL INTEGRATION: SIGMA = 0.40

Figure 11. Test case illustrating Approach 3 using a realistic (WNA) reference site hazard curve (solid line). Median amplification factor is 2.0, $\sigma_{in} = 0.1, 0.2, 0.3, 0.4$. Dotted line, reference hazard times median amplification, very close to Approach 2

which uses mean amplification (mean = median $e^{\frac{\sigma^2}{2}}$). Note the impact of the reference hazard curve change in slope on the differences between Approaches 2 and 3 (full integration).

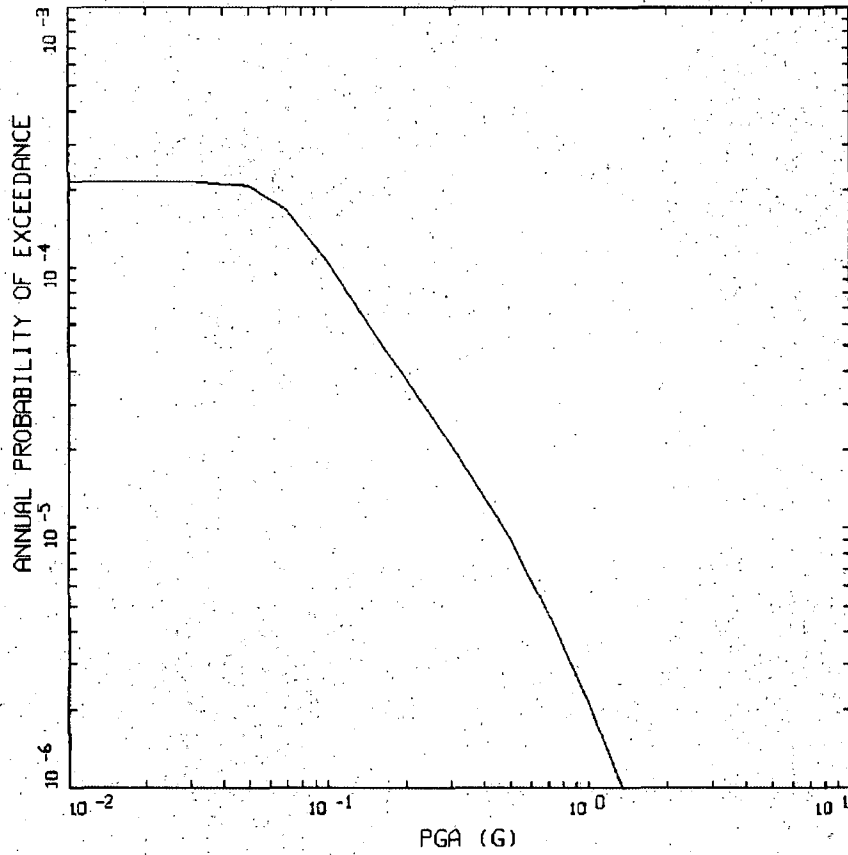


TEST EXAMPLE: PGA HAZARD CURVE
 AMP FACTOR = 2.0, SIGMA=0.30

- LEGEND
- INPUT HAZARD CURVE
 - INPUT HAZARD CURVE SCALED BY AMP=2.0
 - - - APPROACH 3 APPROXIMATE: SIGMA = 0.30
 - x - APPROACH 3 FULL INTEGRATION: SIGMA = 0.30

Figure 12. Test case illustrating Approach 3 using a realistic (WNA) reference site hazard curve (solid line). Median amplification factor is 2.0, $\sigma_{in} = 0.3$. Dotted line, reference hazard times median amplification, very close to Approach 2 which uses

mean amplification (mean = median $e^{\frac{\sigma^2}{2}}$). Dashed line represents approximate Approach 3 (Equation 7), solid crosses line reflects full integration Approach 3 (Equation 5). Note the impact of the reference hazard curve change in slope on the differences between Approaches 2 and 3 and the breakdown for approximate Approach 3 below AFE of 2×10^{-4} , in this case.



DUKE-LEE: HAZARD CURVE, MEAN
HARD ROCK, PGA

— LEGEND
MEAN, PGA

Figure 13. Lee Nuclear Site hard rock horizontal hazard curve for peak acceleration (Duke Energy Carolinas, LLC, 2007).

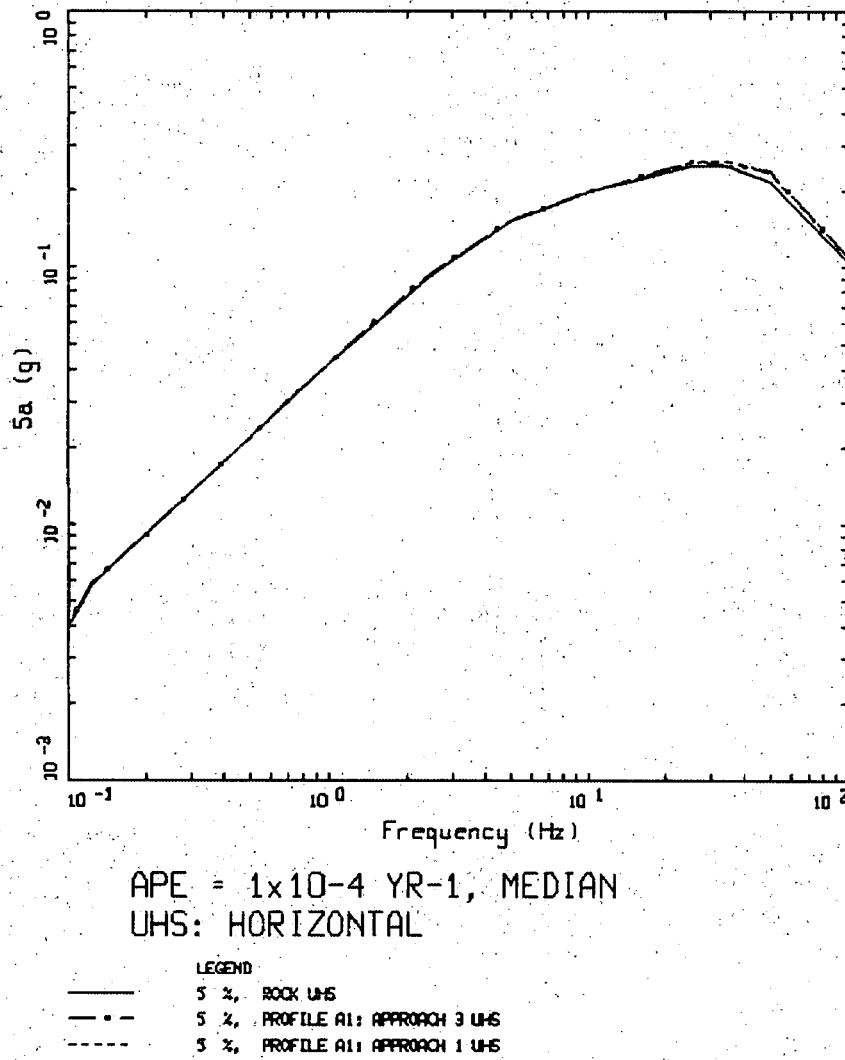


Figure 14. Lee Nuclear Station Unit 1 AEF 10^{-4} horizontal UHS. Hard rock and a comparison between deterministic Approach 1 (or 2, as Approaches 1 and 2 are identical for linear site response) and fully probabilistic Approach 3.

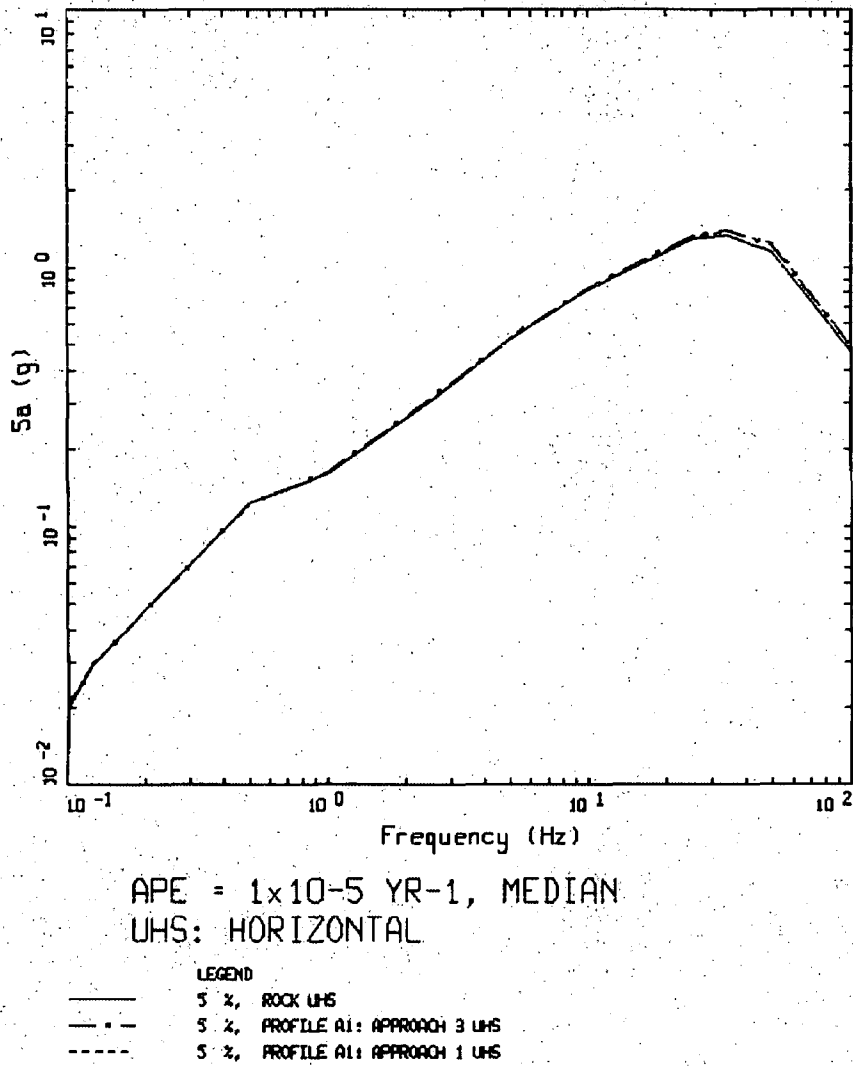


Figure 15. Lee Nuclear Station Unit 1 AEF 10^{-5} horizontal UHS. Hard rock and a comparison between deterministic Approach 1 (or 2, as Approaches 1 and 2 are identical for linear site response) and fully probabilistic Approach 3.

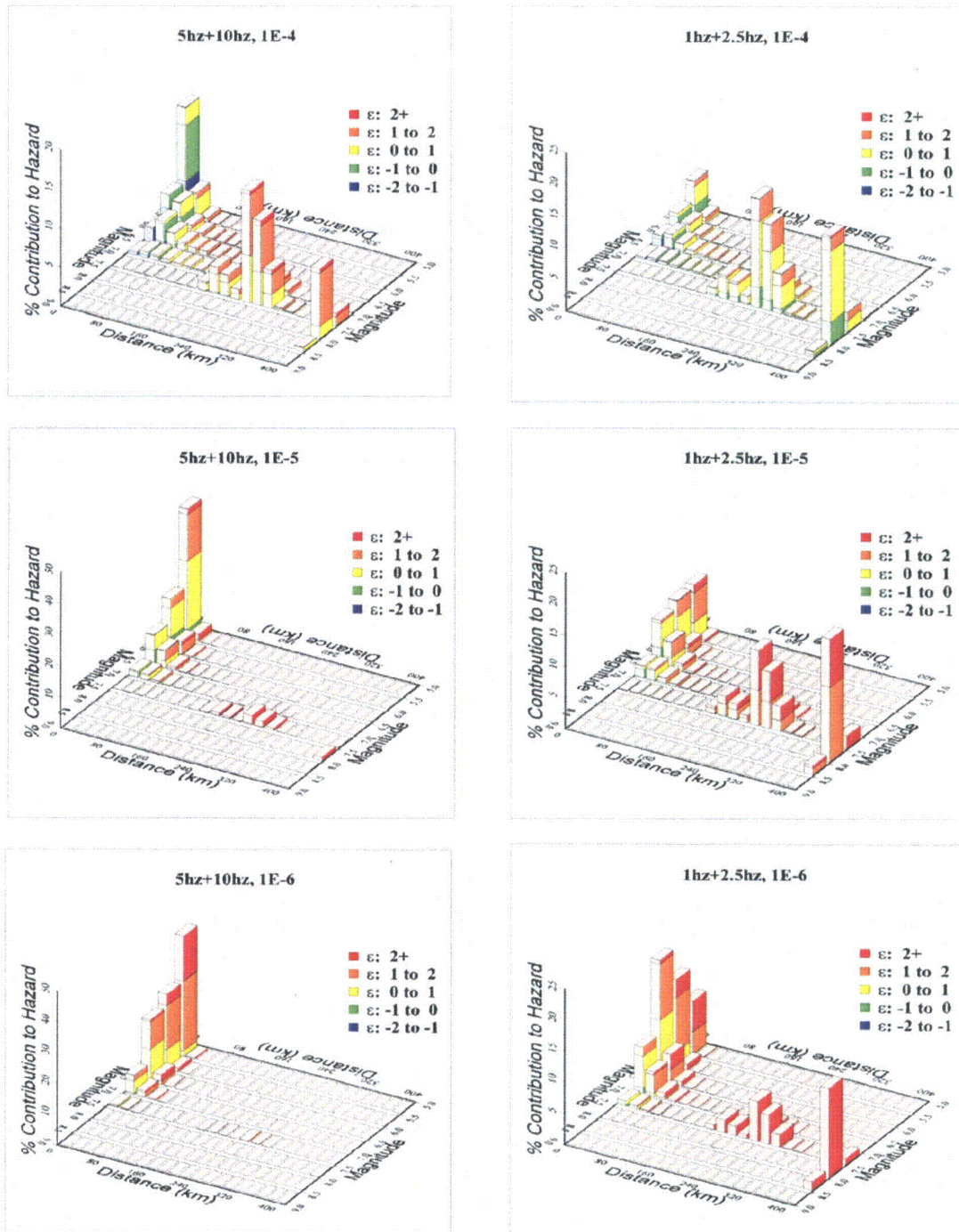
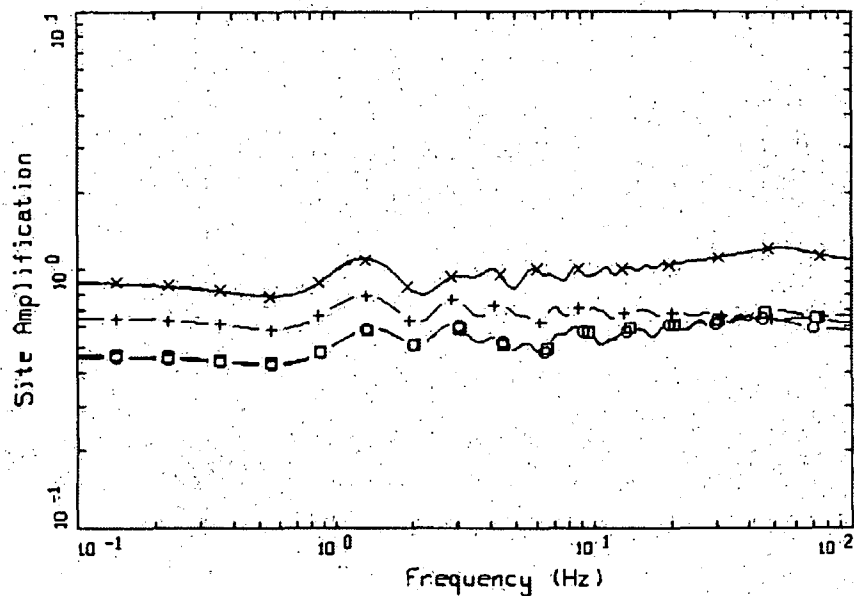


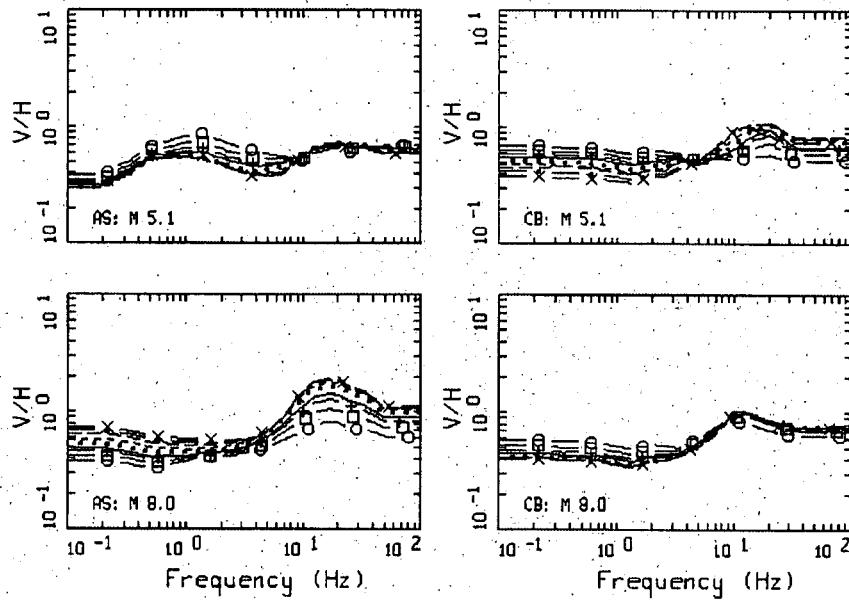
Figure 16. High-frequency (≥ 5 Hz) and low-frequency (≤ 2.5 Hz) hard rock hazard deaggregation for the Lee Nuclear Site (Duke Energy Carolinas, LLC, 2007).



V/H RATIOS
UNIT 1 FIRS

LEGEND	
—○—	50TH PERCENTILE, D = 80 KM, 0.01 g (D= 50 MI, 0.01g)
—□—	50TH PERCENTILE, D = 16 KM, 0.10 g (D= 10 MI, 0.10g)
—+—	50TH PERCENTILE, D = 7 KM, 0.20 g (D= 4 MI, 0.20g)
—x—	50TH PERCENTILE, D = 0 KM, 0.30 g (D= 0 MI, 0.30g)
—	50TH PERCENTILE, D = 0 KM, 0.50 g (D= 0 MI, 0.50g)

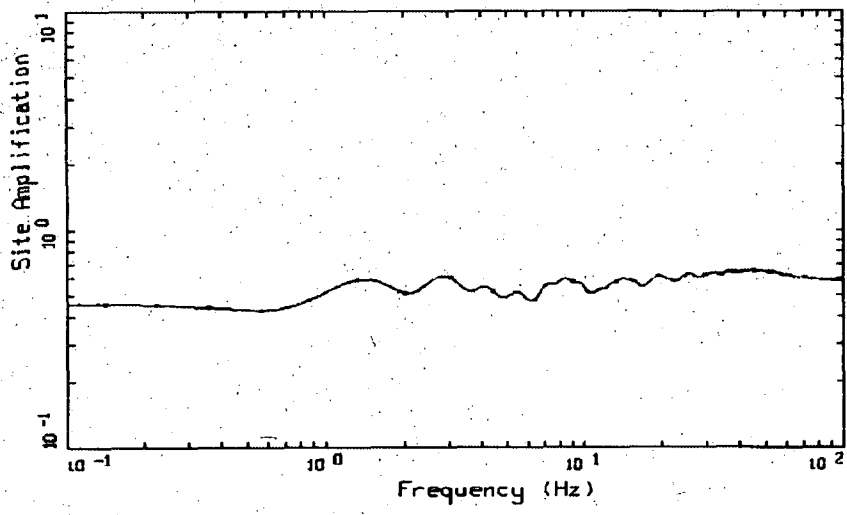
Figure 17. Site-specific median V/H ratios computed for the Lee Nuclear Station Unit 1 for M 5.1 at a suite of distances. Due to profile stiffness linear analyses were performed resulting in magnitude independent V/H ratios.



EMPIRICAL V/H RATIOS FOR SOFT ROCK

LEGEND	
—○—	DISTANCE = 57 KM
—□—	DISTANCE = 31 KM
—+—	DISTANCE = 19 KM
—	DISTANCE = 14 KM
.....	DISTANCE = 8 KM
----	DISTANCE = 5 KM
----	DISTANCE = 3 KM
—•—	DISTANCE = 2 KM
—x—	DISTANCE = 1 KM

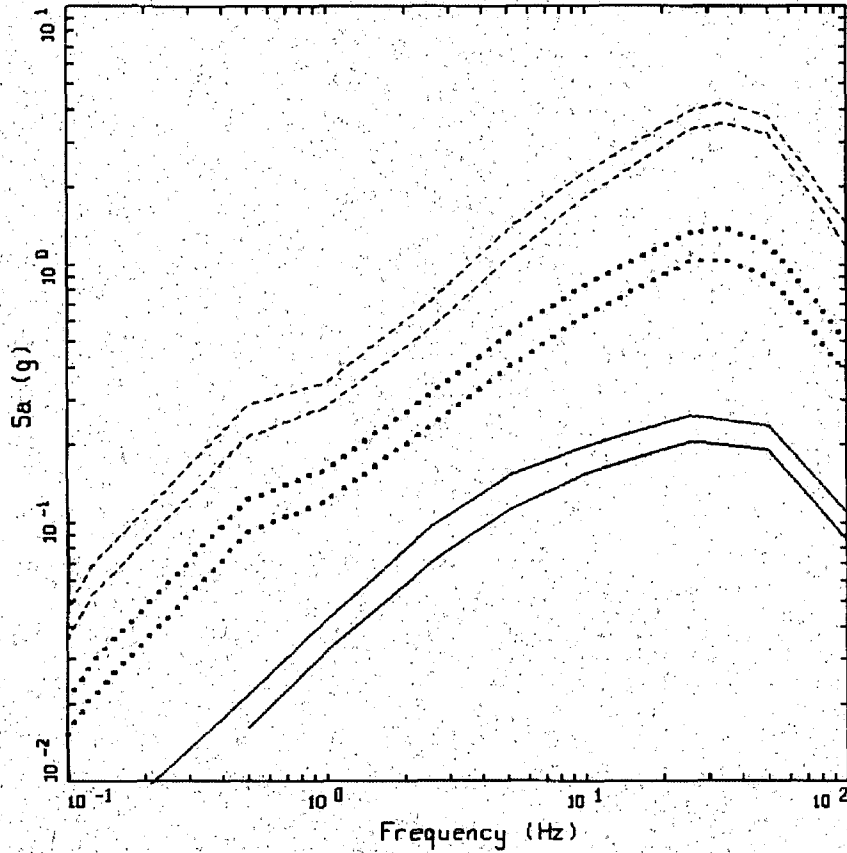
Figure 18. Empirical WNA soft rock median V/H ratios: AS, Abrahamson and Silva, 1997; CB, Campbell and Bozorgnia, 2003 computed for M 5.1 and M 8.0 at a suite of distances.



V/H RATIOS
UNIT 1

- LEGEND
- - - 84TH PERCENTILE
— 50TH PERCENTILE
- - - 16TH PERCENTILE

Figure 19. Site-specific median and ± 1 sigma V/H ratios computed for the Lee Nuclear Station Unit 1 for M 5.1 at a distance of 80 km. Due to profile stiffness linear analyses were performed resulting in magnitude independent V/H ratios. Sigma reflects aleatory variability in shear- and compressional-wave velocities and depth to basement material across the site.



PROFILE A1
UHS: HORIZONTAL AND VERTICAL

- LEGEND
- 5 % HORIZONTAL UHS, MEAN, 1×10^{-6} AEP
 - 5 % VERTICAL UHS, MEAN, 1×10^{-6} AEP
 - 5 % HORIZONTAL UHS, MEAN, 1×10^{-5} AEP
 - 5 % VERTICAL UHS, MEAN, 1×10^{-5} AEP
 - 5 % HORIZONTAL UHS, MEAN, 1×10^{-4} AEP
 - 5 % VERTICAL UHS, MEAN, 1×10^{-4} AEP

Figure 20: Horizontal and vertical component UHS at annual exceedance probabilities 10^{-4} , 10^{-5} , 10^{-6} yr^{-1} : Lee Nuclear Station Unit 1.

8.0 Appendices

Appendix A – Modification of Herrmann's Duration Formula

Appendix B – Criteria for Adjusting Kappa

Appendix C – Limitations of Stochastic Point-source Modeling

Appendix A

Modification of Herrmann's Duration Formula

Table of Contents

List of Tables.....	A2
List of Figures.....	A2
1.0 PURPOSE AND SCOPE.....	A4
2.0 ASSUMPTIONS.....	A4
3.0 DISCUSSION.....	A4
4.0 SUMMARY.....	A6
5.0 REFERENCES.....	A6
6.0 TABLES AND FIGURES.....	A8

List of Tables

Table A1 Model Parameters.....	A8
--------------------------------	----

List of Figures

Figures A1a-c. Example of the empirical duration model developed in Silva et al. (1996). Figures taken from McGuire et. al (2001, NUREG/CR-6728) where the duration model was used to define acceptable ranges in duration based on magnitude, rupture distance, and site condition for development and use of analysis time histories. Magnitudes illustrated are M 5.5, 6.5, and 7.5 in Figures A1a, A1b and A1c respectively.....A9

Figure A2. Median estimates of amplification factors (5% damped response spectra) computed for M 6.0 and a deep firm soil site in the CENA using the EPRI (1993; FSAR Reference 2.5.2-273) modulus reduction and hysteretic damping curves. Comparison using path duration with R-1 and R-10 distance dependencies based on Table A1 model parameters.....A12

Figure A3. Median estimates of reference site (hard CENA rock) and soil site (deep firm CENA soil) response spectra (5% damped) computed for M 6.0 using the EPRI (1993; FSAR Reference 2.5.2-273) modulus reduction and hysteretic damping curves (soil site), reference site median peak acceleration is 0.01g. Comparison using path duration with R-1 and R-10 distance dependencies based on Table A1 model parameters.....A14

Figure A4. Median estimates of reference site (hard CENA rock) and soil site (deep firm CENA soil) response spectra (5% damped) computed for M 6.0 using the EPRI (1993; FSAR Reference 2.5.2-273) modulus reduction and hysteretic damping curves (soil site), reference site median peak acceleration is 0.50g. Comparison using path duration with R-1 and R-10 distance dependencies based on Table A1 model parameters.....A15

Figure A5. Median estimates of reference site (hard CENA rock) and soil site (deep firm CENA soil) response spectra (5% damped) computed for M 6.0 using the EPRI (1993; FSAR Reference 2.5.2-273) modulus reduction and hysteretic damping curves (soil site), reference site median peak acceleration is 1.50g. Comparison using path duration with R-1 and R-10 distance dependencies based on Table A1 model parameters.....A16

1.0 Purpose and Scope

This appendix addresses the use of a modification of Herrmann's duration formula, $T=1/fc+0.05R$, in the site response analysis for Lee Nuclear Station Unit 1. Based on methodologies advanced subsequent to the initial publication of Herrmann's duration formula, the site response analysis utilizes a modification of the path component R. Justification for this modification includes attribution and utilization of an unpublished document (Silva et al., 1996; FSAR Reference 2.5.2-288).

2.0 Assumptions

None.

3.0 Discussion

The propagation path component of the duration was originally developed by Herrmann (1985; Reference 1) based on 1D modeling of Lg wave propagation in Central Eastern North America (CENA), where Lg waves are short-period, higher mode surface waves with a group velocity of about 3.5 kilometers (km) per second. The 0.05R factor was based on judgment from a visual inspection of the increased complexity of the Lg wavetrain at increasing epicentral distances ranging from 1 km to 300 km. The combination of a R^{-1} ($R^{1/2}$, $R > 100$ km) geometrical attenuation with a 0.05R distance dependency in duration (slowly increasing motion durations with increasing distance, conditional on magnitude) resulted in a net time domain dependence at large distance varying approximately as $R^{-5/6}$, the overall distance dependency of peak motions in CENA observed in this time frame.

Subsequently the simple path duration model of Herrmann (1985; Reference 1) has been updated with analyses using CENA as well as Western North America (WNA) data. More recent quantitative criteria for time domain durations appropriate for random vibration theory (RVT) have included the 5% to 75% buildup of normalized Arias Intensity of acceleration (e.g. References 2, 3, and 4) as well as the duration required to match the observed peak velocity and the expected peak velocity based on RVT (Reference 5 and FSAR References 2.5.2-208 and 2.5.2-298). These more recent refinements of the path duration model were intended to provide more accurate estimates of expected motions and were based on data generally exceeding hypocentral distances of about 10 km in WNA and 20 km in CENA. The recent analyses showed that duration increased in a complicated and frequency dependent manner with distance likely due to wave scattering and perhaps dispersion. Some models have adopted a frequency independent but non-monotonic distance dependence for duration (Reference 6 and FSAR Reference 2.5.2-208) while others employ the simple model of 0.05R (References 7 and 8, and FSAR References 2.5.4-219, and 2.5.2-273) because the stochastic model is relatively insensitive to details in the path duration model. For distances beyond about 10 km, the essential aspect of the path duration for the stochastic model is an overall increase with distance at a rate of about five seconds per 100 km (0.05R) (FSAR Reference 2.5.2-298). Also, in view of the neglect of potential frequency dependence of the path duration in the stochastic model due to the relative insensitivity to changes in duration, a simple path model is considered to sufficiently capture the effects of an increase in duration with distance. This is particularly the case for computing site amplification, where the effects of duration largely ("approximately") cancel in taking ratios of soil motions (5% damped spectral acceleration) to rock motions (compare to

RAI Response 02.05.02-010) since to first-order the influence of duration is comparable for the rock input motions and the soil motions that use the same rock motions as input.

The modification of Herrmann's term of $0.05R$ to $R-10$ for WNA was based on results from an empirical duration model developed by Silva et al (1996; FSAR Reference 2.5.2-288). In that model duration was defined as the time between the 5% and 75% normalized Arias Intensity as in the ergodic window defined by Ou and Herrmann (1990; Reference 3). This is approximately the time interval where the slope in the normalized Arias Intensity plot is constant, reflecting a uniform build-up of power and a reasonable measure of duration that is independent of frequency. Based on analyses of the WNA strong motion data available at that time (Reference 9), the empirical model showed a constant duration within a 10 km rupture distance across magnitude and site condition (soft rock and deep firm soil). Figures DUK-PR-022-A1a, DUK-PR-022-A1b and DUK-PR-022-A1c show the distance dependency of the empirical duration model for soft rock sites at magnitudes M 5.5, 6.5, and 7.5 (FSAR Reference 2.5.2-251) respectively. At all three magnitudes the 5% to 75% normalized Arias Intensity duration is constant out to 10 km and the increase in duration due to propagation path effects is approximately 5 seconds per 100 km, consistent with that of Herrmann (1985; Reference 1) for CENA hard rock sites. The duration within 10 km is due principally to the source and site, with little contribution from wave scattering. Also, the source duration for the point-source model is roughly 1, 3, and 9 seconds for magnitudes 5, 6, and 7, also consistent with the empirical duration model at rupture distances within 10 km.

It should also be noted the mixing of rupture and hypocentral distance metrics, while not strictly correct, is conventional due to the use of a point-source model. The distance metric is of no practical consequence because of the relative insensitivity to the differences in path duration within 10 km using rupture versus hypocentral distance. The original $0.05R$ factor developed by Herrmann (1985; Reference 1) was actually an epicentral distance and implemented subsequently as a hypocentral distance (Reference 7 and FSAR Reference 2.5.2-298). The 0.05 ($R-1$) modification to the Herrmann (1985; Reference 1) path duration dependency simply reflects an assumption that there is no contribution to path duration within one kilometer of a source in CENA. This modification has implications for only very small earthquakes at very shallow depths and very close epicentral distances and for magnitude much less than M 5, where the source and path durations have comparable values. In these cases the difference between $R-1$ and R in the path duration can have a significant impact on the expected motions.

However, for all practical applications with M above 4.5 and in particular for computing site amplification, the effects of minor changes in the path duration model have very little impact. This is illustrated in Figure DUK-PR-022-A2, which shows median estimates of amplification of 5% damped spectral acceleration across structural frequency (0.1 Hz to 100 Hz) computed for a deep firm soil site in CENA. In Figure DUK-PR-022-A2 the magnitude is M 6.0 (single-corner source model) and the hard rock median peak acceleration ranges from 0.01g to 1.50g and comparisons are shown between a $R-1$ and a $R-10$ distance dependency in propagation path dependency. As Figure DUK-PR-022-A2 illustrates, across structural frequency and loading level, there is very little difference in amplification between using an $R-1$ or an $R-10$ dependency in the propagation path duration model. To illustrate the effects of the path model on absolute spectra, Figures DUK-PR-022-A3, DUK-PR-022-A4, and DUK-PR-022-A5 show both the hard rock outcrop as well as soil median spectra

(5% damped spectra acceleration) computed with R-1 compared to R-10 path dependencies at 0.01g, 0.50g, and 1.50g hard rock loading levels. As Figures DUK-PR-022-A3, DUK-PR-022-A4, and DUK-PR-022-A5 show, the differences in median estimates between the R-1 and R-10 path models are, as expected, larger than those shown in Figure DUK-PR-022-A2 for the median amplification factors but differences remain quite small. At a loading level of 0.50g, Figure DUK-PR-022-A4 shows the largest difference between the R-1 and R-10 path duration models with the shorter path duration (R-10) exceeding the R-1 model by a maximum of about 6% at high-frequency (5 Hz to 40 Hz). Table DUK-PR-022-A1 summarizes the model parameters and the durations at the three loading level 0.01g, 0.50g, and 1.50g. As Table DUK-PR-022-A1 shows, the largest difference in total duration occurs for 0.50g and is about 15% greater for the R-1 dependency compared to the R-10 path dependency. The maximum difference in median spectra is only 6% in Figure 4 and only about 3% in amplification as shown in Figure DUK-PR-022-A2, illustrating the weak dependency of the model on total duration.

4.0 Summary

Subsequent to 1985, the simple path duration model of Herrmann (1985) (need FSAR reference) has been updated with analyses using Central and Eastern North America as well as Western North America data. These more recent refinements of the path duration model were intended to provide more accurate estimates of expected motions. Calculations show that for all practical applications with M above 4.5 and in particular for computing site amplification, the effects of the minor changes in the path duration model have very little impact on estimated amplifications because of the weak dependency of the point-source model on total duration.

5.0 References:

- 1) Herrmann, R.B. (1985). "An extension of random vibration theory estimates of strong ground motion to large distance." *Bulletin of the Seismological Society of America*, 75(5), 1447-1453.
- 2) Fatehi, A. and R. B. Herrmann (2008). "High-frequency ground-motion scaling in the Pacific Northwest and in Northern and Central California." *Bulletin of the Seismological Society of America*, 98(2), 709-721.
- 3) Ou, G.B., and Herrmann, R.B. (1990). "Estimation theory for strong ground motion." *Seismological Research Letters*, 61(2), 99-107.
- 4) Raoof, M., R. B. Herrmann, and L. Malagnini (1999). "Attenuation and excitation of three-component ground motion in Southern California." *Bulletin of the Seismological Society of America*, 89(4) 888-902.

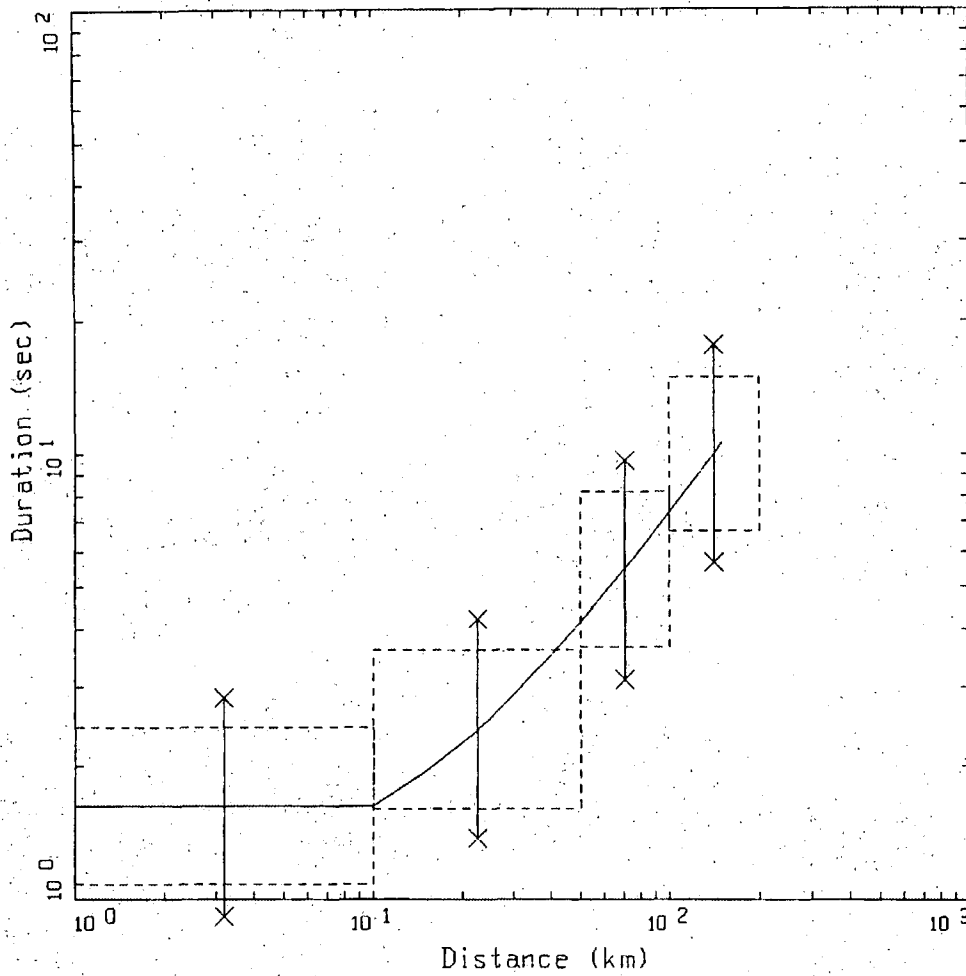
- 5) Atkinson, G.M. (1995). "Attenuation and source parameters of earthquakes in the Cascadia Region." *Bulletin of the Seismological Society of America*, 85(5), 1327-1342.
- 6) Atkinson, G.M. and D.M Boore (2006). "Earthquake ground-motion prediction equations for Eastern North America." *Bulletin of the Seismological Society of America*, 96(6), 2181-2205.
- 7) Atkinson, G.M and W.J. Silva (2000). "Stochastic modeling of California ground motions." *Bulletin of the Seismological Society of America*, 90(2), 255-274.
- 8) Tavakoli, B. and S. Pezeshk (2005). "Empirical-stochastic ground-motion prediction for Eastern North America." *Bulletin of the Seismological Society of America*, 95(6), 2283-2296.
- 9) Abrahamson, N.A and K.M. Shedlock (1997). "Overview." *Seismological Research Letters*, 68(1), 9-23.

6.0 Tables and Figures

Table A1 Model Parameters						
PGA(g)	Distance (km)	T _{source} (sec)	T _{path} (sec)		T _{total} (sec)	
			R-1	R-10	R-1	R-10
0.01	163, 8.0*	2.7	8.1	7.7	10.8	10.4
0.50	5.0, 8.0*	2.7	0.4	0.0	3.1	2.7
1.50	0.1, 3.5*	2.7	0.1	0.0	2.8	2.7

- M = 6.0
- $\Delta\sigma$ = 110 bars
- Q(f) = 670 f^{0.33}
- κ = 0.006 sec
- ρ = 2.71 cgs
- β = 3.52 km/sec
- R_c = 60 km
- T = 1/fc + 0.05 (R-1), R > 1; RVT duration, R = hypocentral distance (km)

* Source depth

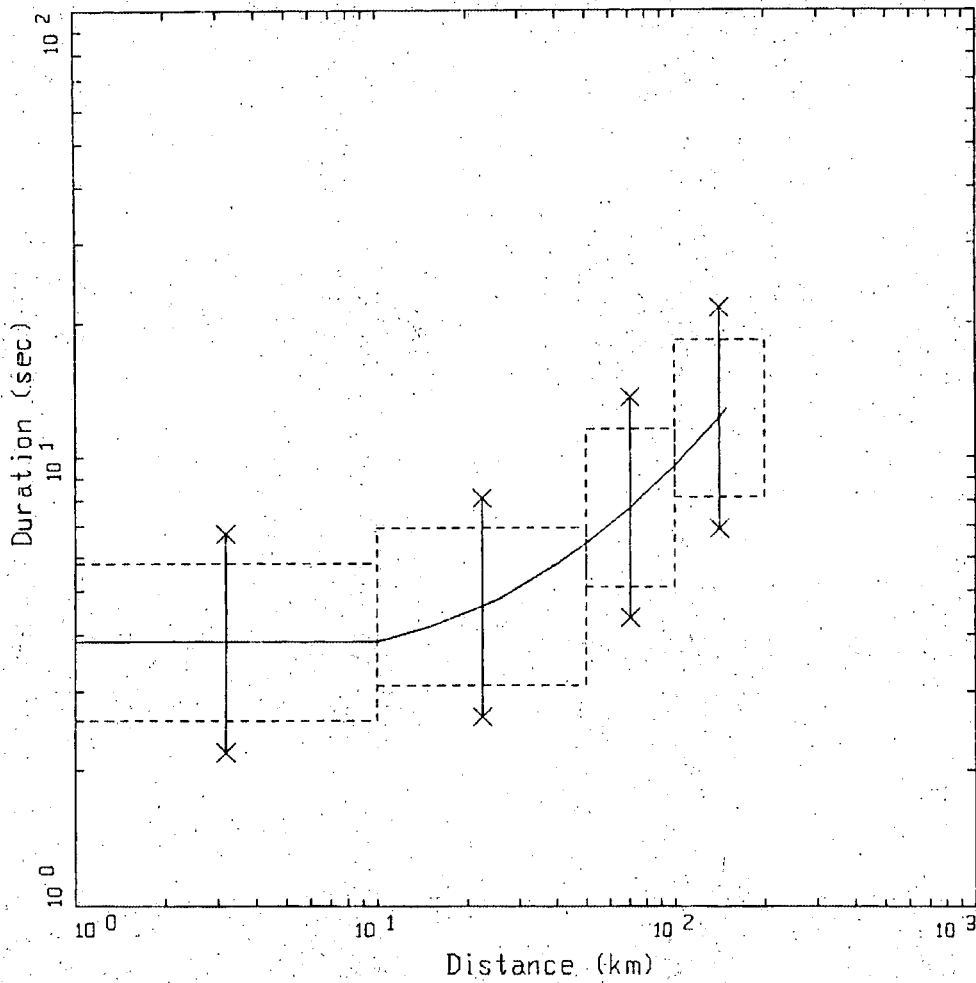


5-75% DURATION
ROCK SITE CONDITIONS, HORIZONTAL, M5.5

LEGEND

5-75% DURATION, HORIZONTAL, M=5.5

Figure A1a. Example of the empirical duration model developed in Silva et al. (1996; FSAR Reference 2.5.2-288). Figures taken from NUREG/CR-6728 (FSAR Reference 2.5.2-251) where the duration model was used to define acceptable ranges in duration based on magnitude, rupture distance, and site condition for development and use of analysis time histories. Magnitude illustrated is M 5.5.

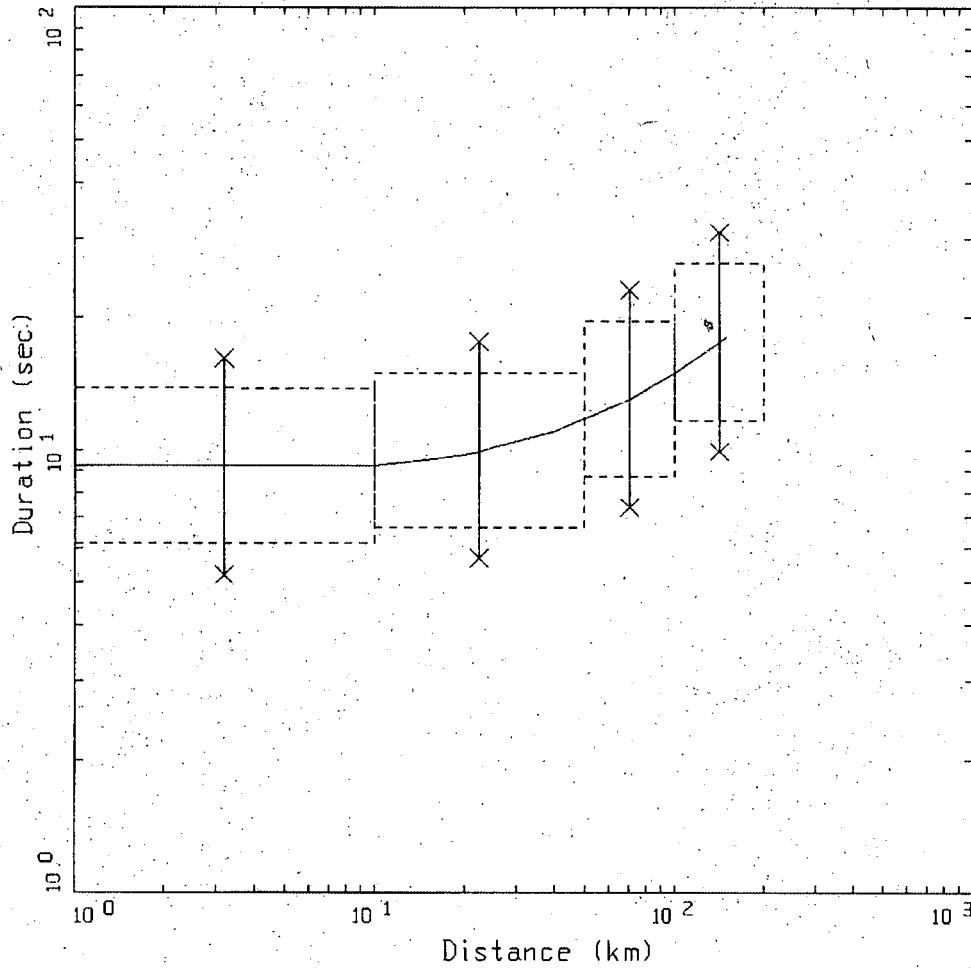


5-75% DURATION
ROCK SITE CONDITIONS, HORIZONTAL, M6.5

LEGEND

— 5-75% DURATION, HORIZONTAL, M=6.5

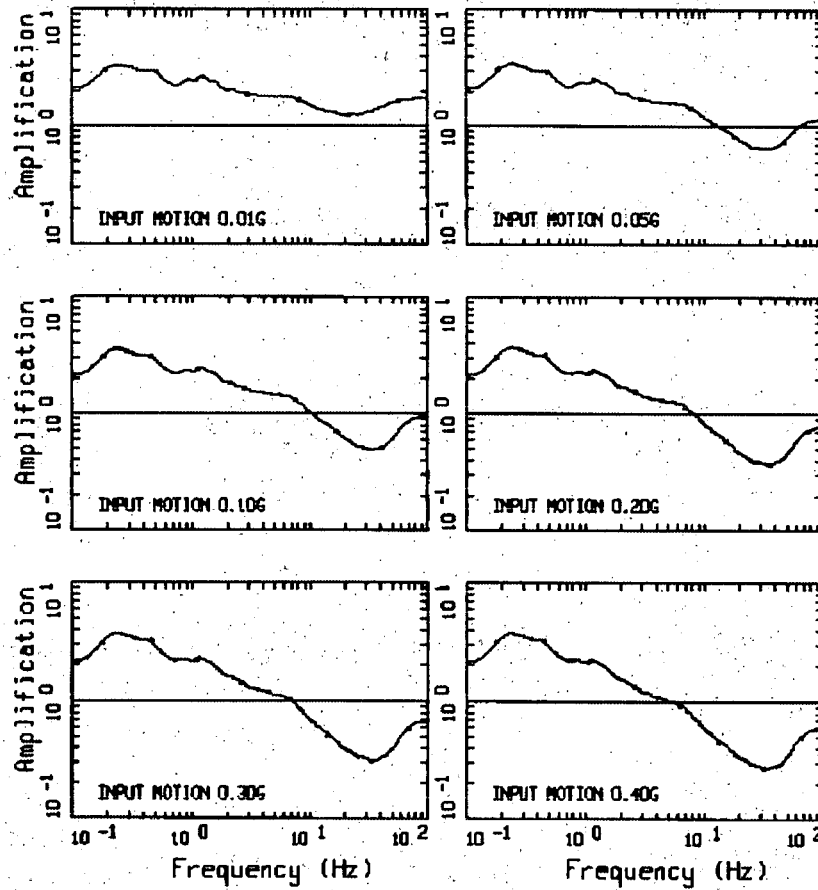
Figure A1b. Example of the empirical duration model developed in Silva et al. (1996; FSAR Reference 2.5.2-288). Figures taken from NUREG/CR-6728 (FSAR Reference 2.5.2-251) where the duration model was used to define acceptable ranges in duration based on magnitude, rupture distance, and site condition for development and use of analysis time histories. Magnitude illustrated is M 6.5.



5-75% DURATION
ROCK SITE CONDITIONS; HORIZONTAL, M7.5

LEGEND
—— 5-75% DURATION, HORIZONTAL, M=7.5

Figure A1c. Example of the empirical duration model developed in Silva et al. (1996; FSAR Reference 2.5.2-288). Figures taken from NUREG/CR-6728 (FSAR Reference 2.5.2-251) where the duration model was used to define acceptable ranges in duration based on magnitude, rupture distance, and site condition for development and use of analysis time histories. Magnitude illustrated is M 7.5.

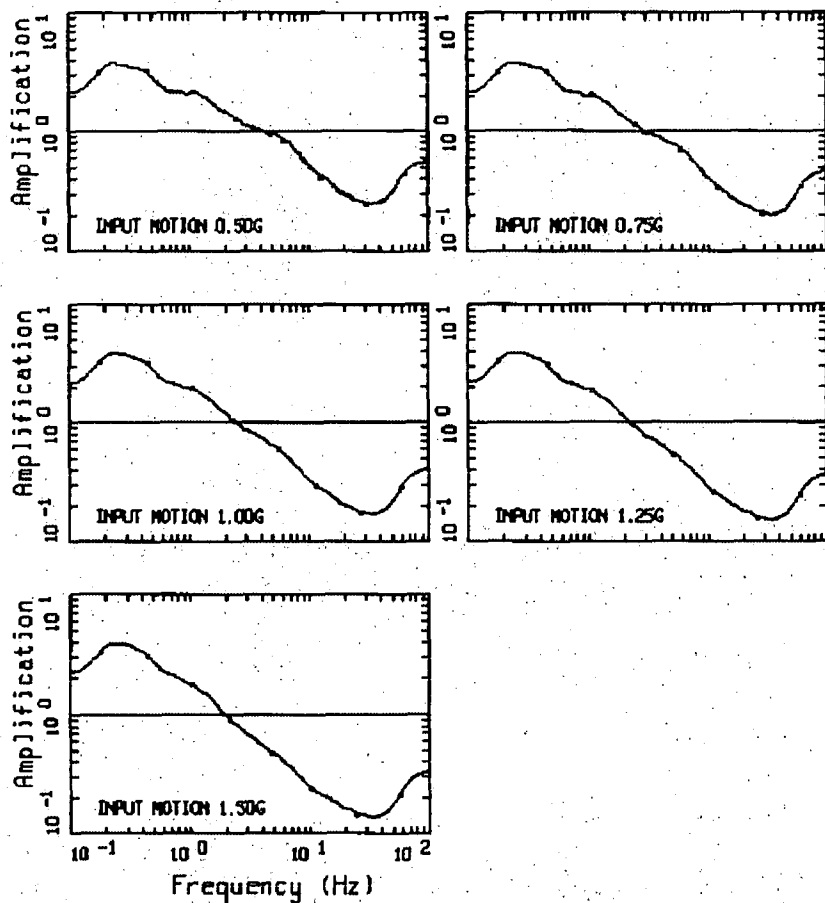


AMPLIFICATION

PAGE 1 OF 2

- LEGEND
- M = 6.00, 1 CORNER, (R-1) ± 0.05
 - - - M = 6.00, 1 CORNER, (R-10) ± 0.05
 - UNITY LINE

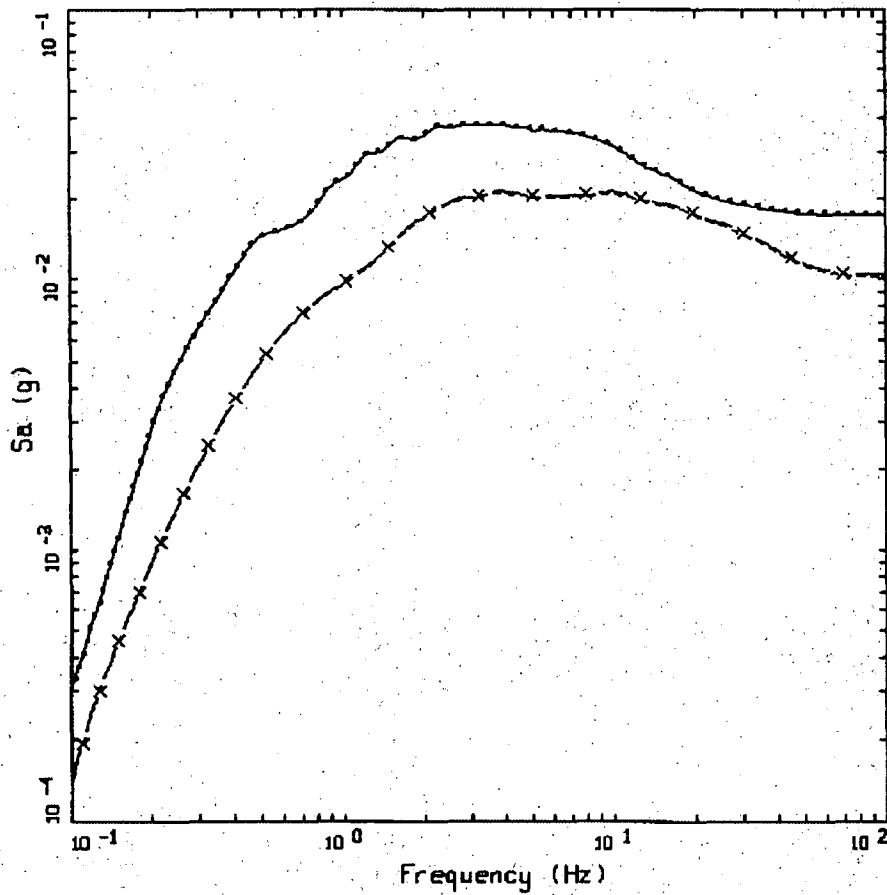
Figure A2. Median estimates of amplification factors (5% damped response spectra) computed for M 6.00 and a deep firm soil site in the CENA using the EPRI (1993; FSAR Reference 2.5.2-273) modulus reduction and hysteretic damping curves. Comparison using path duration with R-1 and R-10 distance dependencies based on Table A1 model parameters.



AMPLIFICATION
 PAGE 2 OF 2

LEGEND
 — M = 6.00, 1 CORNER, (R-1) ± 0.05
 - - - M = 6.00, 1 CORNER, (R-10) ± 0.05
 ——— UNITY LINE

Figure A2. (Continued) Median estimates of amplification factors (5% damped response spectra) computed for M 6.0 and a deep firm soil site in the CENA using the EPRI (1993; FSAR Reference 2.5.2-273) modulus reduction and hysteretic damping curves. Comparison using path duration with R-1 and R-10 distance dependencies based on Table A1 model parameters.

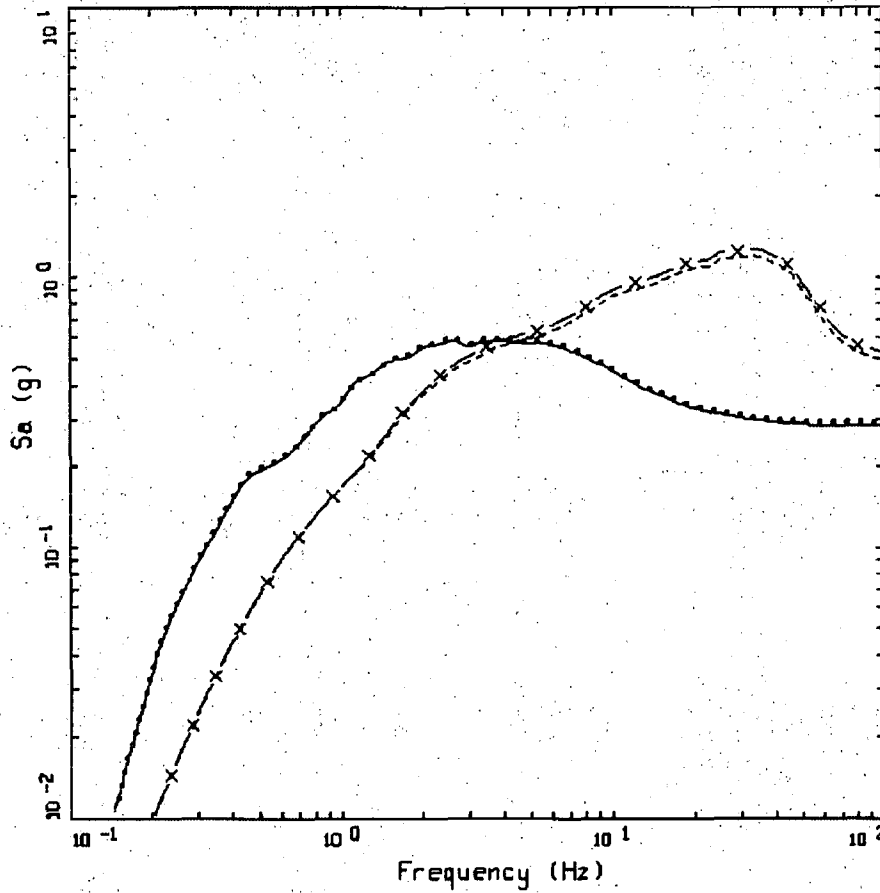


SOIL: M = 6.00, 1 CORNER
REFERENCE MOTION: 0.01 G

LEGEND

- 50TH PERCENTILE, SOIL, (R-1) = 0.05
- 50TH PERCENTILE, SOIL, (R-10) = 0.05
- - - 50TH PERCENTILE, HARD ROCK REFERENCE SITE, (R-1) = 0.05
- x - 50TH PERCENTILE, HARD ROCK REFERENCE SITE, (R-10) = 0.05

Figure A3. Median estimates of reference site (hard CENA rock) and soil site (deep firm CENA soil) response spectra (5% damped) computed for M 6.0 using the EPRI (1993; FSAR Reference 2.5.2-273) modulus reduction and hysteretic damping curves (soil site). reference site median peak acceleration is 0.01g. Comparison using path duration with R-1 and R-10 distance dependencies based on Table A1 model parameters.

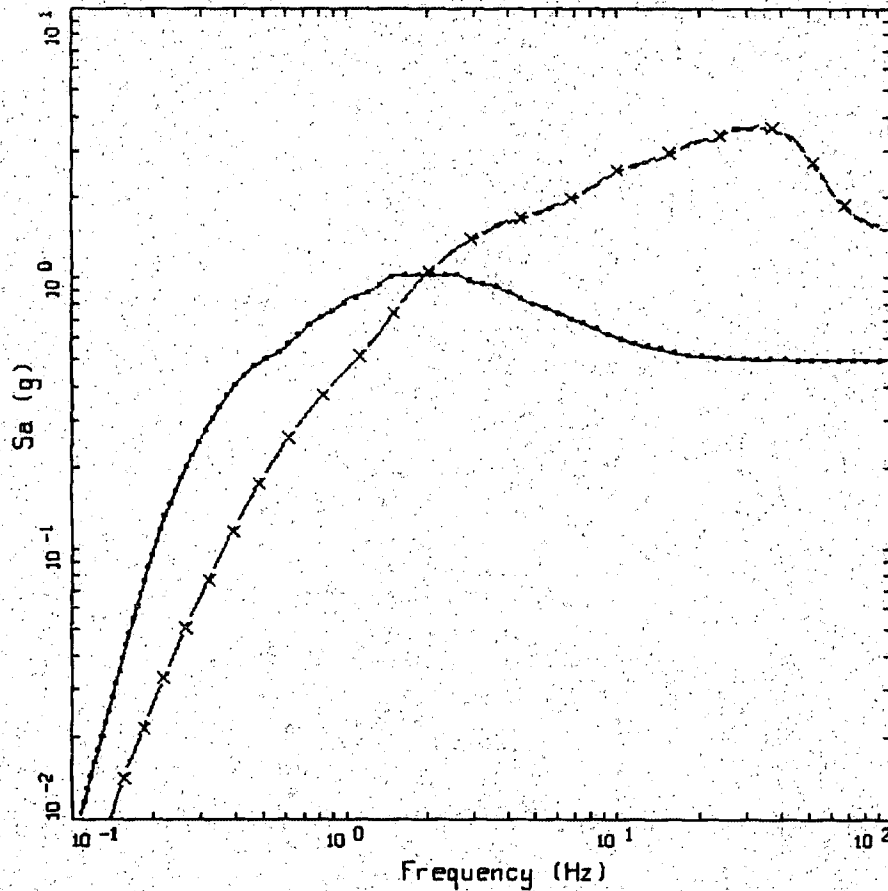


M = 6.00, 1 CORNER
REFERENCE MOTION 0.50 G

LEGEND

- 50TH PERCENTILE, SOIL, (R-1) ± 0.05
- 50TH PERCENTILE, SOIL, (R-10) ± 0.05
- - - 50TH PERCENTILE, HARD ROCK REFERENCE SITE, (R-1) ± 0.05
- x - 50TH PERCENTILE, HARD ROCK REFERENCE SITE, (R-10) ± 0.05

Figure A4. Median estimates of reference site (hard CENA rock) and soil site (deep firm CENA soil) response spectra (5% damped) computed for M 6.0 using the EPRI (1993; FSAR Reference 2.5.2-273) modulus reduction and hysteretic damping curves (soil site), reference site median peak acceleration is 0.50g. Comparison using path duration with R-1 and R-10 distance dependencies based on Table A1 model parameters.



M = 6.00, 1 CORNER
REFERENCE MOTION 1.50 G

- LEGEND
- 50TH PERCENTILE, SOIL, (R-1) ± 0.05
 - 50TH PERCENTILE, SOIL, (R-10) ± 0.05
 - - - 50TH PERCENTILE, HARD ROCK REFERENCE SITE, (R-1) ± 0.05
 - x - 50TH PERCENTILE, HARD ROCK REFERENCE SITE, (R-10) ± 0.05

Figure A5: Median estimates of reference site (hard CENA rock) and soil site (deep firm CENA soil) response spectra (5% damped) computed for M 6.0 using the EPRI (1993; FSAR Reference 2.5.2-273) modulus reduction and hysteretic damping curves (soil site), reference site median peak acceleration is 1.50g. Comparison using path duration with R-1 and R-10 distance dependencies based on Table A1 model parameters.

Appendix B

Criteria for Adjusting Kappa

Table of Contents

List of Figures.....	B2
1.0 PURPOSE AND SCOPE.....	B4
2.0 ASSUMPTIONS.....	B4
3.0 DISCUSSION.....	B4
4.0 SUMMARY.....	B8
5.0 REFERENCES.....	B8
6.0 FIGURES.....	B9

List of Figures

- Figure B1. Comparison of the median spectrum (5% damped) based on thirty simulated profiles with the spectrum computed from the base case profile. The total kappa is 0.04 sec for each profile. M 6.5, single-corner source model, and the reference rock motion is 0.01g. Generic deep firm soil site with \bar{V}_s (30m) = 270m/sec (Walling et. al, 2008)..... B9
- Figure B2. Comparison of the median spectrum (5% damped) based on thirty simulated profiles with the spectrum computed from the base case profile. The total kappa is 0.04 sec for the base case profile and 0.034 sec for each random profile. M 6.5, single-corner source model, and the reference rock motion is 0.01g. Generic deep firm soil site with \bar{V}_s (30m) = 270m/sec (Walling et. al, 2008).....B10
- Figure B3. Comparison of median spectra based on thirty simulated profiles with total kappa values of 0.04 sec (dotted lines) and 0.034 sec (dashed lines) with the spectrum computed using the base case profile with a kappa of 0.04 sec. M 6.5, single-corner source model, and the reference site motion is 0.01g. Generic deep firm soil with \bar{V}_s (30m) = 270m/sec (Walling et. al, 2008). Logarithmic Sa axis.....B11
- Figure B4. Comparison of median spectra based on thirty simulated profiles with total kappa values of 0.04 sec (dotted lines) and 0.034 sec (dashed lines) with the spectrum computed using the base case profile with a kappa of 0.04 sec. M 6.5, single-corner source model, and the reference site motion is 0.01g. Generic deep firm soil with \bar{V}_s (30m) = 270m/sec (Walling et. al, 2008). Linear Sa axis:B12
- Figure B5. Spectral ratios (5% damped) of the median spectra based on thirty simulated profiles divided by the spectrum computed for the base case profile with a total kappa value of 0.04 sec. Simulated profiles have kappa values of 0.04 sec (solid line) and 0.034 sec (dotted lines). Ratios computed at 300 points and are based on the spectra shown in Figures B3 and B4.B13

Figures B6a and B6b. Comparison of the base case profile with the median profile computed from the thirty simulated profiles, $\pm 1\sigma$ estimates are shown along with the median: linear and logarithmic axes. Generic deep firm soil with $\bar{V}_s(30m) = 270m/sec$ (Walling et. al, 2008).B14

Figure B7. Comparison of the median spectrum (5% damped) based on thirty simulated profiles with the spectrum computed from the base case profile. The total kappa is 0.04 sec for each profile. M 6.5, single-corner source model, and the reference rock motion is 0.01g. Generic soft rock site with $\bar{V}_s(30m) = 560m/sec$ (Walling et. al, 2008).B16

Figure B8. Comparison of the median spectrum (5% damped) based on thirty simulated profiles with the spectrum computed from the base case profile. The total kappa is 0.04 sec for the base case profile and 0.038 sec for each random profile. M 6.5, single-corner source model, and the reference rock motion is 0.01g. Generic soft rock site with $\bar{V}_s(30m) = 560m/sec$ (Walling et. al, 2008).B17

Figure B9. Comparison of median spectra based on thirty simulated profiles with total kappa values of 0.04 sec (dotted lines) and 0.038 sec (dashed lines) with the spectrum computed using the base case profile with a kappa of 0.04 sec. M 6.5, single-corner source model, and the reference site motion is 0.01g. Generic soft rock with $\bar{V}_s(30m) = 560m/sec$ (Walling et. al, 2008). Logarithmic Sa axis.B18

Figure B10. Comparison of median spectra based on thirty simulated profiles with total kappa values of 0.04 sec (dotted lines) and 0.038 sec (dashed lines) with the spectrum computed using the base case profile with a kappa of 0.04 sec. M 6.5, single-corner source model, and the reference site motion is 0.01g. Generic soft rock with $\bar{V}_s(30m) = 560m/sec$ (Walling et. al, 2008). Linear Sa axis.B19

Figure B11. Spectral ratios (5% damped) of the median spectra based on thirty simulated profiles divided by the spectrum computed for the base case profile with a total kappa value of 0.04 sec. Simulated profiles have kappa values of 0.04 sec (solid line) and 0.038 sec (dotted lines). Ratios computed at 300 points and are based on the spectra shown in Figures B9 and B10.B20

Figures B12a and B12b. Comparison of the base case profile with the median profile computed from the thirty simulated profiles, $\pm 1\sigma$ estimates are shown along with the median: linear and logarithmic axes. Generic soft rock with $\bar{V}_s(30m) = 560m/sec$ (Walling et. al, 2008).B21

1.0 Purpose and Scope

This appendix addresses the use of adjusted values of kappa, a parameterization of high frequency spectral damping, in the site response analysis for Lee Nuclear Station Unit 1. Justification for adjusting values of kappa includes an attribution to an unpublished document (Silva et al., 1996; FSAR Reference 2.5.2-288). A potential exists for the underestimation of median high-frequency amplification during site response analysis if a kappa correction is not used. Consequently, it is prudent to estimate and correct for any potential bias toward underestimating median amplification produced by using a suite of profiles, random or measured, that have multiple layers of alternating velocities. This appendix provides specific examples of how the kappa correction is calculated and applied to avoid bias.

2.0 Assumptions

None.

3.0 Discussion

It is well known that wave propagation through multiple closely spaced elastic plane layers with alternating velocities results in multiple reflections, giving rise to a depletion of high-frequency energy in the direct wave. The apparent energy loss due to scattering emulates intrinsic wave damping, displaying characteristics quite similar to intrinsic damping. Scattering damping at shallow depths (hundreds to thousands of feet) was initially proposed in exploration geophysics as a contributing factor to the depletion of high-frequency energy with increasing travel time (References 1 and 2). Subsequently, the effects of random fluctuations in wave velocity over the dimensions of fractions of wavelengths in the earth's crust was postulated as a causal mechanism for the generation of coda, the incoherent wave fields that follow direct arrivals observed on accelerograms and seismograms throughout the world. This random scattering also results in an apparent wave damping which is generally considered to be weakly frequency dependent, with damping decreasing as frequency increases (References 3 and 4). For wave propagation through the crust, the energy dissipation is considered to be due to a combination of intrinsic (e.g. hysteretic) damping and scattering due to random fluctuations in velocities. The apparent weak dependence of the net or total damping on frequency reflects an artifact of the combination of the two contributing factors, wave scattering and intrinsic absorption (Reference 4).

For applications to site response analyses it is prudent to estimate and correct for any potential bias toward underestimating median amplification produced by using a suite of profiles, random or measured, that have multiple layers of alternating velocities. To be clear, the scattering due to alternating velocities does not refer to deterministic and stable conditions which may exist across a site (e.g. single or multiple low velocity zones). The alternating velocities that contribute to scattering damping in one-dimensional site response analyses are the apparently random fluctuations in measured velocities that do not correlate between measurements made at multiple locations across a site. It should be emphasized that the issue of a scattering correction in random profiles arises because base case profiles are typically smooth relative to the profiles measured at multiple locations across a site upon which they are based. One-dimensional site response analyses implicitly assume lateral continuity in velocity while in the earth the constant velocity layers interpreted in site measurements typically vary laterally across both soil and rock sites. The motions at any given point are influenced to some degree by nearby velocity structures because, in propagating to the surface the wave fields reflect a horizontal velocity (giving rise to lateral

strains) and because they follow a Fermat path, minimizing the travel time to the surface at each frequency. The fundamental assumption in developing site-specific motions is that a base case velocity profile that is laterally continuous is associated with a total damping at low strains and, consequently, a site-specific spectral shape or multiple shapes that are stable across the areas to which they apply as well as across earthquakes of similar (small or large and distant) magnitudes. The fundamental objective in site response is to develop a mean (log) estimate of amplification that reflects a base case or mean (best) estimate of a velocity profile representative of a given area as well as the variability about the base case profile (and related amplification) across the specific area. Associated with the base case profile and hysteretic damping from the low strain damping in the nonlinear dynamic material properties at low loading levels, is a spectral shape that is assumed to be based on multiple earthquakes sampling over all source azimuths and recorded at multiple locations across the site, sampling multiple in situ velocity columns. This ideal empirical average is replicated in the site response analyses through a Monte Carlo simulation of random profiles and G/G_{max} and hysteretic damping curves. Provided recorded motions from multiple earthquakes were available at multiple closely spaced locations at a well characterized site, the issue of the appropriateness of correcting for the scattering damping introduced in the one-dimensional analyses could be resolved with a comparison between two median spectra, one based on simulations and the other based on observations. Equivalence between the two median spectra would suggest the scattering induced by the one-dimensional analyses is similar to that observed, provided the randomly generated profiles reflect similar statistical properties to the actual profiles. Such a comparison is currently not possible as suitable dense array recordings of strong ground motions are not available across dimensions of a typical foundation footprint. As a result, the necessity of a scattering correction to one-dimensional site response analyses remains an unconfirmed assumption, at least for some cases.

For cases where the total kappa in the profile is not known independently from observations of ground motions at similar profiles (e.g., a constraint on the total low strain damping), the correction for scattering kappa reflects an assumption that the actual scattering in the field may be less than that which occurs in one-dimensional analyses. The kappa correction may be somewhat conservative, depending on the magnitude of the correction. However for cases where the total kappa is known a priori (e.g. very deep soft to firm soil profiles or soft rock at least 1 km to 2 km thick as well as shallow soil overlying thick sequences of soft rock), the median spectral shape based on a suite of random profiles should be constrained to not fall significantly below the spectrum computed with the base case profile and known total kappa. The constraint imposed in the random profiles is applied by reducing the kappa (low strain damping) by the same amount in each of the random profiles. This process of adjusting kappa is done iteratively with the comparison between the median spectrum and the spectrum computed with the base case profile at high-frequency (≥ 1 Hz) as the figure of merit. The criteria for similarity is one of judgment, particularly when the spectrum computed with the base case profile displays peaks and valleys due to resonances while the median spectrum is much smoother. The assessment must then be made by looking at the overall spectral levels over a wide frequency range. The criteria implemented requires the median spectra not to fall below the base case spectrum by more than about 5% over a wide frequency range. Formally one may introduce criteria analogous to that of spectral matching outlined in NUREG/CR-6728 (FSAR Reference 2.5.2-251) by defining a smoothing window, frequency range, and acceptable tolerance. However, use of a realistic profile correlation model (e.g. FSAR Reference 2.5.2-273) that is appropriate for variability over the dimensions of a footprint for both deep firm soil and soft rock sites (a footprint correlation model is not currently available for hard rock sites), produces scattering corrections that are

generally quite small for both deep firm soil and soft rock sites. As a result, prescriptive criteria regarding a scattering correction may not be warranted. The magnitude of the correction is illustrated in examples for a deep soil site and a soft rock site presented in the following discussion.

Considering a generic deep firm soil site (1,000 ft deep to 1 km/sec material) with a \bar{V}_s (30m) of 270 m/sec (Reference 5), Figure B1 shows the median spectrum (as well as \pm one sigma estimates) developed from spectra (5% damped) computed with thirty simulated profiles compared to the spectrum computed with the base-case profiles at very low (linear) loading levels. In the case in Figure B1 all the profiles reflect a total kappa value of 0.04 sec and there is generally good agreement between the median spectrum and that of the base case profile across most of the frequency range, suggesting an acceptably close agreement between the median and base case profiles. However, for frequencies exceeding about 4 Hz, the median spectrum falls slightly below the spectrum computed with the base case profile, with variations of up to about 10% (Figure B1). This trend is attributable to the damping induced by wave scattering due to velocity fluctuations in the one-dimensional analyses. Lowering the total kappa in the simulated profiles to 0.034 sec results in a median spectrum at or slightly above the base case spectrum at high-frequency as shown in Figure B2. The approximately 15% decrease in kappa results in about a 10% increase in the median spectrum at frequencies exceeding about 4 Hz and reflects a typical scattering correction at a deep soil site, removing a potential bias or underestimate of expected spectra at low loading levels. To more clearly illustrate the differences in the uncorrected and corrected median spectra, Figure B3 shows the two median estimates along with the spectrum computed with the base case profile (kappa = 0.04 sec). As Figure B3 illustrates, the uncorrected median estimate is roughly 10% below the base case spectrum between about 5 Hz and 10 Hz and less than 10% below for frequencies exceeding about 10 Hz. Figure B4 shows the same comparison with linear spectral acceleration (Sa) axes and Figure B5 shows the ratios of the uncorrected and corrected median spectra to the base case spectrum with the \pm 10% fiduciaris as dashed lines. As previously discussed, the spectral amplitude oscillations with frequency are due to profile resonances in the spectrum computed with the base case profile that are greatly smoothed in computing the median spectrum as an average over the multiple spectra computed with the simulated profiles. As Figure B5 clearly illustrates, the spectral amplitude maximum bias tolerance criteria of approximately 5% over a wide frequency range is considered to be exceeded by the uncorrected median estimate. Reducing kappa in each simulated profile by about 15% to 0.034 sec eliminates the potential bias in the uncorrected median estimate. Unfortunately the effects of kappa become more pronounced as frequency increases because the kappa model implies a frequency independent hysteretic damping, while the effects of one-dimensional scattering may result in a frequency dependence with the effective damping decreasing with increasing frequency. The effect of a frequency independent kappa leads to a scattering correction that may result in slightly conservative high-frequency motion at very low loading levels that are typically too small to be a design issue. As discussed in the response to RAI 02.05.02-016, all models have limitations and, as with all models, a more sophisticated profile randomization model that would address this issue would be welcome. The approach taken here to compensate or correct for a possible bias resulting in an underestimate of the expected site-specific spectrum is considered physically reasonable and transparent in both its intent and effect.

To illustrate the shear-wave velocity profile randomization results, the base case profile as well as the median and \pm one sigma velocity profile estimates are shown in Figures B6a and

B6b for linear and logarithmic velocity axes, respectively (shear-wave velocities are log-normally distributed in the correlation model, FSAR Reference 2.5.2-273). In general the median estimate is quite close to the base case profile. Over the top approximately 3m to 5m (10 ft to 15 ft) the median velocity exceeds the base case velocity by only about 10% and is significantly closer throughout the remaining roughly 300m of depth. The similarity between the corrected and uncorrected median spectra and that of the base case indicates that an adequate similarity exists between the base case profile and the median profile.

Finally, to illustrate the scattering correction applied to a stiffer profile, Figure B7 through Figures B12a and B12b show a corresponding suite of analyses (linear and logarithmic velocity axes, respectively) for a soft rock shear-wave velocity profile with $\bar{V}_s(30m) = 560\text{m/sec}$ (Reference 5). For the soft rock velocity profile, Figure B7 shows increased similarity between the spectrum computed with the base case profile and the median spectrum, all with a total kappa value of 0.04 sec, compared to firm soil (Figure B1). The kappa correction or reduction needed to satisfy the spectral bias tolerance criteria is only about 5% from 0.04 sec to 0.038 sec and the effect is illustrated in Figures B8, B9, and B10. As Figure B11 shows, the slight reduction in kappa raised the corrected median from a broad low averaging about 5% below the base case spectrum from about 8 Hz to about 15 Hz. Over this frequency range the spectrum of the corrected median estimate was raised to an average of about 3% below that of the base case. As with the deep firm soil results in Figure B5, at frequencies exceeding about 15 Hz, the correction results in slightly conservative motions at very low loading levels.

Completing the soft rock analyses, Figures B12a and B12b shows the base case profile compared to the median and \pm one sigma estimates. As with the soil profiles in Figures B6a and B6b, the agreement between the median profile and the base case profile is acceptably close, based upon the close agreement between the corresponding spectra.

The examples presented illustrate typical ranges in the scattering kappa and the resulting effects on the expected spectra using an approximate numerical criteria for adjusting kappa that requires the median spectra not to fall below the base case spectrum by more than about 5% over a wide frequency range. The kappa adjustments were small, with the largest kappa adjustments of about 15% for a generic deep firm soil site profile (Figure B5). For the stiffer profile, kappa reduction on the order of only 5% is required to avoid deviations from a base case spectrum of more than about 5% over a wide frequency range (Figures B5 and B11). The kappa adjustment is a physically reasonable and appropriate approach to adjust for a possible bias, a bias that if uncorrected can result in underestimation of median high-frequency spectra at very low loading levels.

4.0 Summary

This appendix summarizes how high frequency spectral damping results from several processes. A potential exists for the underestimation of median high-frequency amplification during site response analysis if a kappa correction is not used. Consequently, it is prudent to estimate and correct for any potential bias toward underestimating median amplification produced by using a suite of profiles, random or measured, that have multiple layers of alternating velocities. This appendix provides specific examples of how the kappa correction is calculated and applied to avoid bias. The examples show that the kappa adjustment is relatively small and provides a physically reasonable and appropriate approach to adjust for

a possible bias, a bias that if uncorrected can result in underestimation of median high-frequency spectra at very low loading levels.

5.0 References:

1. O'Doherty, R.F. and N.A. Anstey (1971). "Reflections on amplitudes." *Geophysical Prospecting* **19**, 430-458.
2. Schoenberger, M. and F. K. Levin (1978). "Apparent attenuation due to intrabed multiples, II" *Geophysics*, **43**, 730-737.
3. Aki, K. and P. G. Richards (1980). *Quantitative Seismology Theory and Methods*, W. H. Freeman and Co., San Francisco.
4. Richards, P. G. and W. Menke (1983). "The apparent attenuation of a scattering medium." *Bulletin of the Seismological Society of America*, **73**(4), 1005-1021.
5. Walling, M., W. Silva and N. Abrahamson (2008). "Nonlinear site amplification factors for constraining the NGA models." *Earthquake Spectra*, **24**(1), 243-255.

6.0 Figures

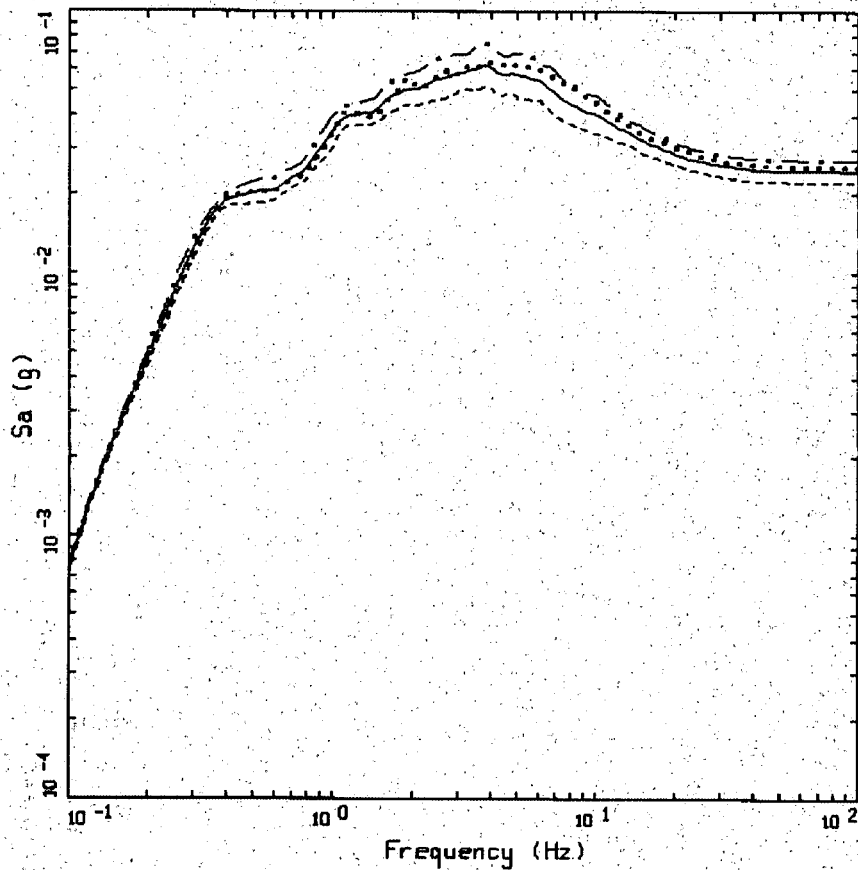
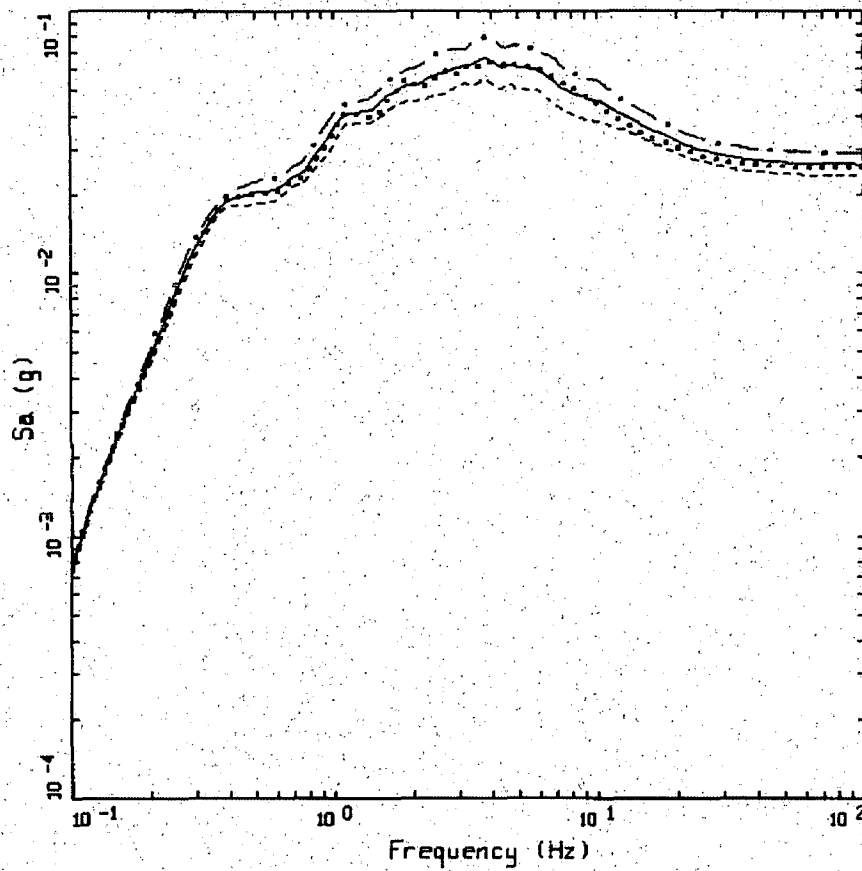


Figure B1. Comparison of the median spectrum (5% damped) based on thirty simulated profiles with the spectrum computed from the base case profile. The total kappa is 0.04 sec for each profile. M 6.5, single-corner source model, and the reference rock motion is 0.01g. Generic deep firm soil site with $\bar{V}_s(30m) = 270m/sec$ (Reference 5).

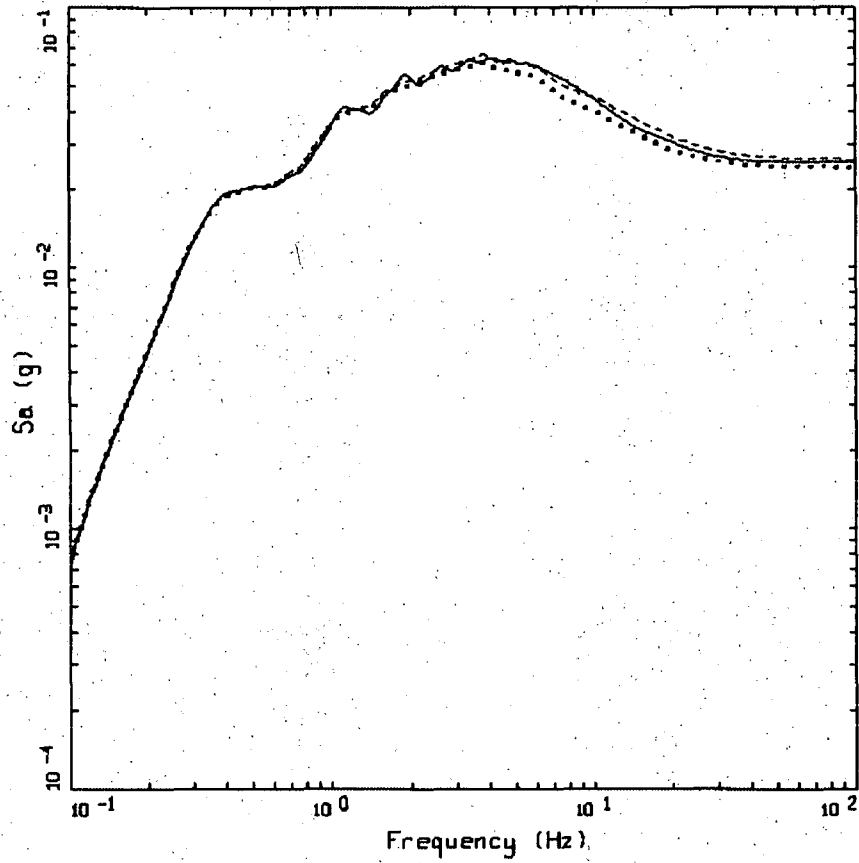


SOIL: M = 6.50, 1 CORNER, VS(30M) = 270 M/SEC
REFERENCE MOTION 0.01 G, K = 0.034 SEC

LEGEND

- 84TH PERCENTILE, PARAMETRIC UNCERTAINTY; PGA = 0.0289 G
- — — 50TH PERCENTILE, PARAMETRIC UNCERTAINTY; PGA = 0.0261 G
- · - · - 16TH PERCENTILE, PARAMETRIC UNCERTAINTY; PGA = 0.0237 G
- · · · · 5 % , BASE CASE; PGA = 0.0251 G

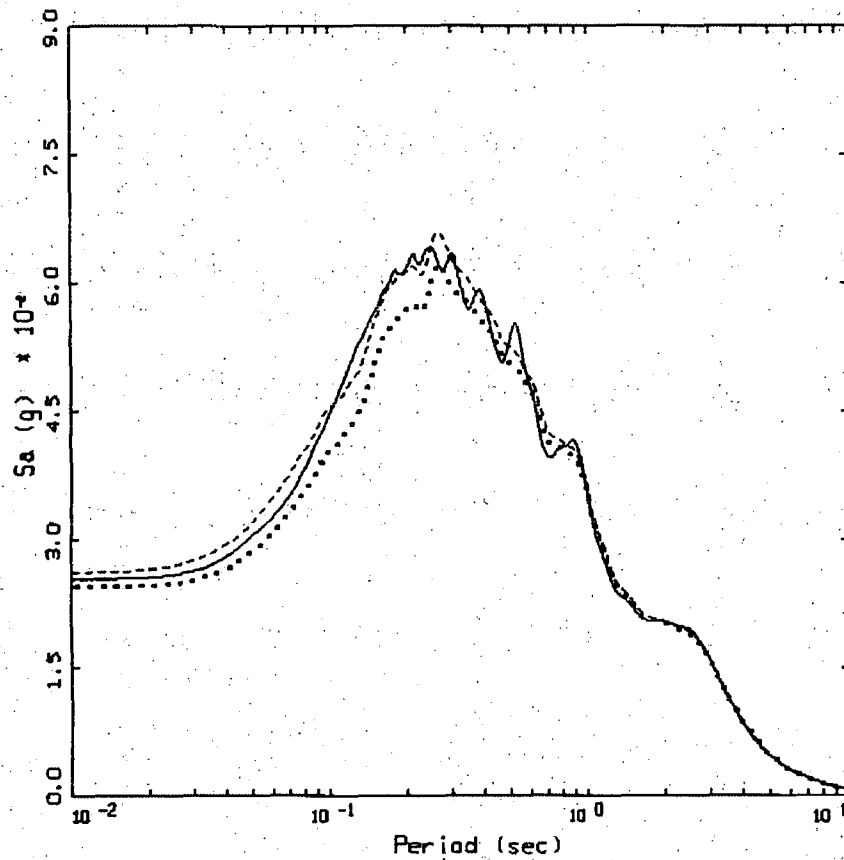
Figure B2. Comparison of the median spectrum (5% damped) based on thirty simulated profiles with the spectrum computed from the base case profile. The total kappa is 0.04 sec for the base case profile and 0.034 sec for each random profile. M 6.5, single-corner source model, and the reference rock motion is 0.01g. Generic deep firm soil site with $\bar{V}_s(30m) = 270m/sec$ (Reference 5).



SOIL: M = 6.50, 1 CORNER, VS(30M) = 270 M/SEC
REFERENCE MOTION 0.01 G

LEGEND
..... 50TH PERCENTILE, PARAMETRIC UNCERTAINTY, K = 0.040 SEC; PGA = 0.0244 G
----- 50TH PERCENTILE, PARAMETRIC UNCERTAINTY, K = 0.034 SEC; PGA = 0.0261 G
———— 5 %, BASE CASE; PGA = 0.0251 G

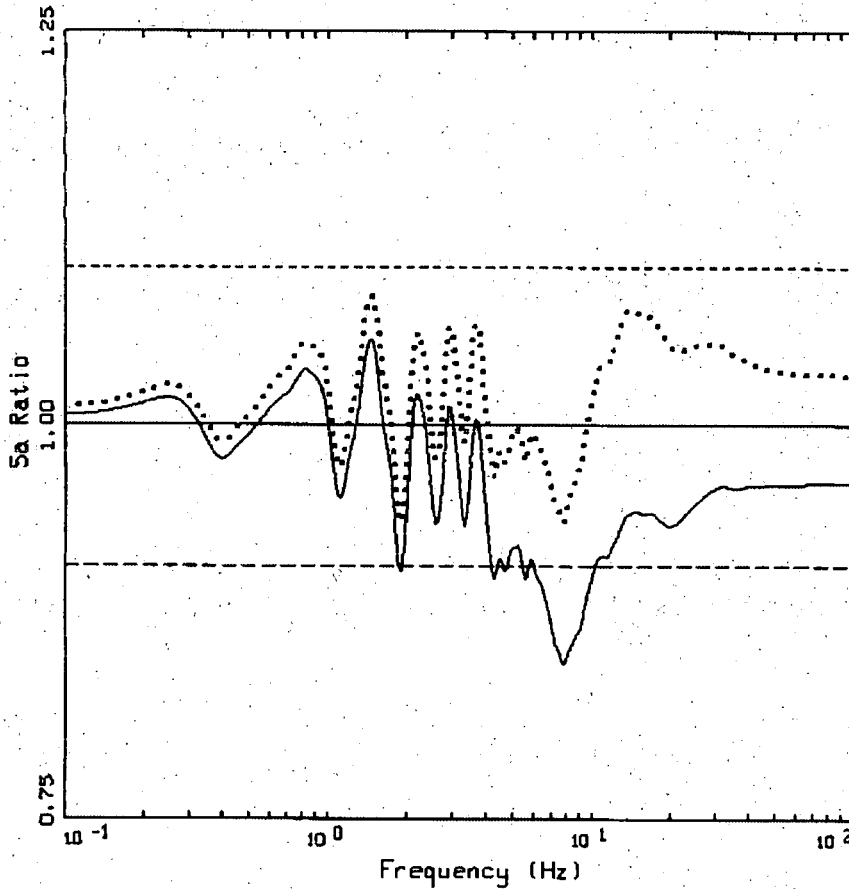
Figure B3. Comparison of median spectra based on thirty simulated profiles with total kappa values of 0.04 sec (dotted lines) and 0.034 sec (dashed lines) with the spectrum computed using the base case profile with a kappa of 0.04 sec. M 6.5, single-corner source model, and the reference site motion is 0.01g. Generic deep firm soil with $\bar{V}_s(30m) = 270m/sec$ (Reference 5). Logarithmic Sa axis.



SOIL: M = 6.50, 1 CORNER, VS(30M) = 270 M/SEC
REFERENCE MOTION 0.01 G

LEGEND
..... 50TH PERCENTILE, PARAMETRIC UNCERTAINTY, K = 0.040 SEC; PGA = 0.0244 G
----- 50TH PERCENTILE, PARAMETRIC UNCERTAINTY, K = 0.034 SEC; PGA = 0.0261 G
———— 5 %, BASE CASE; PGA = 0.0251 G

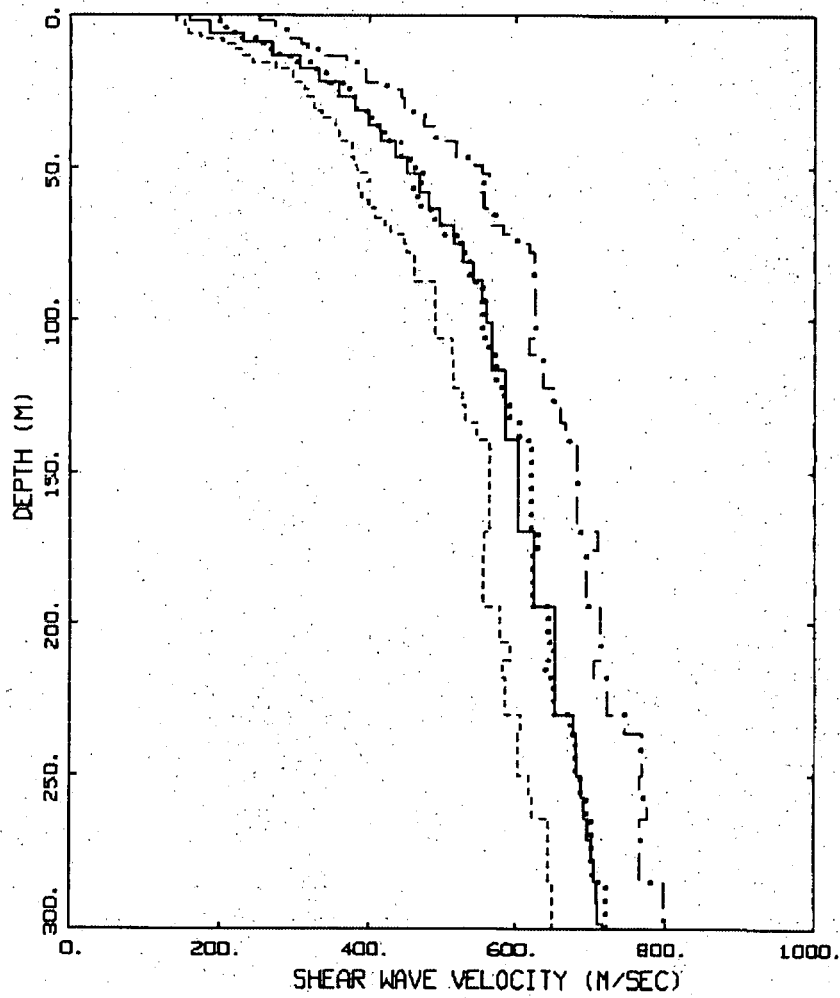
Figure B4. Comparison of median spectra based on thirty simulated profiles with total kappa values of 0.04 sec (dotted lines) and 0.034 sec (dashed lines) with the spectrum computed using the base case profile with a kappa of 0.04 sec. M 6.5, single-corner source model, and the reference site motion is 0.01g. Generic deep firm soil with $\bar{V}_s(30m) = 270m/sec$ (Reference 5). Linear Sa axis.



SOIL: M = 6.50, 1 CORNER, VS(30M) = 270 M/SEC
REFERENCE MOTION 0.01 G, SPECTRAL RATIOS

- LEGEND
- SA RATIO: MEDIAN(K = 0.040 SEC) / BASE CASE
 - SA RATIO: MEDIAN(K = 0.034 SEC) / BASE CASE
 - UNITY
 - UNITY + 1.1
 - UNITY - 1.1

Figure B5. Spectral ratios (5% damped) of the median spectra based on thirty simulated profiles divided by the spectrum computed for the base case profile with a total kappa value of 0.04 sec. Simulated profiles have kappa values of 0.04 sec (solid line) and 0.034 sec (dotted lines). Ratios computed at 300 points and are based on the spectra shown in Figures 022-B4.



SOIL, $V_s(30M) = 270$ M/SEC

- LEGEND
- 16TH PERCENTILE
 - 50TH PERCENTILE
 - . - . 84TH PERCENTILE
 - _____ BASE CASE

Figure B6a. Comparison of the base case profile with the median profile computed from the thirty simulated profiles, $\pm 1\sigma$ estimates are shown along with the median: linear axes. Generic deep firm soil with $\bar{V}_s(30m) = 270m/sec$ (Reference 5).

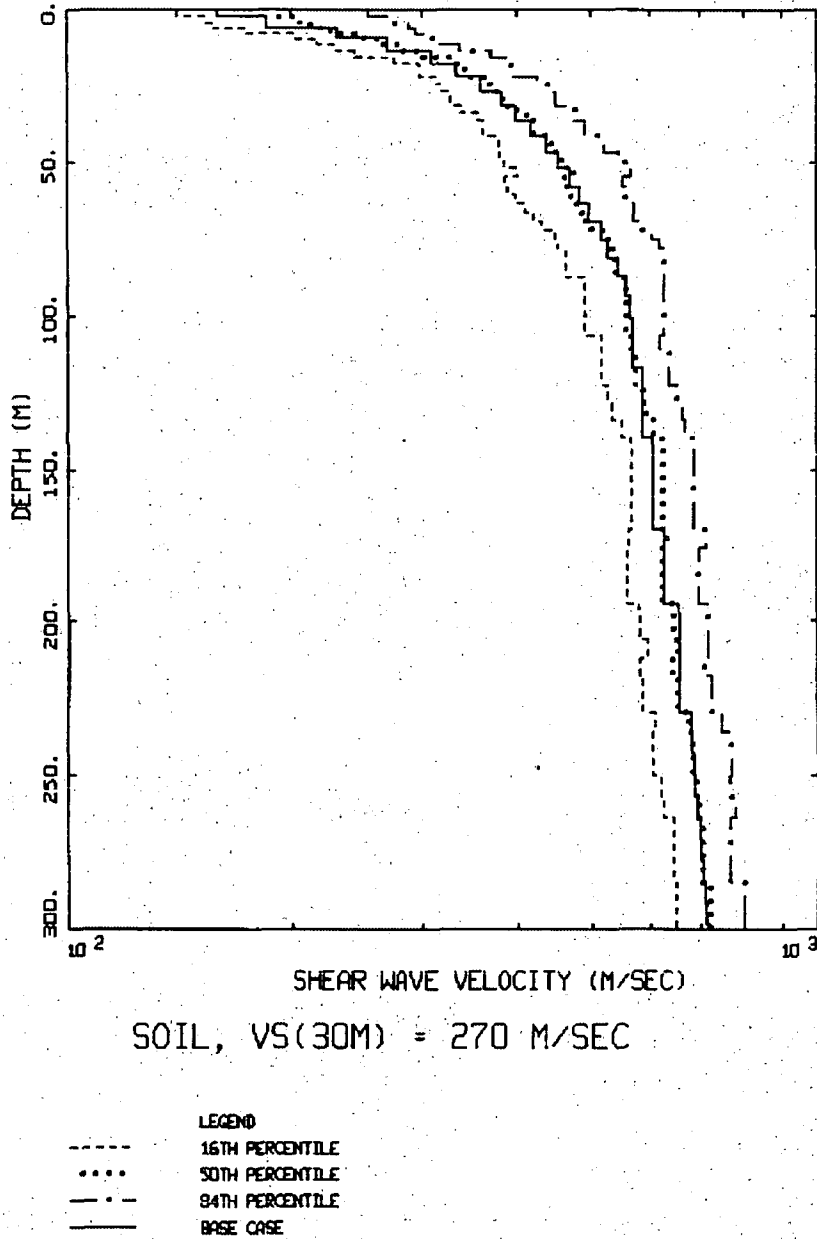
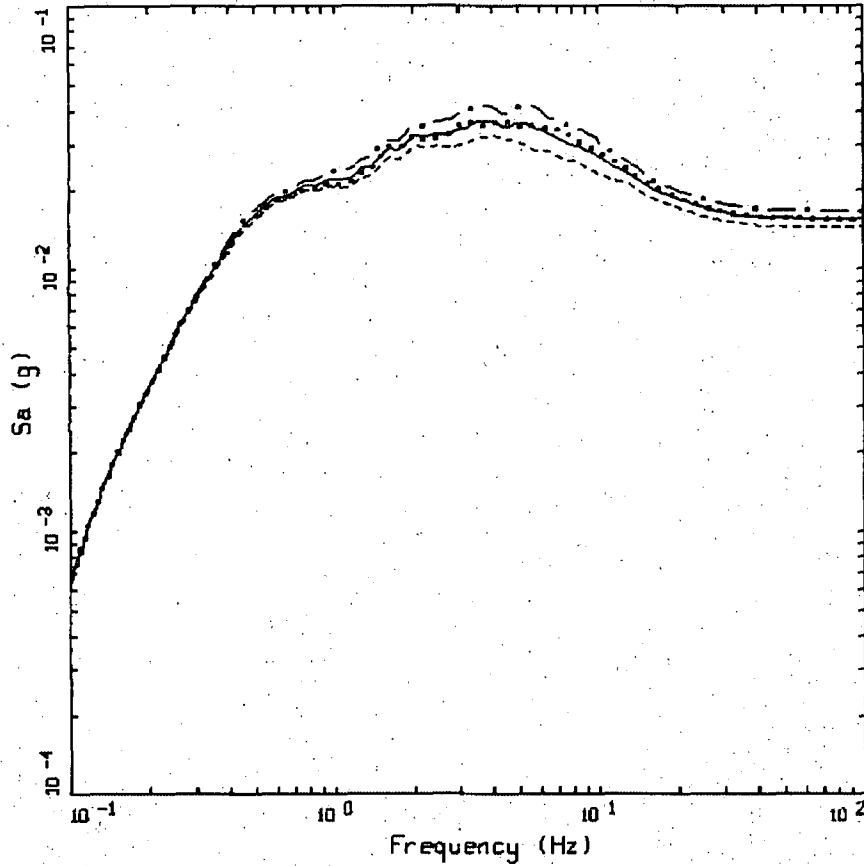


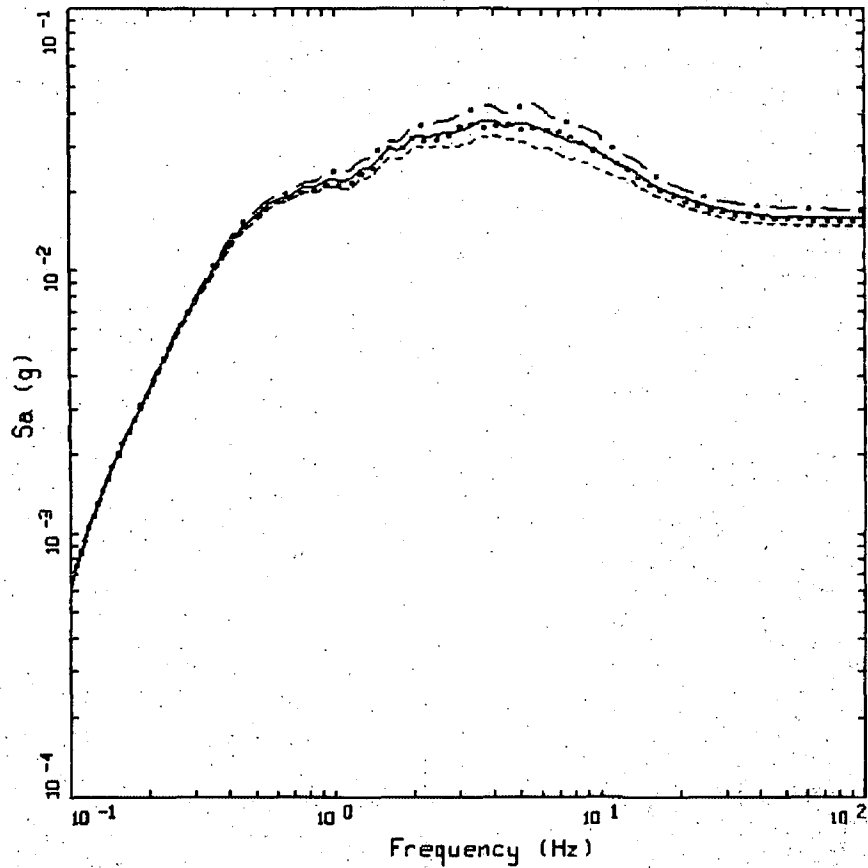
Figure B6b: Comparison of the base case profile with the median profile computed from the thirty simulated profiles, $\pm 1\sigma$ estimates are shown along with the median: logarithmic shear wave velocity axes. Generic deep firm soil with $\bar{V}_S(30m) = 270m/sec$ (Reference 5).



ROCK: M = 6.50, 1 CORNER, VS(30M) = 560 M/SEC
REFERENCE MOTION 0.01 G, K = 0.040 SEC

LEGEND
- - - 84TH PERCENTILE, PARAMETRIC UNCERTAINTY; PGA = 0.0166 G
— 50TH PERCENTILE, PARAMETRIC UNCERTAINTY; PGA = 0.0155 G
- - - 16TH PERCENTILE, PARAMETRIC UNCERTAINTY; PGA = 0.0144 G
- . . . 5 % BASE CASE; PGA = 0.0155 G

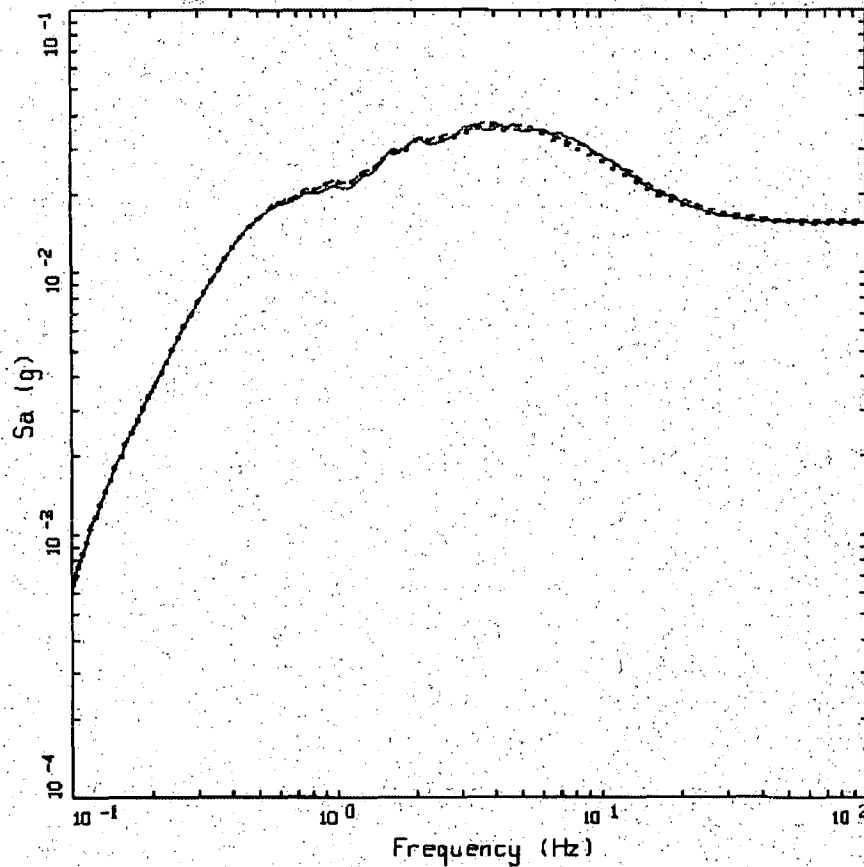
Figure B7. Comparison of the median spectrum (5% damped) based on thirty simulated profiles with the spectrum computed from the base case profile. The total kappa is 0.04 sec for each profile. M 6.5, single-corner source model, and the reference rock motion is 0.01g. Generic soft rock site with $\bar{V}_s(30m) = 560m/sec$ (Reference 5).



ROCK: M = 6.50, 1 CORNER, VS(30M) = 560 M/SEC
REFERENCE MOTION 0.01 G, K = 0.038 SEC

LEGEND
- - - 84TH PERCENTILE, PARAMETRIC UNCERTAINTY; PGA = 0.0170 G
_____ 50TH PERCENTILE, PARAMETRIC UNCERTAINTY; PGA = 0.0158 G
- - - - 16TH PERCENTILE, PARAMETRIC UNCERTAINTY; PGA = 0.0147 G
..... 5 %, BASE CASE; PGA = 0.0153 G

Figure B8. Comparison of the median spectrum (5% damped) based on thirty simulated profiles with the spectrum computed from the base case profile. The total kappa is 0.04 sec for the base case profile and 0.038 sec for each random profile. M 6.5, single-corner source model, and the reference rock motion is 0.01g. Generic soft rock site with $\bar{V}_s(30m) = 560m/sec$ (Reference 5).

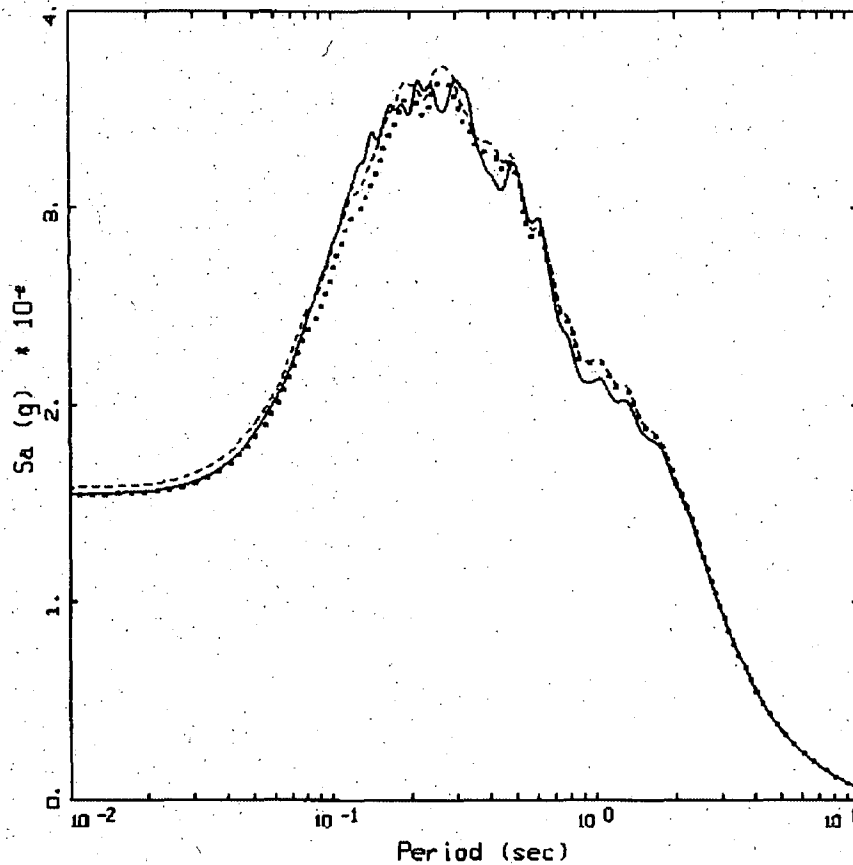


ROCK: M = 6.50, 1 CORNER, VS(30M) = 560 M/SEC
REFERENCE MOTION 0.01 G

LEGEND

- 50TH PERCENTILE, PARAMETRIC UNCERTAINTY, K = 0.040 SEC; PGA = 0.0155 G
- 50TH PERCENTILE, PARAMETRIC UNCERTAINTY, K = 0.038 SEC; PGA = 0.0158 G
- 5. % BASE CASE; PGA = 0.0155 G

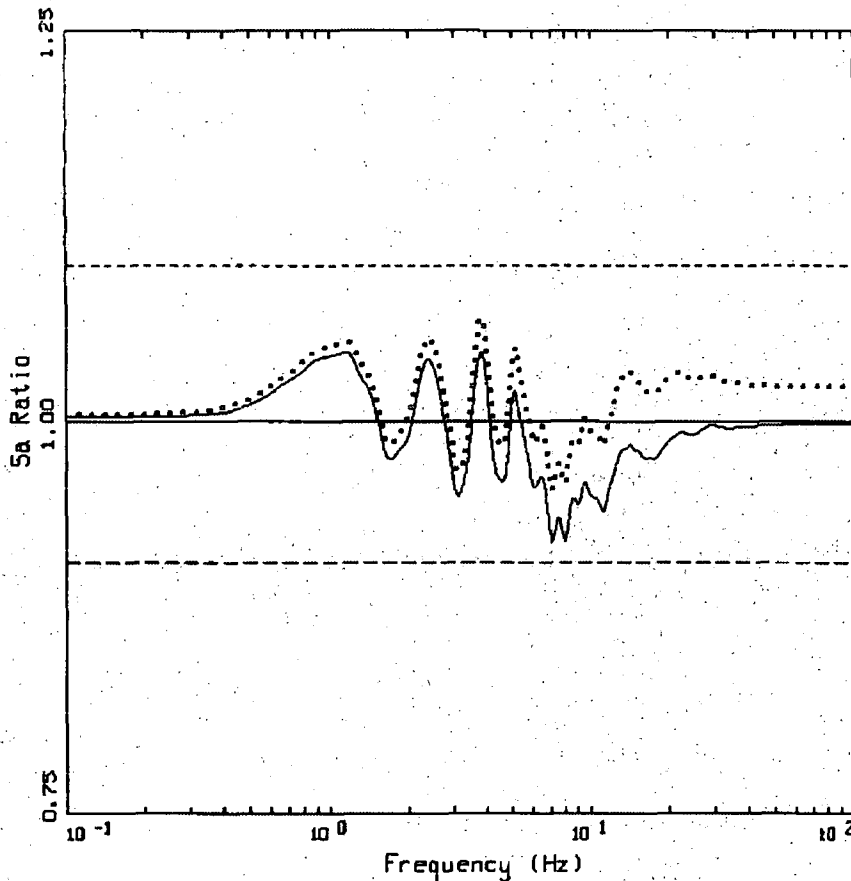
Figure B9. Comparison of median spectra based on thirty simulated profiles with total kappa values of 0.04 sec (dotted lines) and 0.038 sec (dashed lines) with the spectrum computed using the base case profile with a kappa of 0.04 sec. M 6.5, single-corner source model, and the reference site motion is 0.01g. Generic soft rock with $\bar{V}_s(30m) = 560m/sec$ (Reference 5). Logarithmic Sa axis.



ROCK: M = 6.50, 1 CORNER, $V_S(30M) = 560$ M/SEC
REFERENCE MOTION 0.01 G

LEGEND
..... 50TH PERCENTILE, PARAMETRIC UNCERTAINTY, $\kappa = 0.040$ SEC; $PGA = 0.0155$ G
----- 50TH PERCENTILE, PARAMETRIC UNCERTAINTY, $\kappa = 0.038$ SEC; $PGA = 0.0158$ G
———— 5 %, BASE CASE; $PGA = 0.0155$ G

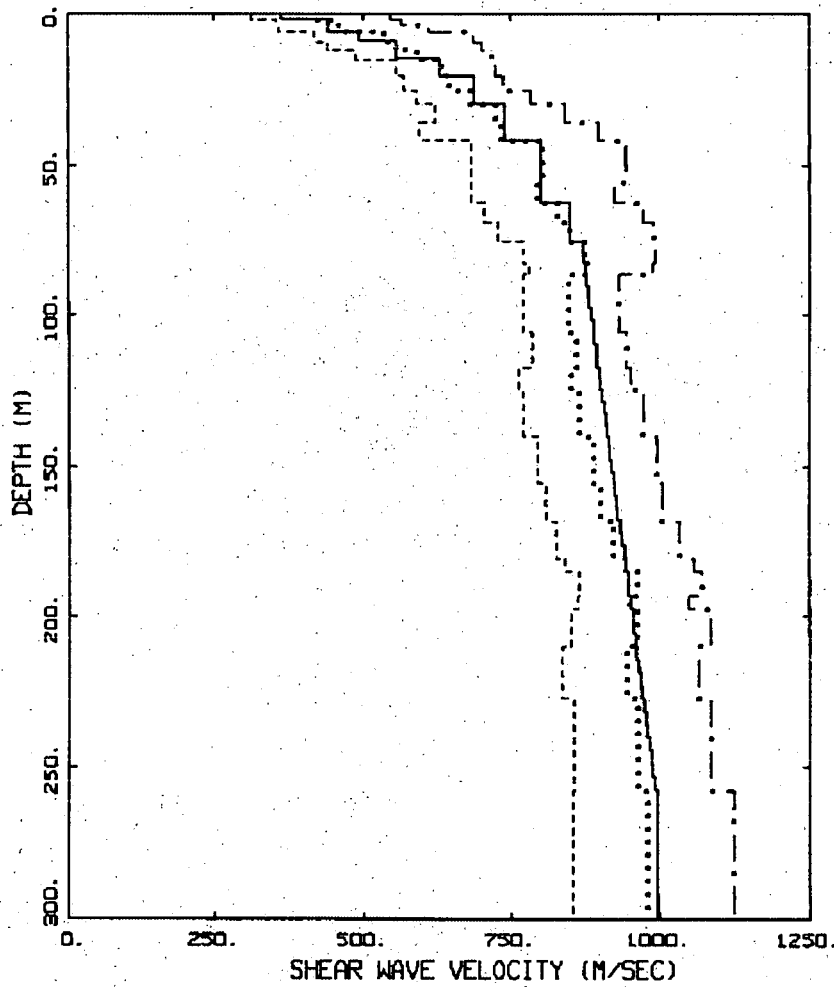
Figure B10. Comparison of median spectra based on thirty simulated profiles with total kappa values of 0.04 sec (dotted lines) and 0.038 sec (dashed lines) with the spectrum computed using the base case profile with a kappa of 0.04 sec. M 6.5, single-corner source model, and the reference site motion is 0.01g. Generic soft rock with $\bar{V}_s(30m) = 560m/sec$ (Reference 5). Linear S_a axis.



ROCK: M = 6.50, 1 CORNER, VS(30M) = 560 M/SEC
REFERENCE MOTION 0.01 G, SPECTRAL RATIOS

- LEGEND
- SA RATIO: MEDIANIK = 0.040 SEC / BASE CASE
 - SA RATIO: MEDIANIK = 0.038 SEC / BASE CASE
 - UNITY
 - - - UNITY * 1.1
 - - - UNITY / 1.1

Figure B11. Spectral ratios (5% damped) of the median spectra based on thirty simulated profiles divided by the spectrum computed for the base case profile with a total kappa value of 0.04 sec. Simulated profiles have kappa values of 0.04-sec (solid line) and 0.038 sec (dotted lines). Ratios computed at 300 points and are based on the spectra shown in Figures B9 and B10.



ROCK, $V_s(30M) = 560$ M/SEC

- LEGEND
- 16TH PERCENTILE
 - 50TH PERCENTILE
 - . - . 84TH PERCENTILE
 - _____ BASE CASE

Figure B12a. Comparison of the base case profile with the median profile computed from the thirty simulated profiles, $\pm 1\sigma$ estimates are shown along with the median: linear axes. Generic soft rock with $\bar{V}_s(30m) = 560m/sec$ (Reference 5).

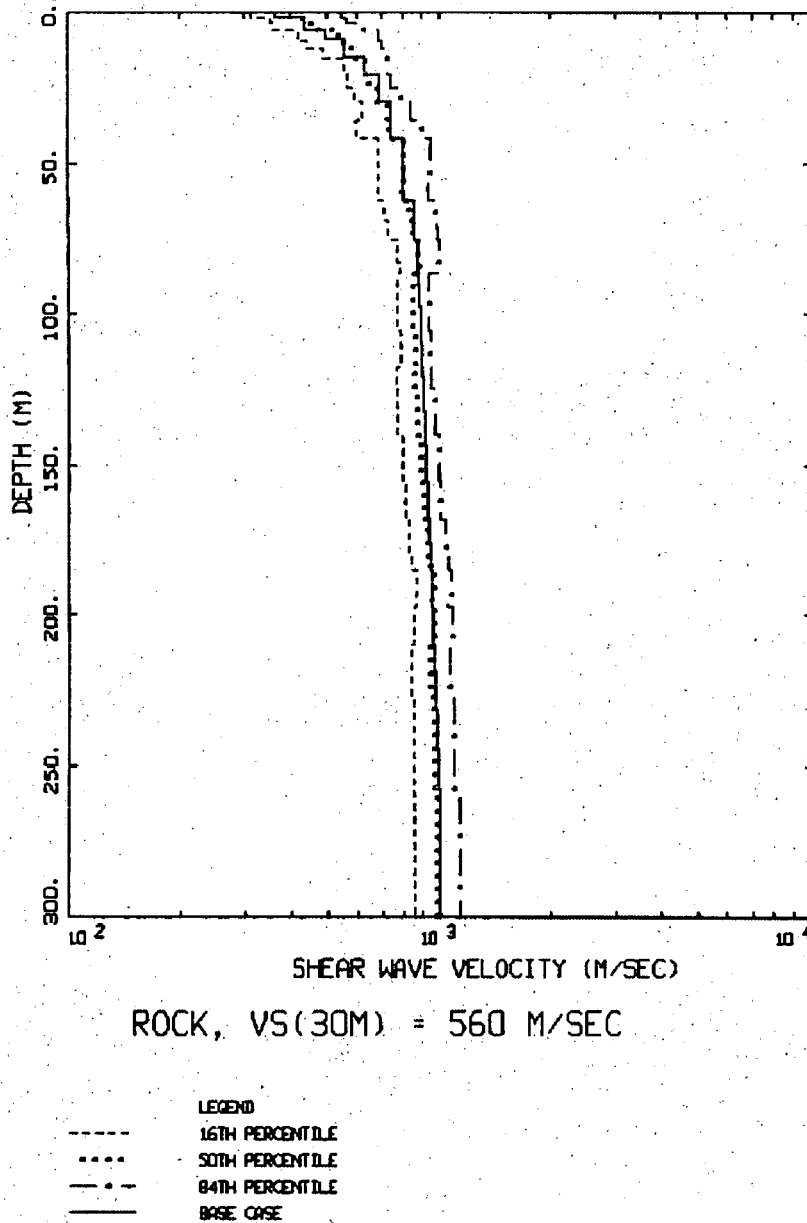


Figure B12b. Comparison of the base case profile with the median profile computed from the thirty simulated profiles, $\pm 1\sigma$ estimates are shown along with the median: logarithmic shear wave velocity axes. Generic soft rock with $\overline{V}_s(30m) = 560m/sec$ (Reference 5).

Appendix C

Limitations of Stochastic Point-source Modeling

Table of Contents

List of Figures.....	C2
1.0 PURPOSE AND SCOPE.....	C3
2.0 ASSUMPTIONS.....	C3
3.0 DISCUSSION.....	C3
4.0 SUMMARY.....	C5
5.0 REFERENCES.....	C5
6.0 FIGURES.....	C6

List of Figures

Figure C1. Comparison of empirical WNA spectral shapes (PEER, 2008; Reference 7) with those computed using the single- and double-corner source models moment magnitudes are 5.5, 6.5, and 7.5 and the rupture distance is 25 km from a vertical strike-slip earthquake with the top-of-rupture at the surface. The site condition is soft rock (Geomatrix category A and B) with a \bar{v}_s (30m) of 550m/sec..... C6

Figure C2. Comparison of empirical WNA spectral shapes (PEER, 2008; Reference 7) with those computed using the single- and double-corner source models moment magnitudes are 5.5, 6.5, and 7.5 and the rupture distance is 200 km from a vertical strike-slip earthquake with the top-of-rupture at the surface. The site condition is soft rock (Geomatrix category A and B) with a \bar{v}_s (30m) of 550m/sec..... C9

1.0 Purpose and Scope

This appendix addresses the computational validity of the point-source model in the site response analysis for Lee Nuclear Station Unit 1. Silva et al. (FSAR Reference 2.5.2-288) demonstrated that the point-source model underpredicts intermediate period absolute spectral amplitudes for $M \geq 6.5$ and distances beyond 100 km. New calculations were performed to demonstrate that the point-source model compares very favorably with the recent 2008 NGA empirical Ground Motion Prediction Equations (GMPE) (PEER, 2008; Reference 7) across both period and magnitude over a wide distance range in a relative sense, the manner in which the point source model is used to estimate amplifications for the site response analysis for Lee Nuclear Station Unit 1.

2.0 Assumptions

None.

3.0 Discussion

It is important to clarify the difference in model accuracy in an absolute sense as discussed in the Silva et al. (1997; Reference 1) unpublished report, and model accuracy in a relative sense, as used in developing amplification factors. In applications of Approach 3, to cover the range in reference site (e.g. hard rock in Central Eastern North America (CENA)) hazard from high to low probability (range 10^{-2} to 10^{-7}), amplification factors are developed for a suite of reference site peak acceleration values from 0.01g to about 1.50g at a sufficiently dense grid to permit linear (log) interpolation. To adjust the reference site peak acceleration to the desired values, source distance is iteratively adjusted. The corresponding soil motion is then developed by placing the site-specific soil column on top of the hard rock profile, in the case of CENA hard rock reference hazard. As a result of "fixing" the reference site peak acceleration, the model has been used to produce relative (amplitude ratios) rather than absolute motion. The amplification (amplitude ratio) implementation of the model then places far less stringent criteria on absolute motion accuracy. In general, for the application of developing site-specific amplification factors, the essential criteria of the model is most properly viewed or specified through its ability to produce acceptably accurate response spectral shapes. That is, does the model reflect an acceptably close agreement with empirical response spectral shapes across structural frequency at fixed magnitude as well as the change in spectral shape with magnitude and distance. To illustrate the agreement between the point-source model and empirical spectral shapes, the comparison of shapes at M 6.5 with four Next Generation Attenuation (NGA) ground motion prediction equations (GMPE) shown in the response to RAI 02.05.02-021 has been expanded to include M 5.5 and M 7.5. Since spectral shapes vary weakly with distance (Silva and Green, 1989; Reference 2), shapes computed at a distance of 25 km are appropriate for distances ranging out to at least 50 km and perhaps for somewhat larger distances. Also 25 km reflects a distance for which significant data exist across magnitude M 5.5 to M 7.5. Figure C1 shows the comparisons for M 5.5, 6.5, and 7.5 at a distance of 25 km for a soft rock site (V_s (30m)), the stiffest site condition near which significant recordings exist over a wide magnitude range. In general, either the single-or double-corner model shapes are within about 10% of the empirical shapes. The overall weak effect of spectral shape on amplification, conditional on peak acceleration (Bazzurro and Cornell, 2004; Reference 3) and further illustrated in Figure 5 showing a 25% difference in amplification for a 100% difference in control motion, suggest the effects of a 10% to 20% difference in control motion shape would result in a negligible difference in amplification.

At larger distances, Figure C2 illustrates an extreme case comparing model and NGA spectral shapes at a distance of 200 km, the largest distance of applicability of the NGA GMPEs. At large distances, beyond about 100 km in Western North America (WNA) (Silva and Green, 1989; Reference 2), frequency dependent crustal damping ($Q(f) = Q_0 f^h$) is dominant over kappa, reducing high frequency motions and resulting in a shift in spectral shapes to longer period. This trend is easily observed in the shift of the peaks from about 0.2 sec (5 Hz) at a distance of 25 km (Figure C1) to about 0.3 sec (≈ 3 Hz) at 200 km (Figure C2). The shift in the empirical spectra places upper limits on Q_0 to about 200, for an h of 0.6, the values used herein. From Figure C2 the effects of the decrease in the quantity of empirical data, particularly for M 5.5, is evidenced by the increased range in empirical shapes compared to those computed for a distance of 25 km (Figure C1). In general the point-source model, either single- or double-corner, remain generally within the range of the empirical shapes. This is particularly evident for periods shorter than about two seconds, which is the period range that dominates approximately the top 500 ft of soil profiles where nonlinearity is most pronounced (Silva et al., 1997; Reference 1). Recall for linear site response analyses, control motion spectral shape has an effect only at very short periods, very low levels of motion, and at large distance due to the depletion of short period energy in control motions by crustal damping (Subsection 2.5.2.7.1.1.1.1, Duke FSAR).

It is also important to point out that for applications to soft or firm rock reference site conditions, base-of-soil rock conditions are distinctly different at shallow depths than rock outcrop, where there typically exists a steep velocity gradient (Silva et al, 1997 (Reference 1); Boore, 2003 (Reference 4)). Such conditions can have a significant impact on high-frequency motions, resulting in amplification that is not present for base-of-soil rock conditions. If appropriate corrections are not made to the soft or firm rock reference site control motions, the site response analyses may overdrive the soil column resulting in unconservative amplification at high frequency. Because the appropriate reference site soft or firm rock profile will likely be poorly known, the base-of-soil correction will likely result in a control motion that is less accurate than the point-source model illustrated in Figure C1.

Additionally, for hard rock reference site conditions in the CENA, since the model(s) used to develop hard rock hazard is (are) dominated by the point-source model, the use of a point-source to drive a site-specific soil column is not an issue. This is the case provided the point-source models used in the site response adequately span the range in models, e.g. single- and double-corner, that is accommodated in developing the reference site hazard.

To summarize, although the point-source model has been shown to underpredict intermediate period motions for $M \geq 6.5$ and distances beyond 100 km in an absolute sense (Silva et al., 1996; Reference 6), the model compares quite favorably with the recent NGA (2008; Reference 5) empirical GMPEs across both period and magnitude over a wide distance range in a relative sense, the manner in which the model is implemented. Considering response spectral shapes, both the single- and double-corner point-source models produce motions (5% damped pseudo absolute response spectra) that either exceed or are within the range of the recently developed NGA GMPEs. For applications to the CENA, where the GMPEs are dominated by the point-source model, the appropriateness of the model to serve as control motions in site amplification analyses is less of an issue.

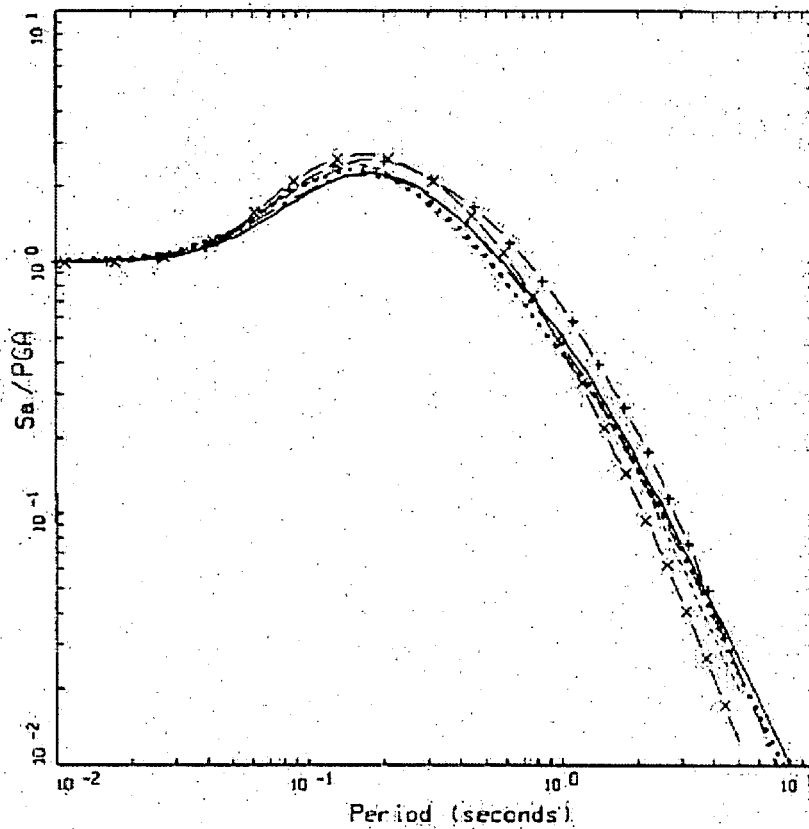
4.0 Summary

Although the point-source model had been shown by Silva et al. (FSAR Reference 2.5.2-288) to underpredict intermediate period absolute spectral amplitudes for $M \geq 6.5$ and distances beyond 100 km, this appendix provides new calculations that show that the point-source model compares quite favorably with the recent 2008 NGA empirical GMPEs (PEER, 2008; Reference 5) across both period and magnitude over a wide distance range in a relative sense, the manner in which the point source model is used to estimate amplifications for the site response analysis for Lee Nuclear Station Unit 1.

5.0 References

1. Silva, W.J., N. Abrahamson, G. Toro, C. Costantino (1997). "Description and validation of the stochastic ground motion model." Report Submitted to Brookhaven National Laboratory, Associated Universities, Inc. Upton, New York.
2. Silva, W.J., and Green, R.K. (1989). "Magnitude and distance scaling of response spectral shapes for rock sites with applications to North American tectonic environment." *Earthquake Spectra*, 5(3), 591-624.
3. Bazzurro, Paolo and C.A. Cornell (2004). "Nonlinear soil-site effects in probabilistic seismic-hazard analysis." *Bulletin of the Seismological Society of America*, 94(6), 2110-2123.
4. Boore, D.M. (2003) "Simulation of ground motions using the stochastic method" *Pure and Applied Geophysics*, 160(2003), 635-676.
5. Pacific Engineering Research Center (PEER) (2008), Next Generation of Ground Motion Attenuation Models (NGA), "Special issue on the next generation attenuation project," Technical editors, J. Stewart, R. Archuleta, M. Power, *Earthquake Spectra*, vol. 24(1).
6. Silva, W.J., N. Abrahamson, G. Toro and C. Costantino. (1996). "Description and validation of the stochastic ground motion model." Report Submitted to Brookhaven National Laboratory, Associated Universities, Inc. Upton, New York 11973, Contract No. 770573.

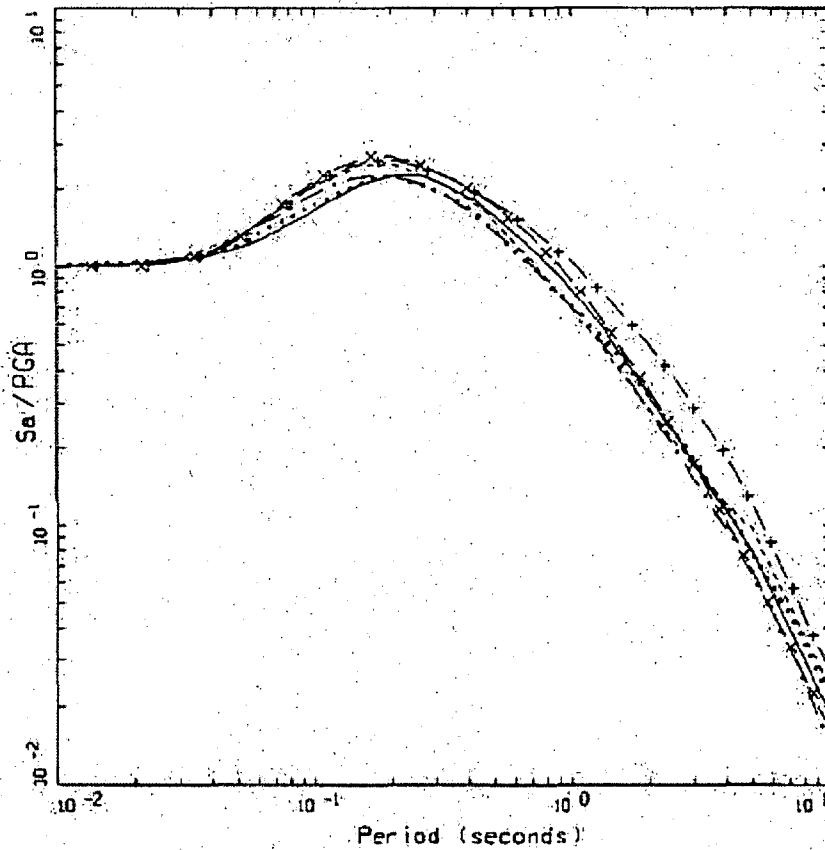
6.0 Figures



NGA 2008, M = 5.5, D = 25 KM, STRIKE-SLIP
550 M/SEC (GAB)

- LEGEND
- ABRAHAMSON & SILVA
 - BOORE & ATKINSON
 - - - CAMPBELL & BOZORCHIAN
 - - - OHICU & YOUNG
 - x - 2-CORNER, K = 0.05 SEC
 - + - 1-CORNER, K = 0.05 SEC

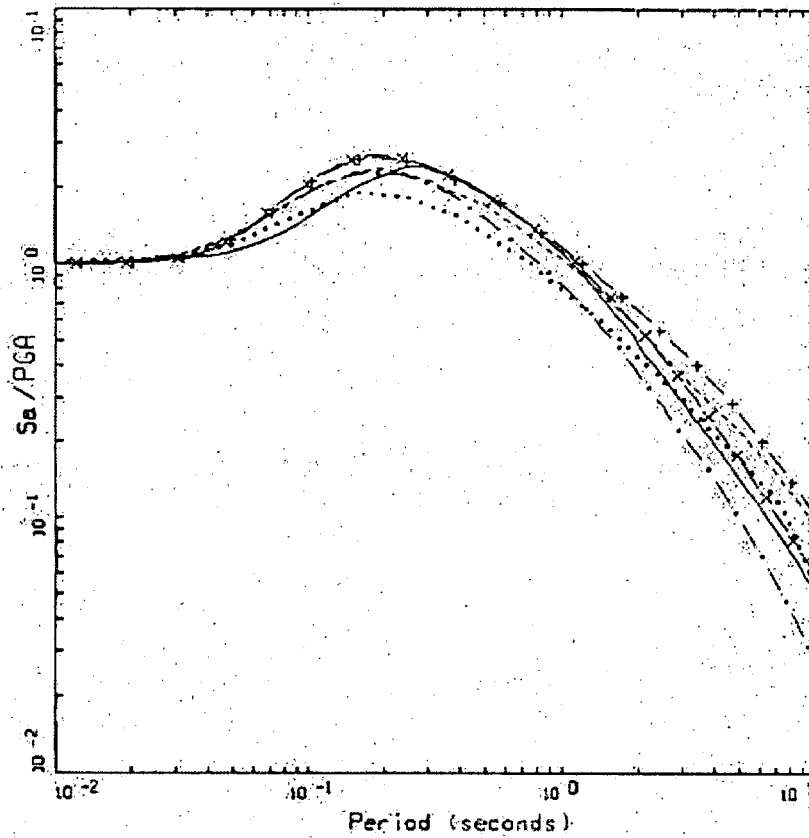
Figure C1. Comparison of empirical WNA spectral shapes (PEER, 2008; Reference 7) with those computed using the single- and double-corner source models moment magnitudes are 5.5, 6.5, and 7.5 and the rupture distance is 25 km from a vertical strike-slip earthquake with the top-of-rupture at the surface. The site condition is soft rock (Geomatrix category A and B) with a \bar{v}_s (30m) of 550m/sec.



NGA 2008, M = 6.5, D = 25 KM, STRIKE-SLIP
550 M/SEC (GAB)

- LEGEND
- ABRAHAMSON & SILVA
 - BOORE & ATKINSON
 - - - CAMPBELL & BOZORGNIA
 - · - CHIYOU & YOUNGS
 - x - 2-CORNER, K = 0.05 SEC
 - + - 1-CORNER, K = 0.05 SEC

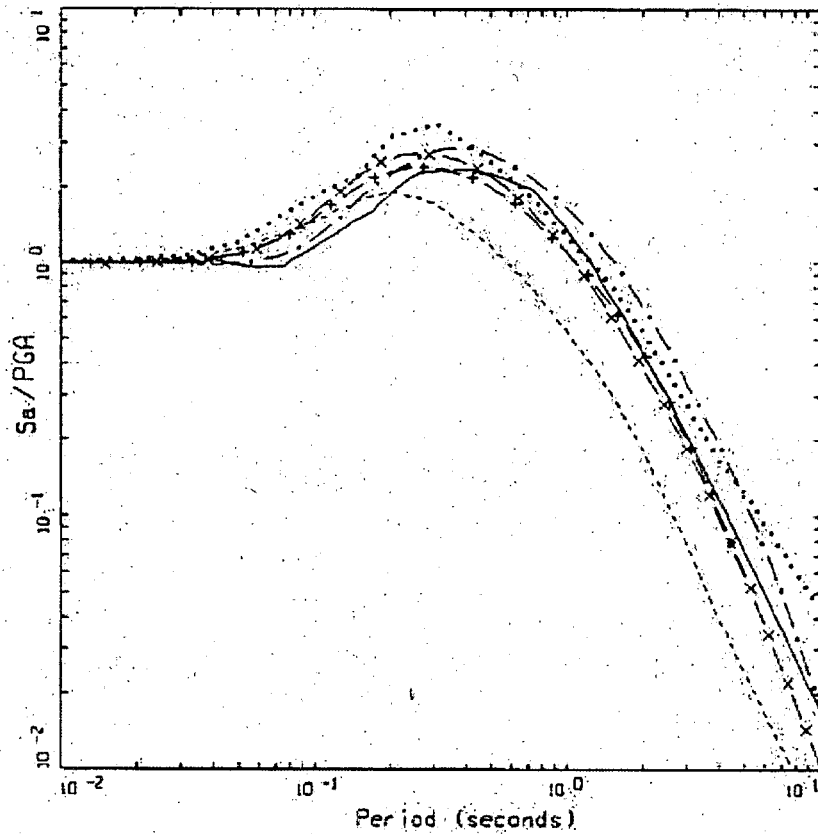
Figure C1. (continued) Comparison of empirical WNA spectral shapes (PEER, 2008; Reference 7) with those computed using the single- and double-corner source models moment magnitudes are 5.5, 6.5, and 7.5 and the rupture distance is 25 km from a vertical strike-slip earthquake with the top-of-rupture at the surface. The site condition is soft rock (Geomatrix category A and B) with a \bar{V}_s (30m) of 550m/sec.



NGA 2008, $M = 7.5$, $D = 25$ KM, STRIKE-SLIP
550 M/SEC (GAB)

- LEGEND
- ABRAHAMSON & SILVA
 - BOORE & ATKINSON
 - - - CAMPBELL & BOZORGHIA
 - · - CHIU & YOUNG
 - x - 2-CORNER, $K = 0.05$ SEC
 - + - 1-CORNER, $K = 0.05$ SEC

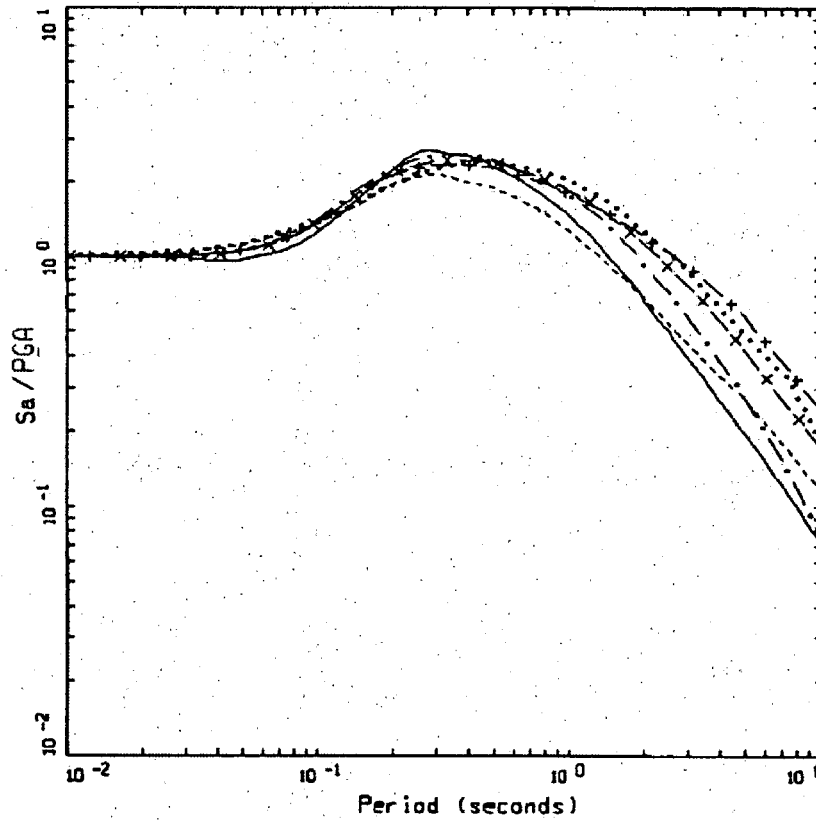
Figure C1. (continued) Comparison of empirical WNA spectral shapes (PEER, 2008; Reference 7) with those computed using the single- and double-corner source models moment magnitudes are 5.5, 6.5, and 7.5 and the rupture distance is 25 km from a vertical strike-slip earthquake with the top-of-rupture at the surface. The site condition is soft rock (Geomatrix category A and B) with a \bar{V}_s (30m) of 550m/sec.



NGA 2008, M = 5.5, D = 200 KM, STRIKE-SLIP
550 M/SEC (GAB)

- LEGEND
- ABRAHAMSON & SILVA
 - BOORE & ATKINSON
 - CAMPBELL & BOZORCHIA
 - · - · CHIOU & YOUNG
 - x - 2-CORNER, K = 0.05 SEC
 - + - 1-CORNER, K = 0.05 SEC

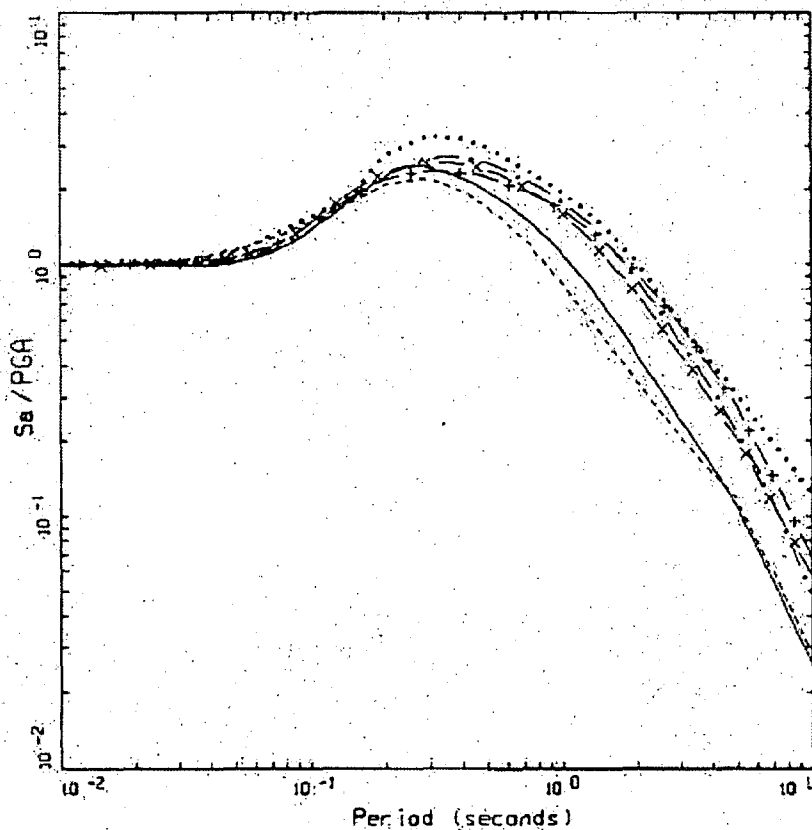
Figure C2. Comparison of empirical WNA spectral shapes (PEER, 2008; Reference 7) with those computed using the single- and double-corner source models moment magnitudes are 5.5, 6.5, and 7.5 and the rupture distance is 200 km from a vertical strike-slip earthquake with the top-of-rupture at the surface. The site condition is soft rock (Geomatrix category A and B) with a \bar{V}_s (30m) of 550m/sec.



NGA 2008, $M = 7.5$, $D = 200$ KM, STRIKE-SLIP
550 M/SEC (GAB)

- LEGEND
- ABRAHAMSON & SILVA
 - BOORE & ATKINSON
 - - - CAMPBELL & BOZORGNIA
 - · - CHIYOU & YOUNGS
 - x - 2-CORNER, $K = 0.05$ SEC
 - + - 1-CORNER, $K = 0.05$ SEC

Figure C2. (continued) Comparison of empirical WNA spectral shapes (PEER, 2008; Reference 7) with those computed using the single- and double-corner source models moment magnitudes are 5.5, 6.5, and 7.5 and the rupture distance is 200 km from a vertical strike-slip earthquake with the top-of-rupture at the surface. The site condition is soft rock (Geomatrix category A and B) with a \bar{v}_s (30m) of 550m/sec.



NGA 2008, $M = 6.5$, $D = 200$ KM, STRIKE-SLIP
550 M/SEC (GAB)

- LEGEND
- ABRAHAMSON & SILVA
 - BOORE & ATKINSON
 - - - CAMPBELL & BOZORGNIA
 - · - CHIQU & YOUNGS
 - x - 2-CORNER, $K = 0.05$ SEC
 - + - 1-CORNER, $K = 0.05$ SEC

Figure C2. (continued) Comparison of empirical WNA spectral shapes (PEER, 2008; Reference 7) with those computed using the single- and double-corner source models moment magnitudes are 5.5, 6.5, and 7.5 and the rupture distance is 200 km from a vertical strike-slip earthquake with the top-of-rupture at the surface. The site condition is soft rock (Geomatrix category A and B) with a \bar{V}_s (30m) of 550m/sec.